UNIVERSITY OF CALIFORNIA

Santa Barbara

Greening azacycle synthesis and ester amidation using flow chemistry powered by heterogeneous catalysis

A thesis submitted in partial satisfaction of the

requirements for the degree Master of Science

in Chemistry

by

Melvin Thomas

Committee in charge:

Professor Susannah L. Scott, Chair

Professor Mattanjah S de Vries

Professor Songi Han

September 2022

The thesis of Melvin Thomas is approved.

_____

Songi Han

_____

Mattanjah S de Vries

_____

Susannah L. Scott, Committee Chair

September 2022

Greening azacycle synthesis and ester amidation using flow chemistry powered by heterogeneous catalysis

ACKNOWLEDGEMENTS

I am greatly indebted to many people without whose support and encouragement this thesis would not have been possible.

To begin with, I wish to express my sincere gratitude to Prof. Susannah Scott for guiding me throughout my research work. I am deeply indebted to her for the consistent encouragement and invaluable criticism, which lent me a hand in completing this work.

I would like to thank my committee members, Prof. Mattanjah de Vries and Songi Han, for their kind help and support.

I extend my heartfelt thanks to Dr. Allison Wesley for teaching me the fundamentals of flow chemistry.

I sincerely thank Dr. Jing Wu and Costanza Leonardi for their help and support during the projects.

I thank Dr. Bryan Li (Pfizer) and Dr. Joel Hawkins (Pfizer) for their suggestions and support.

I sincerely thank all my friends at UC Santa Barbara for their time and efforts in helping me.

I am thankful to the authorities and staff of UCSB for helping me on various occasions.

For being the indomitable force behind me, I wholeheartedly thank my family.

ABSTRACT

Greening azacycle synthesis and ester amidation using flow chemistry powered by heterogeneous catalysis

Melvin Thomas

Flow chemistry is one of the most efficient ways of practicing chemistry. The development of reliable flow chemistry methods is of great significance from an industrial perspective since safety and ease in scaling up processes are this technology's key advantages. Herein we discuss the development of novel flow methodologies for making azacycles and amides.

Azacycles are an essential class of pharmaceutically active compounds whose synthesis is generally conducted in batch by methods involving highly functionalized reagents and a homogeneous catalyst with or without a promoter. A more direct route to azacycles, for example, from ethers, would enable more streamlined, efficient, and sustainable processes. This work synthesized a wide range of N-substituted pyrrolidines, piperidines, and pyrroles by the direct reaction of cyclic ethers or furans with primary amines. Amorphous silica-alumina, a simple and readily available solid acid, catalyzes the cyclocondensation reaction for both aromatic and aliphatic amines and allows the reaction to be conducted continuously in a packed-bed reactor. When the reactant is a simple ether that can also serve as the solvent, *N*-substituted azacycles are obtained in high yield by simple solvent removal without further workup. The solid acid-catalyzed reaction in flow provides a simple and efficient route to *N*-substituted azacycles.

Amide bond formation is a crucial transformation in pharmaceutical manufacturing. Conventional protocols involve harsh conditions or the stoichiometric usage of toxic coupling agents such as HATU or EDC. Amidation of esters is a promising strategy because it requires cheap, stable, and readily available methyl or ethyl esters and produces volatile alcohol as the only byproduct. In this project, we have developed an efficient continuous flow protocol with short residence times using amorphous silica-alumina as the catalyst.

TABLE OF CONTENTS

Chapter 1. Introduction

1.1 Background 1

1.2 Azacycle synthesis: state of the art 4

1.3 Ester amidation: state of the art 7

References 13

Appendix 1 21

Chapter 2. Azacycles synthesis in flow

2.1 Introduction 31

2.2 Experimental Methods 34

2.3 Computational Methods 36

2.4 Results and Discussion 38

2.5 Conclusion 53

References 55

Appendix 2 67

Chapter 3. Ester amidation in flow

3.1 Introduction 99

3.2 Experimental Methods 101

3.3 Results and discussion 104

3.4 Conclusion 116

References 118

Appendix 3 127

Conclusion 143

1. Introduction

1.1 Background

There are two main ways to achieve chemical transformations in the pharmaceutical industry: batch and flow protocols. In batch protocols, all the starting materials are added under ambient conditions; upon reaction completion, product separation and purification are typically carried out by extensive workup, including chromatography. Even though batch processes are established and versatile, they have some limitations when scaling up. In particular, safe handling of explosive gases and toxic reagents is challenging in batch protocols. In addition, heat and mass transfer irregularities can lower the yield and form byproducts.[1]

Flow chemistry is an alternative approach in which reactants are continuously added, reacted, and isolated. Starting materials are always supplied at one end of the reactor, and the product is constantly collected from the other. In flow chemistry, the reaction rate is determined by the concentration of reagents. Reaction time in flow conditions is expressed in residence time. When a catalyst is present (usually the case), it is defined as the ratio of the catalyst void volume to the overall flow rate.

Advantages and applications of flow chemistry

Inherent advantages of flow technology include efficient heat exchange, high reproducibility, fast mixing, high throughput, safety, and the ability to do multi-step syntheses.[2] Most importantly, using flow technology, we can perform large-scale chemistry, which is difficult under batch conditions, including large-scale photochemistry and electrochemistry. For example, many efficient microwave-assisted reactions at a small scale

are either challenging to scale up or lose efficiency upon scaling up. Such processes can be easily scaled up using flow technology without compromising efficiency.[3]

Since the required volume of a flow reactor is much smaller than needed for a batch reactor to achieve the same throughput, the surface area to volume ratio of the flow reactor is comparatively high, which helps improve heat transfer. Additionally, precise parameter control is possible in flow. The improved mixing and heat transfer reduces unwanted by/side products caused by inhomogeneities in concentration and temperature.[1]

Since the nature of the technology is continuous addition and removal, there is no accumulation of large amounts of reactive species at any moment, which mitigates several safety issues. Risky reactions involving toxic and explosive intermediates can be achieved safely using flow technology. Hydrogenation, halogenation, nitration, generation of diazomethane, reactions involving organic azides, etc., are potentially hazardous transformations that can be achieved safely using flow.[4a-b] Highly exothermic reactions can be more readily controlled in the flow because of efficient heat transport. The chances for thermal runaway reactions are minimized since the feed of reactants can be stopped easily. Since the chemistry happens in narrow tubes, fine-tuning internal pressure is possible with the help of a back pressure regulator and HPLC pump. The high-pressure conditions that can be attained safely increase the boiling points of solvents, enabling faster and unconventional reactions that are difficult under ambient reflux conditions.

A flow reactor is an efficient option for gas-liquid biphasic mixtures due to improved interfacial mixing and the opportunity to achieve high pressure more safely. Moreover, controlling the stoichiometry of gases is possible with a mass-flow controller.[5] The reported protocols for ozonolysis of alkenes, quenching of Grignard reagents with CO_2 to afford

carboxylic acids, and palladium-catalyzed carbonylation reactions using CO are some successful examples of the safe handling of gases in flow.[6,7]

Advantages of heterogeneous catalysis in packed bed reactors

Heterogeneous catalysis is vital in many industrial processes. Ease of separation from the product and the possibility of reuse make heterogeneous catalysts attractive. Continuous flow technology makes heterogeneous catalysis simplifies operations by combining reaction and isolation into a single step.[8,9]

There are two main flow reactors for heterogeneous catalyzed reactions: continuously stirred tank reactors and packed bed reactors. This thesis will focus on the packed bed reactor. These reactors are generally tubular and are often made of stainless steel. The catalysts (for example, in the case of simple redox reactions, transition metals deposited on a solid support material) can be packed inside the reactor. The particle size of the heterogeneous catalyst is crucial. Big particles have a relatively low surface-to-volume ratio, and conversion might be lower since the reaction occurs on the surface. Porous particles have higher surface areas, but mass transport limitations can prevent access of reactants to the active sites, and side-products can clog the pores. Small particles may cause high back pressure.[10]

Inert packing materials such as silica beads and glass wool can provide additional support to the catalyst bed. The packed bed reactor can be mounted in a heating block, with a back pressure regulator to control the system pressure. A liquid, gas, or mixed mobile phase is pumped through the catalyst bed. The high catalyst-to-substrate ratio in the reactor can enable high conversion and lower reaction time. Since the products and by-products are continuously removed, the chances of catalyst poisoning are reduced. Most importantly, continuous use of

the catalyst is possible in most cases. However, there are some potential issues, such as irregularities in pressure and possibilities for catalyst deactivation and leaching.[11]

1.2 Azacycle Synthesis: State of the art

Nitrogen-containing 5- and 6-membered rings are present in many bioactive molecules and valuable materials (Figure **1.1**).[12a-d] There are several methods to make these motifs.

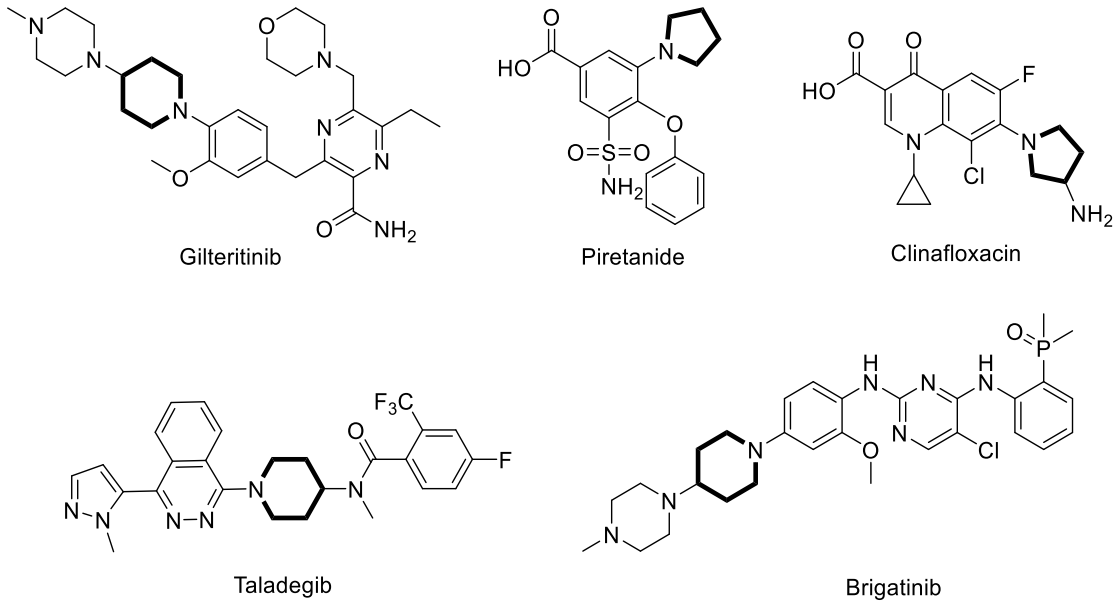

Figure 1.1 Selected bioactive molecules containing 5- or 6-membered azacycles.

N, N-dialkylation reaction of amines with dihalides or diols is a classical approach. Recent examples of this approach are shown in **Scheme 1.1**. Their limitations include difficulty scaling up, expensive catalysts, and long reaction times. [13,14]

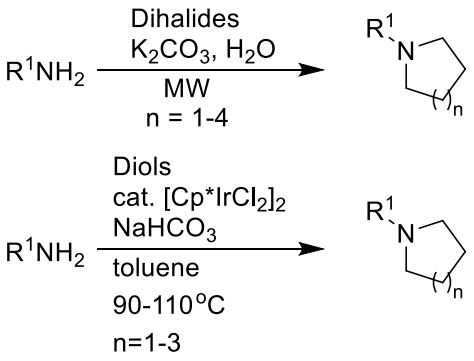

Scheme 1.1 Azacycles from dihalides and diols

Reductive amination of dicarbonyl compounds is another reliable route (**Scheme 1.2**). Dialdehydes can be subjected to reductive amination to furnish azacycles using $KHFe(CO)_4$,[15] $HFe(CO)_4^-$, n-Bu_2SnClH-HMPA,[16] $NaBH_4$,[17] etc., as reducing agents. Reducing diesters under hydrogenation conditions in the presence of $Ru(acac)_3$ and triphos required a high temperature (220 °C) to limit the scope of reaction of aniline derivatives.[18] Reductive amination of dicarboxylic acids and various amines in the presence of an N-heterocyclic carbene complex of iron(0), $Fe(CO)_4$(IMes), has also been reported.[19] Here, the difficulty lies in the preparation of the catalyst.

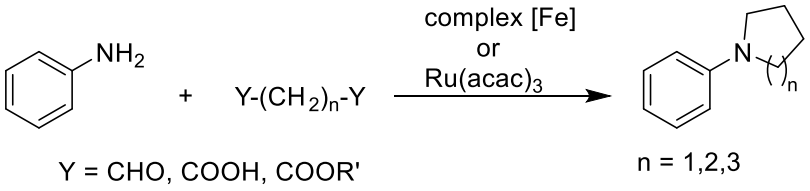

Scheme 1.2 Reductive amination of dicarbonyl compounds

Another well-established route is the transition metal-catalyzed C-N coupling of aryl or alkyl halides with amines (**Scheme 1.3**).[20a-d]

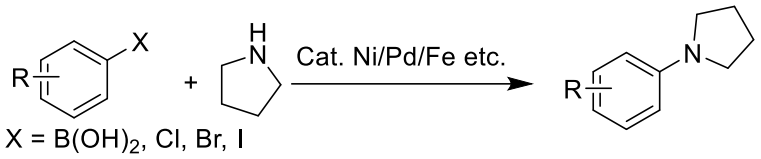

Scheme 1.3 Transition metal-catalyzed C-N coupling

In 2021, Wang et al. developed a novel intramolecular radical cyclization pathway (**Scheme 1.4**), using copper acetate as the catalyst.[21]

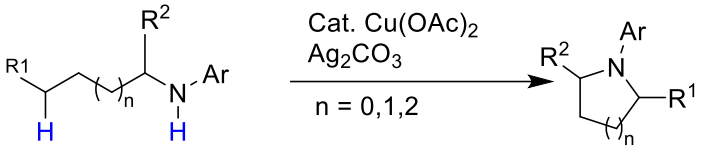

Scheme 1.4 Radical cyclization pathway towards azacycle

Even though the protocols mentioned above are successful, the direct reaction of amines and cyclic ethers to form N-substituted azacycles is very appealing since water is the only byproduct (**Scheme 1.5**). Many reported protocols are promoted by stoichiometric or excess amounts of Brønsted acids like HI,[22] or Lewis acids such as $BF_3.Et_2O$,[23] $AlMe_3$,[24] $AlCl_3$,[25] $TiCl_4$,[26] etc.

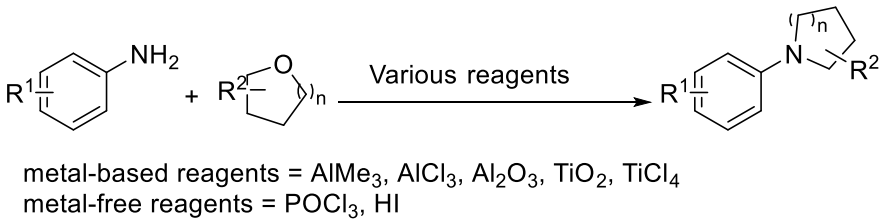

Scheme 1.5 Direct reaction of amines and cyclic ethers to form N-substituted azacycles

In 2016, Zhang et al. developed a method applying frustrated Lewis pair chemistry using *p*-TSA.H_2O and $B(C_6F_5)_3$ to synthesize azacycles from cyclic ethers and amines in a sealed vessel (**Scheme 1.6**).[27]

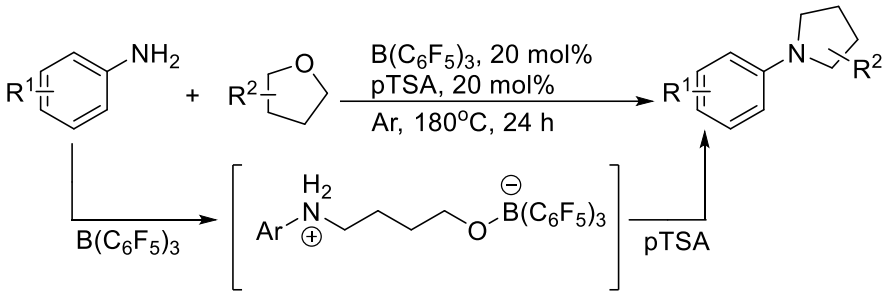

Scheme 1.6 Frustrated Lewis pair chemistry for furnishing azacycles

Solid acids like TiO_2[28] and Al_2O_3[29a-b] also have been applied to this transformation. However, their scope was limited to a few vapor phase reactions requiring high temperature (ca. 400 ^oC); hence, there is a lack of a versatile method for direct, continuous synthesis of azacycles from cyclic ethers and alkyl/aryl amines. Chapter 2 of this thesis describes the development of a protocol to address this scenario.

1.3 Ester amidation: State of the art

Amide bond formation is a crucial transformation in pharmaceutical manufacturing (**Figure 1.2**).[30a] For example, Pfizer's Covid drug PF-07321332 contains four amide bonds.[30b] Conventional protocols involve harsh conditions or the stoichiometric usage of toxic coupling agents such as HATU or EDC.[31] Amidation of esters is a promising strategy because it requires cheap, stable, and readily available methyl or ethyl esters and produces volatile alcohol as the only byproduct.

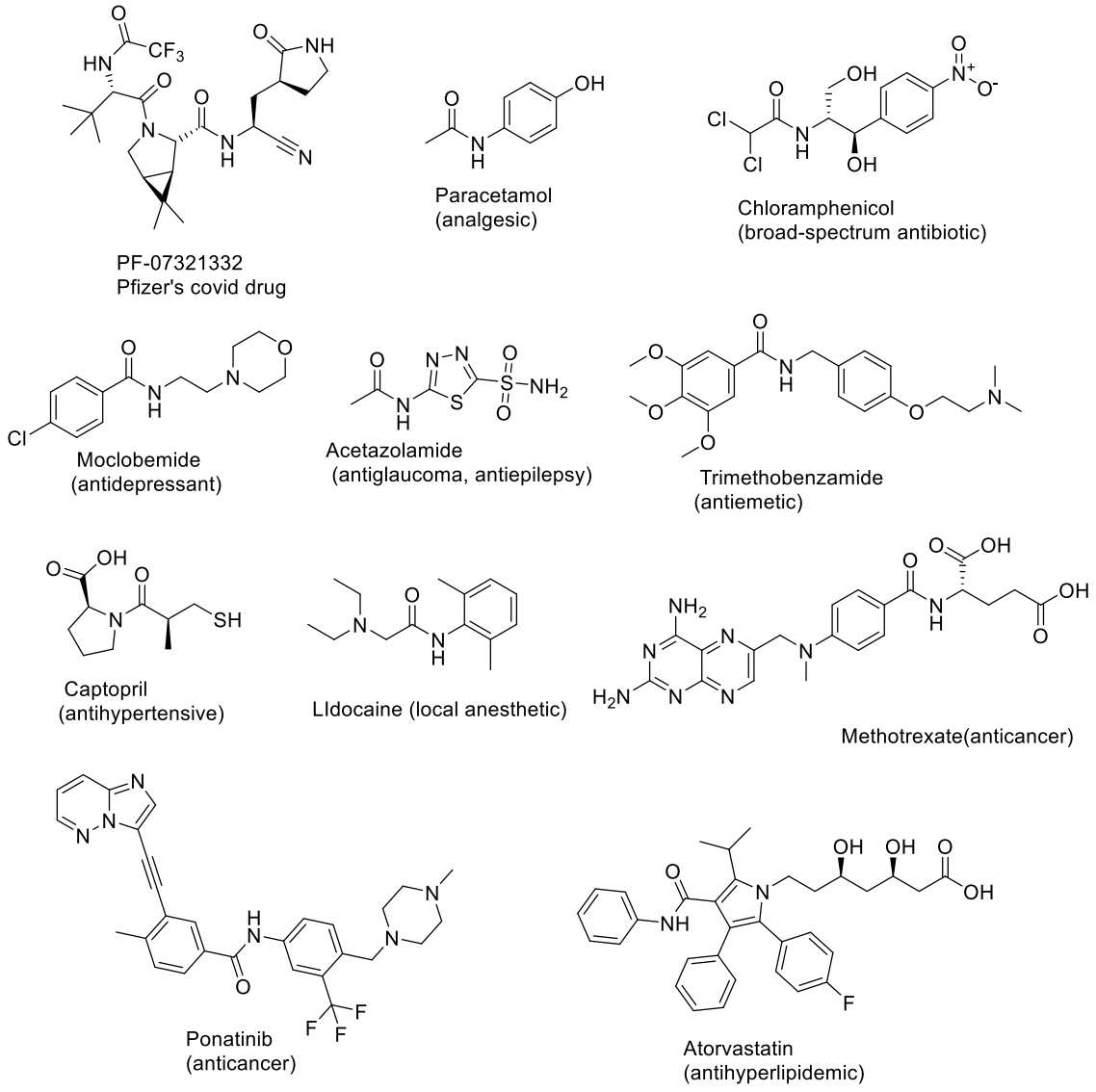

Figure 1.2 Selected amide-containing pharmaceutical drugs

Direct amide bond formation from amines and unactivated esters is undermined due to the need to deprotonate the amine with organometallic reagents like $AlMe_3$,[32] isopropyl magnesium chloride,[33] acutely toxic tin reagents,[34] etc. Despite attempts to develop milder versions of this method,[35a-m] issues with epimerizable stereocenters, functional group tolerance, and the need for excess amine limit its general utility. For example, Ranu and Gupta

reported a protocol with a catalytic amount of non-toxic indium triiodide and excess amine (**Scheme 1.7**),[36] but the reaction was unsuccessful with secondary amines.

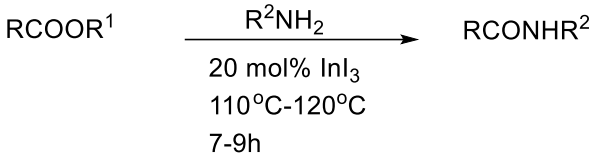

Scheme 1.7 Indium triiodide-catalyzed amidation of esters

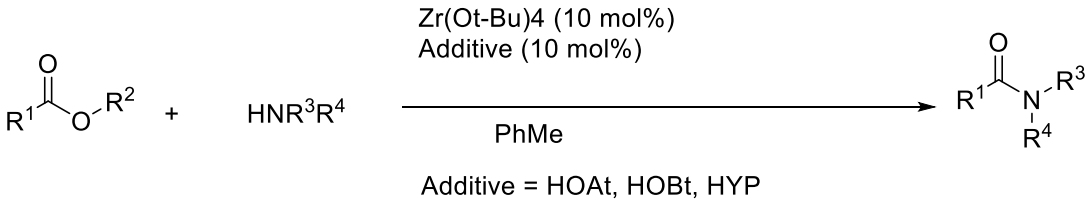

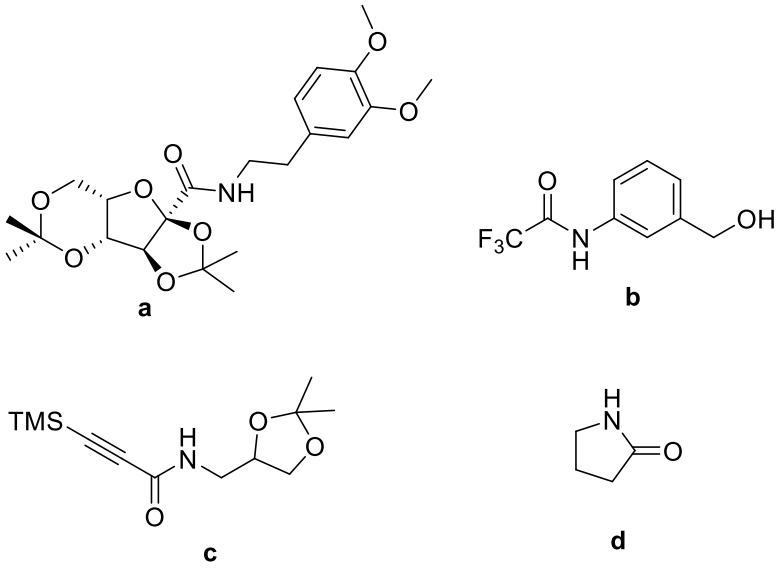

Scheme 1.8 $Zr(O\text{-}tBu)_4$ -catalyzed amidation of esters

Even though there are protocols based on other metal catalysts[35b] like zinc dust, palladium acetate, antimony (III) ethoxide, ligated iridium, and ruthenium catalysts, $Zr(O\text{-}tBu)_4$ stands

out with an impressive substrate scope including amides a-c in **Scheme 1.8** and an intramolecular example d.[35j]

In addition to transition metal catalysts, organocatalysts have been successfully applied to achieve the amidation of esters. However, most of these protocols require amino alcohols as starting materials since they proceed via transesterification.[35b] The organocatalyst 1,5,7-triazabicyclo[4.4.0]dec-5-ene (TBD) does not have this limitation (**Scheme 1.9**).[35h] It has been applied to synthesizing secondary and tertiary amides from alkyl or aryl esters with various amines under solvent-free conditions in 60-94% yields.

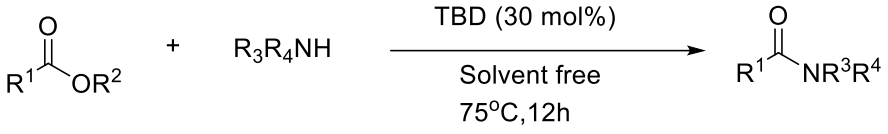

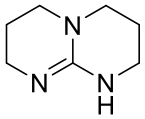

TBD= 1,5,7-triazabicyclo[4.4.0]dec-5-ene

Scheme 1.9 TBD-catalyzed amidation of esters

The reliability and application of this procedure have been further demonstrated in a pilot-plant scale process as a key step for synthesizing a human hematopoietic prostaglandin D synthase inhibitor (H-PGDS, 54) to supply preclinical trials (**Scheme 1.10**).[37]

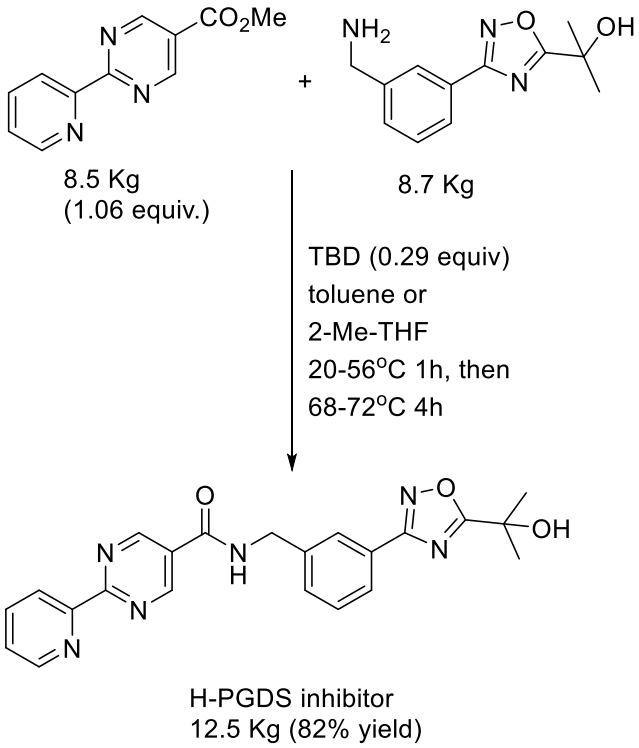

Scheme 1.10 Pilot-plant scale synthesis of H-PGDS via TBD catalysis

Since catalyst-product separation is challenging in these homogeneous systems, heterogeneous catalysis is an appealing strategy. Shimizu and co-workers developed the first heterogeneous catalytic system for ester amidation. Their batch protocol used Nb_2O_5 catalyst at 140 °C for 30 h. (**Scheme 1.11**) [38]

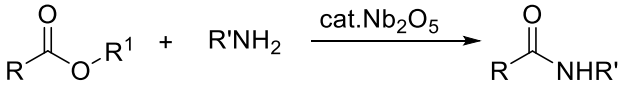

Scheme 1.11 Nb_2O_5 catalyzed ester amidation in batch

In 2021, Kobayashi et al. developed a continuous flow protocol catalyzed by amorphous zirconium oxide. (**Scheme 1.12**) [39]

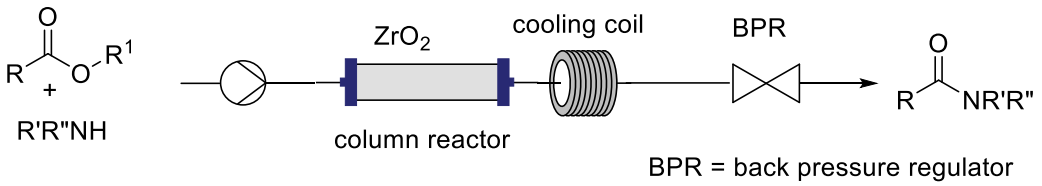

Scheme 1.12 Zirconium oxide catalyzed ester amidation in flow.

While this is a remarkable achievement, relatively high catalyst loading and usage of toxic diglyme as the reaction medium leave room for improvement. Chapter 3 of this thesis is an attempt to address this.

References

1. Plutschack, M. B.; Pieber, B.; Gilmore, K.; Seeberger, P. H. The Hitchhiker's Guide to Flow Chemistry. *Chem. Rev.* **2017**, *117* (18), 11796–11893.

2. McQuade, D. T.; Seeberger, P. H. Applying Flow Chemistry: Methods, Materials, and Multistep Synthesis. *J. Org. Chem.* **2013**, *78* (13), 6384–6389.

3. (a) Glasnov, T. N.; Kappe, C. O. The Microwave-to-Flow Paradigm: Translating High-Temperature Batch Microwave Chemistry to Scalable Continuous-Flow Processes. *Chemistry – A European Journal* **2011**, *17* (43), 11956–11968. (b)Wegner, J.; Ceylan, S.; Kirschning, A. Ten Key Issues in Modern Flow Chemistry. *Chemical Communications* **2011**, *47* (16), 4583–4592. (c) Wegner, J.; Ceylan, S.; Kirschning, A. Flow Chemistry – A Key Enabling Technology for (Multistep) Organic Synthesis. *Advanced Synthesis & Catalysis* **2012**, *354* (1), 17–57.

4. (a) Hessel, V.; Kralisch, D.; Kockmann, N.; Noël, T.; Wang, Q. Novel Process Windows for Enabling, Accelerating, and Uplifting Flow Chemistry. *ChemSusChem* **2013**, *6* (5), 746–789. (b) Movsisyan, M.; P. Delbeke, E. I.; T. Berton, J. K. E.; Battilocchio, C.; V. Ley, S.; V. Stevens, C. Taming Hazardous Chemistry by Continuous Flow Technology. *Chemical Society Reviews* **2016**, *45* (18), 4892–4928.

5. Yamamoto, A.; Oshibe, H.; Nakamura, H.; Tezuka, T.; Hasegawa, S.; Maruta, K. Stabilized Three-Stage Oxidation of Gaseous n-Heptane/Air Mixture in a Micro Flow Reactor with a Controlled Temperature Profile. *Proceedings of the Combustion Institute* **2011**, *33* (2), 3259–3266.

6. Cantillo, D.; Oliver Kappe, C. Halogenation of Organic Compounds Using Continuous Flow and Microreactor Technology. *Reaction Chemistry & Engineering* **2017**, *2* (1), 7–19.

7. Ley, S. V. On Being Green: Can Flow Chemistry Help? *The Chemical Record* **2012**, *12* (4), 378–390.

8. Kirschning, A.; Solodenko, W.; Mennecke, K. Combining Enabling Techniques in Organic Synthesis: Continuous Flow Processes with Heterogenized Catalysts. *Chemistry – A European Journal* **2006**, *12* (23), 5972–5990.

9. Irfan, M.; Glasnov, T. N.; Kappe, C. O. Heterogeneous Catalytic Hydrogenation Reactions in Continuous-Flow Reactors. *ChemSusChem* **2011**, *4* (3), 300–316.

10. *Volume 1 Flow Chemistry – Fundamentals*; De Gruyter, 2014.

11. Hii, K. K. (Mimi); Hellgardt, K. Catalysis in Flow: Why Leaching Matters. In *Organometallic Flow Chemistry*; Noël, T., Ed.; Topics in Organometallic Chemistry; Springer International Publishing: Cham, 2016; pp 249–262.

12. (a) Liang, X.; Yang, Q.; Wu, P.; He, C.; Yin, L.; Xu, F.; Yin, Z.; Yue, G.; Zou, Y.; Li, L.; Song, X.; Lv, C.; Zhang, W.; Jing, B. The Synthesis Review of the Approved Tyrosine Kinase Inhibitors for Anticancer Therapy in 2015–2020. *Bioorganic Chemistry* **2021**, *113*, 105011. (b) Fischer, J.; IUPAC; Ganellin, C. R. *Analogue-Based Drug Discovery*; John Wiley & Sons, 2006. (c) Wang, Y.; Damu, G. L. V.; Lv, J.-S.; Geng, R.-X.; Yang, D.-C.; Zhou, C.-H. Design, Synthesis and Evaluation of Clinafloxacin Triazole Hybrids as a New Type of Antibacterial and Antifungal Agents. *Bioorganic & Medicinal Chemistry Letters* **2012**, *22* (17), 5363–5366. (d)

Ghirga, F.; Mori, M.; Infante, P. Current Trends in Hedgehog Signaling Pathway Inhibition by Small Molecules. *Bioorganic & Medicinal Chemistry Letters* **2018**, *28* (19), 3131–3140.

13. Ju, Y.; Varma, R. S. An Efficient and Simple Aqueous N-Heterocyclization of Aniline Derivatives: Microwave-Assisted Synthesis of N-Aryl Azacycloalkanes. *Org. Lett.* **2005**, *7* (12), 2409–2411.

14. Fujita, K.; Fujii, T.; Yamaguchi, R. Cp*Ir Complex-Catalyzed N-Heterocyclization of Primary Amines with Diols: A New Catalytic System for Environmentally Benign Synthesis of Cyclic Amines. *Org. Lett.* **2004**, *6* (20), 3525–3528.

15. Watanabe, Y.; Shim, S. C.; Uchida, H.; Mitsudo, T.; Takegami, Y. The Reducive Amination of Phthalaldehyde by Tetracarbonylhydridoferrate: Synthesis of 2-Arylisoindoles. *Tetrahedron* **1979**, *35* (11), 1433–1436.

16. Suwa, T.; Sugiyama, E.; Shibata, I.; Baba, A. Chemoselective Reductive Amination of Aldehydes and Ketones by Dibutylchlorotin Hydride-HMPA Complex. *Synthesis* **2000**, *2000* (6), 789–800.

17. Katritzky, A. R.; Fan, W.; Fu, C. The Chemistry of Benzotriazole. A Novel Method for the Synthesis of Symmetrical Vicinal Tertiary and Secondary Diamines. *J. Org. Chem.* **1990**, *55* (10), 3209–3213.

18. Shi, Y.; J. Kamer, P. C.; J. Cole-Hamilton, D.; Harvie, M.; F. Baxter, E.; C. Lim, K. J.; Pogorzelec, P. A New Route to N-Aromatic Heterocycles from the Hydrogenation of Diesters in the Presence of Anilines. *Chemical Science* **2017**, *8* (10), 6911–6917.

19. Wei, D.; Netkaew, C.; Wu, J.; Darcel, C. Iron-Catalyzed Hydrosilylation of Diacids in the Presence of Amines: A New Route to Cyclic Amines. *ChemCatChem* **2020**, *12* (21), 5449–5455.

20. (a) Rout, L.; Jammi, S.; Punniyamurthy, T. Novel CuO Nanoparticle Catalyzed C−N Cross Coupling of Amines with Iodobenzene. *Org. Lett.* **2007**, *9* (17), 3397–3399. (b) Guo, D.; Huang, H.; Xu, J.; Jiang, H.; Liu, H. Efficient Iron-Catalyzed N-Arylation of Aryl Halides with Amines. *Org. Lett.* **2008**, *10* (20), 4513–4516. (c) Yong, F.-F.; Teo, Y.-C. Manganese-Catalyzed Cross-Coupling Reactions of Aliphatic Amines with Aryl Halides. *Tetrahedron Letters* **2010**, *51* (30), 3910–3912. (d)Ando, S.; Hirota, Y.; Matsunaga, H.; Ishizuka, T. Nickel-Catalyzed N-Arylation of Amines with Arylboronic Acids under Open Air. *Tetrahedron Letters* **2019**, *60* (18), 1277–1280.

21. Jin, R.-X.; Dai, J.-C.; Li, Y.; Wang, X.-S. Copper-Catalyzed Intramolecular Amination of C(Sp3)–H Bond of Secondary Amines to Access Azacycles. *Org. Lett.* **2021**, *23* (2), 421–426. (22) Hou, T.; Zhang, C.; Wang, Y.; Liu, Z.; Zhang, Z.; Wang, F. Metal-Free Protocol for the Synthesis of N-Arylpyrrolidines Catalyzed by Hydrogen Iodine. *Catalysis Communications* **2017**, *94*, 56–59.

23. Hu, S.; Huo, Y.; Wang, Z. Boron Trifluoride-Mediated Synthesis of N-Aryl-Substituted Pyrrolidines from Tetrahydrofuran and Amines. *Chem Heterocycl Comp* **2017**, *53* (12), 1365–1368.

24. L. Korbad, B.; Lee, S.-H. Synthesis of N -Aryl Substituted, Five- and Six-Membered Azacycles Using Aluminum-Amide Complexes. *Chemical Communications* **2014**, *50* (64), 8985–8988.

25. Olsen, C. J.; Furst, A., N-Phenylpyrrolidine. J. Am. Chem. Soc. 1953, 75 (12), 3026-3026.

26. Sun, Z.; Hu, S.; Huo, Y.; Wang, Z. Titanium Tetrachloride-Mediated Synthesis of N -Aryl-Substituted Azacycles from Cyclic Ethers. *RSC Advances* **2017**, *7* (8), 4363–4367.

27. Zhang, Z.; Miao, C.; Xia, C.; Sun, W. Synergistic Acid-Catalyzed Synthesis of N-Aryl-Substituted Azacycles from Anilines and Cyclic Ethers. *Org. Lett.* **2016**, *18* (7), 1522–1525.

28. Hargis, D. C.; Shubkin, R. L. Gem-Cyclodialkylation A Facile Synthetic Route to N-Substituted Heterocycles. *Tetrahedron Letters* **1990**, *31* (21), 2991–2994.

29. (a) Walkup, R. E.; Searles, S. Synthesis of Sterically Hindered 1-Arylpyrrolidines and 1-Arylpiperidines by Condensation of Primary Aromatic Amines with Cyclic Ethers or Diols. *Tetrahedron* **1985**, *41* (1), 101–106. (b) Amara, Z.; Streng, E. S.; Skilton, R. A.; Jin, J.; George, M. W.; Poliakoff, M. Automated Serendipity with Self-Optimizing Continuous-Flow Reactors. *European Journal of Organic Chemistry* **2015**, *2015* (28), 6141–6145.

30. (a) Kumari, S.; Carmona, A. V.; Tiwari, A. K.; Trippier, P. C. Amide Bond Bioisosteres: Strategies, Synthesis, and Successes. *J. Med. Chem.* **2020**, *63* (21), 12290–12358. (b) Owen, D. R.; Allerton, C. M. N.; Anderson, A. S.; Aschenbrenner, L.; Avery, M.; Berritt, S.; Boras, B.; Cardin, R. D.; Carlo, A.; Coffman, K. J.; Dantonio, A.; Di, L.; Eng, H.; Ferre, R.; Gajiwala, K. S.; Gibson, S. A.; Greasley, S. E.; Hurst, B. L.; Kadar, E. P.; Kalgutkar, A. S.; Lee, J. C.; Lee, J.; Liu, W.; Mason, S. W.; Noell, S.; Novak, J. J.; Obach, R. S.; Ogilvie, K.; Patel, N. C.; Pettersson, M.; Rai, D. K.; Reese, M. R.; Sammons, M. F.; Sathish, J. G.; Singh, R. S. P.; Steppan, C. M.; Stewart, A. E.; Tuttle, J.

B.; Updyke, L.; Verhoest, P. R.; Wei, L.; Yang, Q.; Zhu, Y. An Oral SARS-CoV-2 Mpro Inhibitor Clinical Candidate for the Treatment of COVID-19. *Science* **2021**, *374* (6575), 1586–1593.

31. Dunetz, J. R.; Magano, J.; Weisenburger, G. A. Large-Scale Applications of Amide Coupling Reagents for the Synthesis of Pharmaceuticals. *Org. Process Res. Dev.* **2016**, *20* (2), 140–177.
32. Basha, A.; Lipton, M.; Weinreb, S. M. A Mild, General Method for Conversion of Esters to Amides. *Tetrahedron Letters* **1977**, *18* (48), 4171–4172.
33. M. Muñoz, J. de; Alcázar, J.; Hoz, A. de la; Díaz-Ortiz, Á.; Diego, S.-A. A. de. Preparation of Amides Mediated by Isopropylmagnesium Chloride under Continuous Flow Conditions. *Green Chemistry* **2012**, *14* (5), 1335–1341.
34. Wang, W. B.; Roskamp, E. J. Tin(II) Amides: New Reagents for the Conversion of Esters to Amides. *J. Org. Chem.* **1992**, *57* (23), 6101–6103.
35. (a) Allen, C. L.; Williams, J. M. J. Metal-Catalysed Approaches to Amide Bond Formation. *Chem. Soc. Rev.* **2011**, *40* (7), 3405–3415. (b) de Figueiredo, R. M.; Suppo, J.-S.; Campagne, J.-M. Nonclassical Routes for Amide Bond Formation. *Chem. Rev.* **2016**, *116* (19), 12029–12122. (c) Tsuji, H.; Yamamoto, H. Hydroxy-Directed Amidation of Carboxylic Acid Esters Using a Tantalum Alkoxide Catalyst. *J. Am. Chem. Soc.* **2016**, *138* (43), 14218–14221. (d) Morimoto, H.; Fujiwara, R.; Shimizu, Y.; Morisaki, K.; Ohshima, T. Lanthanum (III) Triflate Catalyzed Direct Amidation of Esters. *Org. Lett.* **2014**, *16* (7), 2018–2021. (e) Movassaghi, M.; Schmidt, M. A. N-Heterocyclic Carbene-Catalyzed Amidation of Unactivated Esters with Amino Alcohols. *Org. Lett.* **2005**, *7* (12), 2453–2456. (f) Kumar, A.; Espinosa-Jalapa, N. A.; Leitus, G.; Diskin-Posner, Y.;

Avram, L.; Milstein, D. Direct Synthesis of Amides by Dehydrogenative Coupling of Amines with Either Alcohols or Esters: Manganese Pincer Complex as Catalyst. *Angewandte Chemie* **2017**, *129* (47), 15188–15192. (g) Kim, B. R.; Lee, H.-G.; Kang, S.-B.; Sung, G. H.; Kim, J.-J.; Park, J. K.; Lee, S.-G.; Yoon, Y.-J. Tert-Butoxide-Assisted Amidation of Esters under Green Conditions. *Synthesis* **2012**, *44* (01), 42–50. (h) Sabot, C.; Kumar, K. A.; Meunier, S.; Mioskowski, C. A Convenient Aminolysis of Esters Catalyzed by 1,5,7-Triazabicyclo[4.4.0]Dec-5-Ene (TBD) under Solvent-Free Conditions. *Tetrahedron Letters* **2007**, *48* (22), 3863–3866. (i) Gnanaprakasam, B.; Milstein, D. Synthesis of Amides from Esters and Amines with Liberation of H2 under Neutral Conditions. *J. Am. Chem. Soc.* **2011**, *133* (6), 1682–1685. (j) Han, C.; Lee, J. P.; Lobkovsky, E.; Porco, J. A. Catalytic Ester−Amide Exchange Using Group (IV) Metal Alkoxide−Activator Complexes. *J. Am. Chem. Soc.* **2005**, *127* (28), 10039–10044. (k) Lenstra, D. C.; Nguyen, D. T.; Mecinović, J. Zirconium-Catalyzed Direct Amide Bond Formation between Carboxylic Esters and Amines. *Tetrahedron* **2015**, *71* (34), 5547–5553. (l)Sultan, S.; Kumar, M.; Devari, S.; Mukherjee, D.; Ali Shah, B. Copper–Manganese Spinel Oxide Catalyzed Synthesis of Amides and Azobenzenes via Aminyl Radical Cations. *ChemCatChem* **2016**, *8* (4), 703–707. (m) Caldwell, N.; Jamieson, C.; Simpson, I.; Tuttle, T. Organobase-Catalyzed Amidation of Esters with Amino Alcohols. *Org. Lett.* **2013**, *15* (10), 2506–2509.

36. Ranu, B. C.; Dutta, P. A Simple and Convenient Procedure for the Conversion of Esters to Secondary Amides. *Synthetic Communications* **2003**, *33* (2), 297–301.

37. Weiberth, F. J.; Yu, Y.; Subotkowski, W.; Pemberton, C. Demonstration on Pilot-Plant Scale of the Utility of 1,5,7-Triazabicyclo[4.4.0]Dec-5-Ene (TBD) as a Catalyst in the

Efficient Amidation of an Unactivated Methyl Ester. *Org. Process Res. Dev.* **2012**, *16* (12), 1967–1969.

38. Ali, Md. A.; Siddiki, S. M. A. H.; Kon, K.; Shimizu, K. A Heterogeneous Niobium(V) Oxide Catalyst for the Direct Amidation of Esters. *ChemCatChem* **2015**, *7* (17), 2705–2710.
39. Rashed, Md. N.; Masuda, K.; Ichitsuka, T.; Koumura, N.; Sato, K.; Kobayashi, S. Zirconium Oxide-Catalyzed Direct Amidation of Unactivated Esters under Continuous-Flow Conditions. *Advanced Synthesis & Catalysis* **2021**, *363* (10), 2529–2535.

Appendix 1

Flow Reactor Operating Procedure

The flow reactor shown in Figure A1.1 was constructed using seamless Swagelok 316/316L stainless steel tubing (1/4″ o.d., 0.18″ i.d., 0.035″ wall thickness, 26 cm length) and standard valves, a back-pressure regulator (Warr, Inc.) and a piston pump (MXT class, Chrom Tech). The reactor was heated to the desired temperature with the help of heat tape while flowing solvent before introducing the reactant solution. The solid catalyst (~0.5 g) was packed into the reactor. The catalyst bed was supported at each end by fused granular quartz (4– 20 mesh, Sigma) and glass wool.

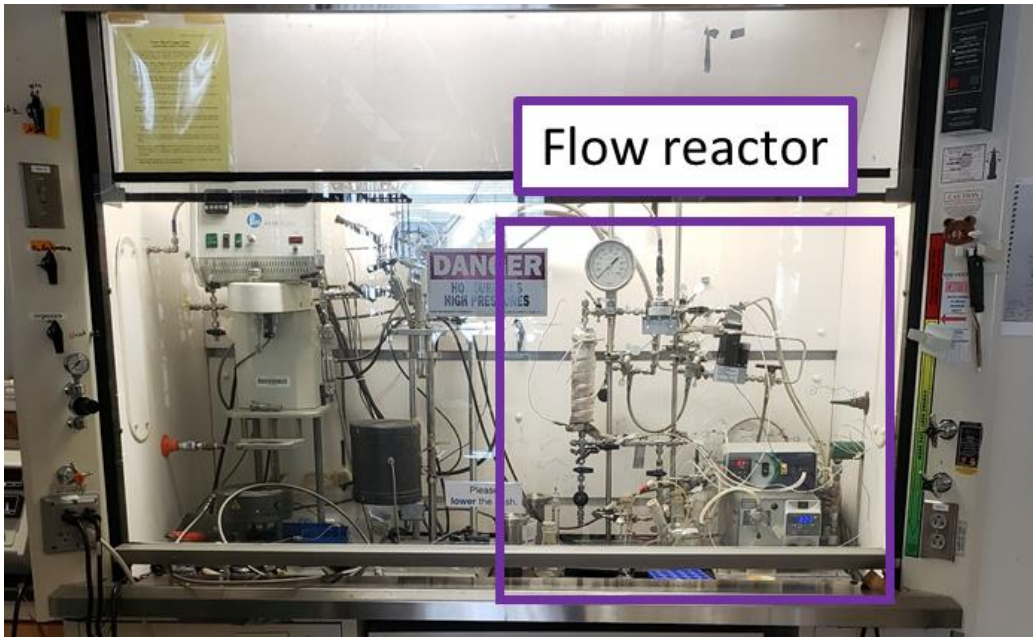

Figure A1.1 Flow reactor in the fume hood

The protocol for operating the flow reactor is given below.

1. Prepare solvent
    a. Fill the flask or cylinder with the solvent of choice (ex. toluene, THF).

b. Add a stopper with a small syringe needle to allow the gas to escape.
c. In a fume hood, connect a long syringe needle to the N_2 line and lace it through a stopper so the line ends towards the bottom of the flask.
d. Purge the flask with N_2 gas for ~15 min.
e. Remove the N_2 line after purging is complete.
f. Sonicate the solution for ~15 min.

2. Check isopropyl alcohol (IPA) to pump
    a. Isopropyl alcohol (IPA) is located in a small flask at the back of the fume hood.
    b. Fill the IPA if the level is low.
    c. To keep the pump head clean, replace the IPA 1 to 2 times per week.
3. Pack the reactor with catalyst, silica, and glass wool according to the schematic below (Figure A1.2).
    a. Add a small amount of glass wool into the reactor.
    b. Use the flat end of the C or D (Figure A1.2) tool to press the wool in place.
    c. Repeat for the other six layers of the reactor bed.
        i. When adding the granular quartz and catalyst into the reactor, drop in small amounts and tap the reactor to ensure good packing. Repeat until all material is added.
        ii. The catalyst bed should be in the middle of the reactor.

iii. To do this, for 0.5 g of amorphous silica-alumina, use 0.7 mg of granular quartz.

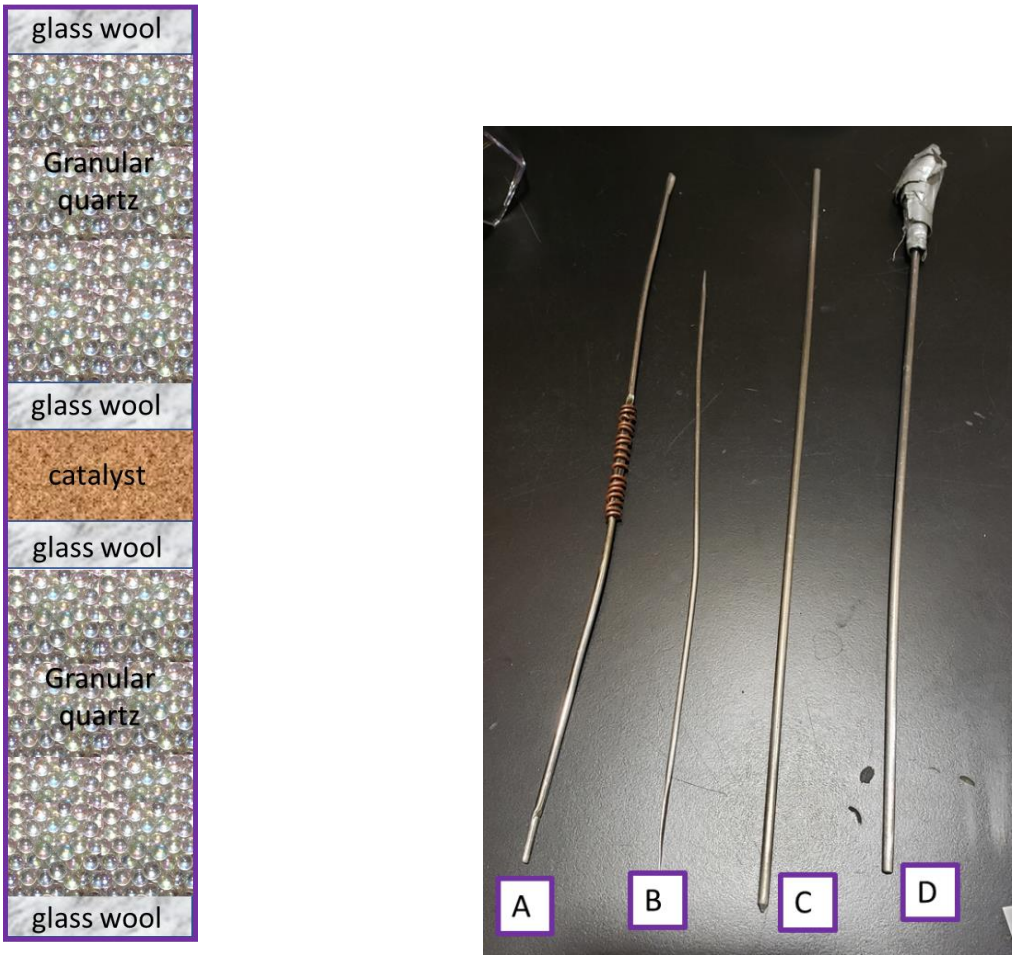

Figure A1.2 Reactor packing schematic and reactor packing as well as cleaning tools

4. Load the reactor into the setup and tighten connections with a wrench.
5. Add clamp to the bottom of the reactor to hold up heat block and tighten block with Allen wrench.
6. Wrap heating tape around the block and secure it with a clamp. (see Figure A1.3)

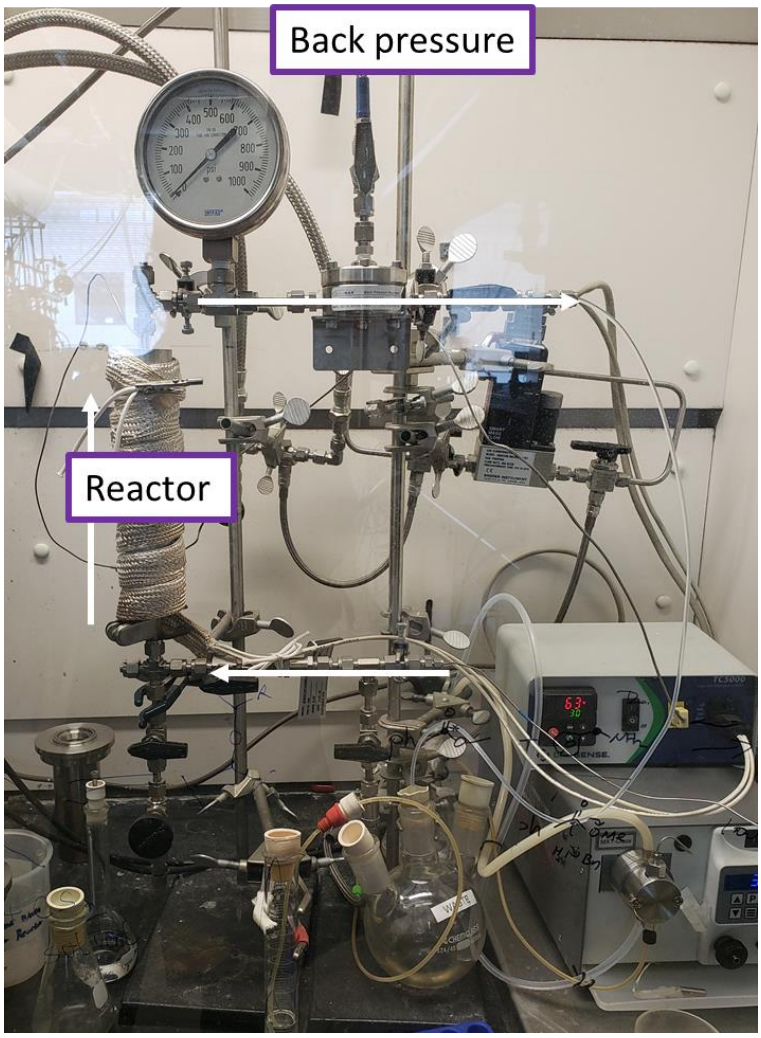

Figure A1.3 Reactor flow and back pressure gauge

7. Prepare substrate solution
    a. Measure the liquid substrate into a volumetric flask using a pipette.
    b. Add the solvent to a specific volume to make the reactant mixture.
    c. Degas the mixture by bubbling it with N_2 for 20 min as described above.
    d. Sonicate for 30 min before introducing it into the flow reactor pump.
    e. If too much gas is present in the solvent, it will accumulate in the pump head and stop pumping.

f. Make sure there is no solid particle in the mixture or solvent before you use it, or it will damage the flow reactor pump. Sonication should help, but filter the mixture if solid particles are still observed.

8. Start solvent flow
    a. Turn on the pump. (Figure A1.4)
    b. Set flow rate using up and down arrows.
    c. Press the start button. (>‖)
    d. Run at 2 mL/min while pressurizing.

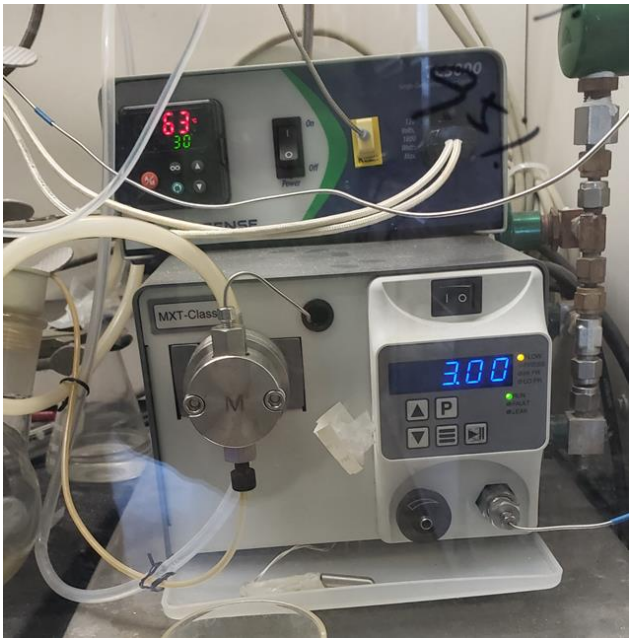

Figure A1.4 Pump and temperature controller

9. Once the solvent has made its way throughout the setup (by seeing solvent flow into the waste container), close the exit valve (valve D) to build pressure. (Figure A1.5)
    a. CAUTION: Keep watch as pressure builds. *Be careful not to let the pressure be above 1000 psi, or the gauge may break.*
    b. Slowly builds pressure until ~200 psi and then ramps quickly.

c. Pause flow at desired set point.

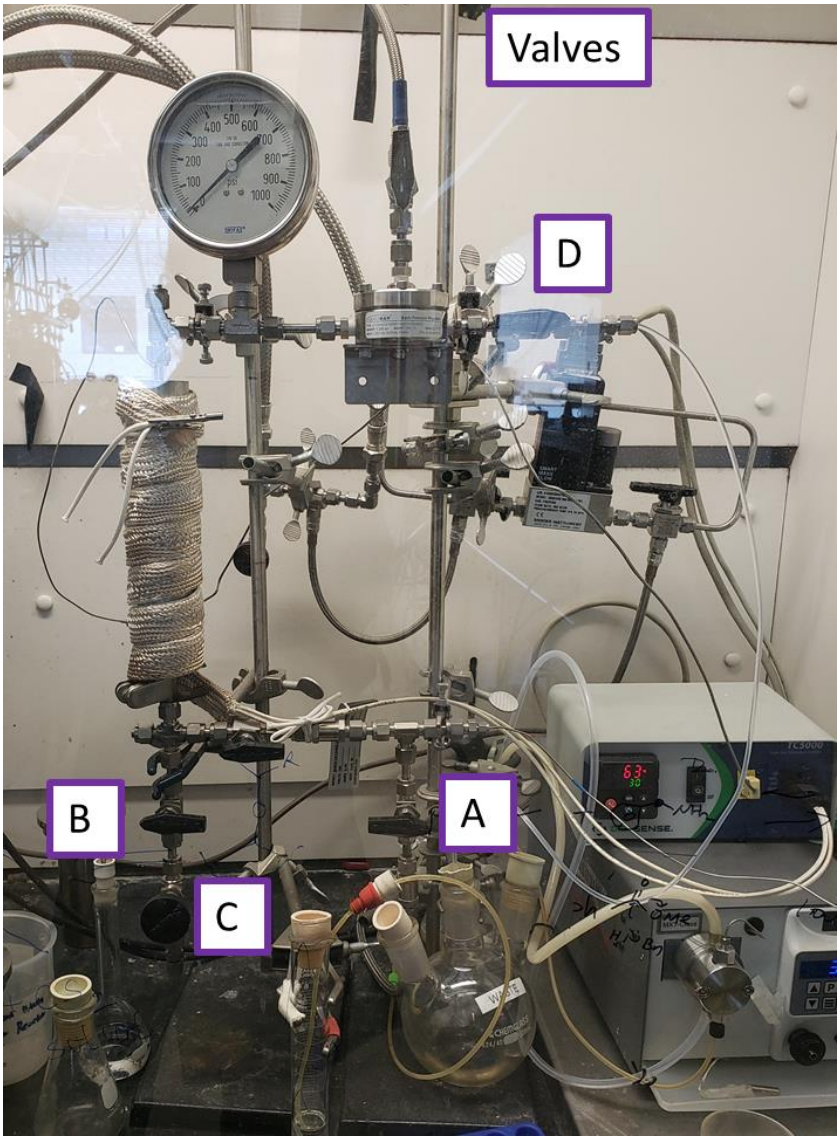

Figure A1.5 Reactor valves

10. Crack open the N_2 cylinder for pressure. (Figure A1.7)

    a. Set the pressure in the tank so that the pressure at the back pressure gauge is correct.

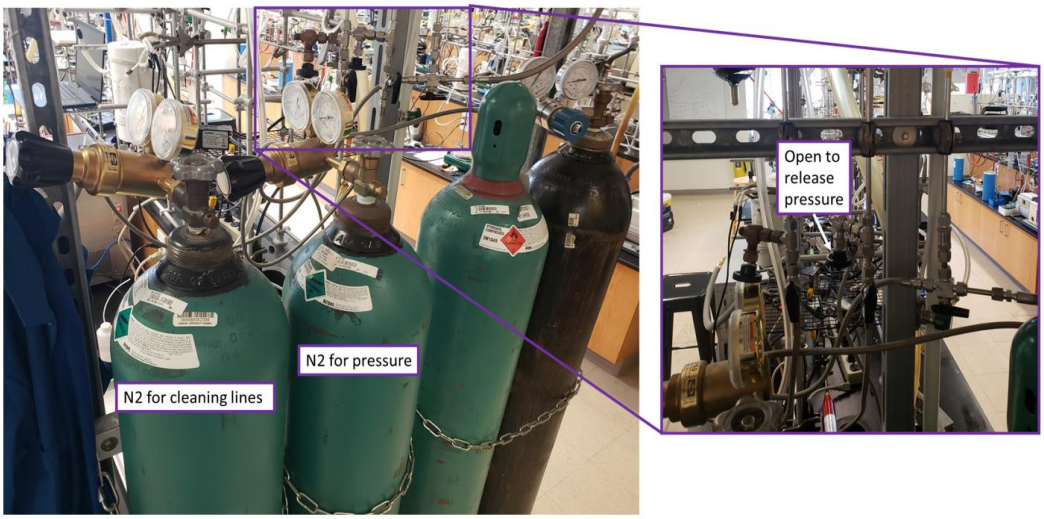

FIGURE A1.7 N_2 cylinder

11. Check for leaks while pressurized.
    a. Should hold pressure if the cylinder is closed.
    b. If pressure drops, first check reactor connections.
    c. Still leave the cylinder cracked throughout the reaction for any slow leak.
12. Lower the flow rate on the pump to 1 mL/min.
    a. Open flow outlet valve. (valve D)
    b. Start the flow.
13. Set temperature
    a. Turn on the unit. (see switch controller in Figure A1.4)
    b. Use up and down arrows to set the reaction temperature.
14. When ready to start the reaction, switch the solvent flask for substrate solution.
15. Start pump flow.
    a. Set the flow rate at 1 mL/min for ~7 mins for the solution to reach the reactor bed.

b. Then change to the desired flow.

c. Depending on the flow, it may take several hours before the products reach the outlet.

d. For example, at 0.04 mL/min, it will take 4.2 hours to reach the outlet. Also, the first ~10 mL will be during the transient start-up phase. Therefore, the first sample collection can begin 8.3 hours after the substrate has reached the reactor bed.

16. Collect samples for analysis

a. After the start-up period, use 15 mL sample vials to collect ~10 mL of solution at the system outlet.

b. One sample at 0.4 mL/min will take ~ 4 hours to collect.

c. The reaction may be stopped if the first two samples show similar yields.

17. To stop the reaction, turn off the temperature controller.

a. Pause substrate flow.

18. When the reaction is complete, collect the remaining reactants and products still in line.

a. Switch substrate solution with the solvent.

b. Set and start flow at 1 mL/min for several minutes. (~4 mins)

c. Stop the flow of the solvent.

19. Depressurize reactor

a. Close N_2 cylinder.

b. Slowly open valve above cylinder to vent. (labeled in Figure A1.7)

20. Dry reactor set up.

a. Open N_2 cylinder. (far left in Figure A1.7)
b. Hold on to the outlet line into the waste container and slowly crack open valve A in Figure A1.5 to remove the remaining solvent in the lines
c. Close the valve.

21. Wash reactor set up by flowing solvent through the bottom line first
    a. Set flow at 3 mL/min and start the flow.
    b. Open valves B and C and run for ~2 mins.
    c. Pause the flow.
    d. Crack open the N_2 line. (valve A in Figure A1.5)
    e. Repeat steps a. through e. 3-5 times.
22. Then flow through the reactor for ~100 mL. (more if changing solvent for next run)
    a. Repeat the same steps to wash and dry as described above.
    b. Now may be a good time to check the flow rate to ensure it is calibrated correctly.
    c. Set flow, and using a cylinder, record the time it takes to fill a certain amount of mL.
    d. Stop flow.
23. Dry the whole system with N_2 flow for several minutes.
24. Remove the reactor.
    a. Remove heating tape and block.
    b. Loosen fittings.
    c. A gentle tap on the reactor to release and remove from the line.

d. Wipe inlet and outlet with Kimwipe.

25. Now system is ready for the next reaction.

2. Azacycles synthesis in flow

2.1 Introduction

In the past decade, investigations of heterogeneous catalysts in organic synthesis have significantly expanded the chemical design space.[1-4] Solid heterogeneous catalysts can facilitate and improve chemical process design by virtue of their inherent adaptability to continuous flow synthesis, with broad applicability in the field of pharmaceutical manufacturing.[5-15] The benefits offered by flow chemistry compared to batch techniques include higher process efficiency and improved catalyst handling, with the advantage of the simple separation of the product from the catalyst.[16] In addition, flow chemistry offers the advantages of easy scale-up and superior environmental compatibility.

N-substituted azacycles such as piperidines, pyrrolidines, and pyrroles are key building blocks for pharmaceuticals and agrochemicals, as well as pyrrole-based functional materials.[22-27] Notably, the *N*-substituted azacycle motif is present in a wide array of pharmacologically active molecules.[28-33] For example, *N*-alkyl-substituted pyrrolidines and piperidines play a vital role in pharmaceutical agents such as procyclidine, an anticholinergic drug, and haloperidol, an antipsychotic medication. Despite the ubiquity of N-substituted azacycle structure, classical synthetic approaches suffer from step- and atom-economy limitations. For example, synthetic methods include reduction of tertiary lactams or azacyclodienes formed by condensation of amine with dicarbonyl compounds;[34-37] *N*,*N*-dialkylation of arylamines with dihalides or diols;[38-40] and cross-coupling of alkyl or aryl halides with *N*-unsubstituted azacycles.[41-42] Each method involves activated starting materials that require extra purification steps and generate waste. In this context, there is a strong interest in developing catalytic methods to synthesize N-substituted azacycles more efficiently.

The direct reaction of cyclic ethers with primary amines is a straightforward and appealing alternative to accessing N-substituted azacycles. This strategy involves widely available and inexpensive starting materials, with water as the only by-product. This transformation has been reported in the literature with both homogeneous (soluble) and heterogeneous (insoluble) promoters. Specifically, the process in homogeneous conditions has been demonstrated with either stoichiometric or excess amounts of Brønsted acids such as HI,[43-44] or Lewis acids such as $BF_3.Et_2O$,[45] $AlCl_3$,[46] $TiCl_4$,[47-48] and $AlMe_3$,[49] as well as $POCl_3$ in combination with DBU.[50-51] In a synergistic approach, Brønsted and Lewis acidity (*p*-TSA.H_2O and $B(C_6F_5)_3$) were combined via a reaction mechanism involving a frustrated Lewis pair formed by the interaction between $B(C_6F_5)_3$ and the amine.[52-53]

Heterogeneous metal oxides can display both Lewis and Brønsted acid and base sites on their surfaces. These materials are used extensively as catalysts in commodity chemical production,[17-18] and have also been used successfully in synthesizing fine chemicals, including pharmaceuticals and agrochemicals.[19-20] Their activity is a function of their physiochemical properties: namely, acid and base site strength, surface density, pore size, and size distribution. The possibility of tuning the acidity of a solid catalyst is particularly appealing in acid-catalyzed processes involving amines as starting materials and/or products. The active sites must have sufficient acid density and strength to promote the reaction without being deactivated by strong amine adsorption.[21] The Lewis acid sites can be further tuned to bind and activate hard or soft donors, even discriminating between light donor atoms such as O and N.

TiO_2[54] and g-Al_2O_3[55-56] have been evaluated for oxidative C-N coupling, but their use in packed-bed reactors with vapor-phase reactants resulted in a limited scope, high required

temperatures (up to 400 °C), and low product yields. During our recent investigation of the flow deprotection of *N*-Boc-aniline catalyzed by solid acids,[61] we discovered that when using THF as the solvent, aniline reacts readily to give *N*-phenylpyrrolidine at moderately elevated temperatures. Upon further investigation, the reaction was found to be both general and quantitative. Here we describe the synthesis of *N*-substituted pyrrolidines, piperidines, and pyrroles from the corresponding primary amines (both *N*-aryl and *N*-alkyl) by flowing the amine through a catalyst bed of amorphous silica-alumina (ASA) with either a cyclic ether or furan, **Scheme 2.1**. Notably, this strategy enables access to *N*-alkyl-substituted azacycles which are challenging to obtain due to the low intrinsic reactivity of alkylamines. Moreover, the C-O bonds of the oxacycles are directly activated by the heterogeneous catalyst without derivatization (as would be required for alcohol displacement, e.g., by mesylation)[62] or a redox reaction (as in the so-called H-borrowing strategy).[63-64]

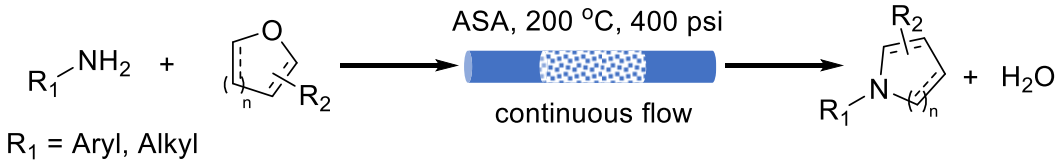

Scheme 2.1 Atom-efficient continuous flow synthesis of *N*-substituted azacycles, catalyzed by amorphous silica-alumina (ASA), as described in this work.

The double alkylation of primary aliphatic and aromatic amines by cyclic ethers or furans was performed under continuous-flow conditions. The ASA catalyst is active at lower temperatures (ca. 200 °C) than previously reported solid acid catalysts, including g-Al_2O_3 (275-340 °C) and TiO_2 (250-300 °C).[58-60] A mechanism involving simultaneous activation of both reactive partners by Brønsted acidic and basic sites on the catalyst surface is supported

by DFT calculations.

2.2 Experimental methods

General. Commercially available compounds and solvents were purchased from Sigma-Aldrich, Fisher, or Alfa Aesar and were used without further purification. Amorphous silica-alumina (ASA, Davicat SIAL 3113, 7.6 wt % Al on a dry basis, B.E.T. surface area 573 m^2/g, pore volume 0.76 cm^3/g) was provided by Grace-Davison (Columbia, MD). HY zeolite (Si/Al = 10, 730 m^2/g) was obtained from Alfa Aesar, while γ-Al_2O_3 (186 $m^2\ g^{-1}$, pore volume 0.50 $cm^3\ g^{-1}$) was purchased from Strem. Except where noted, all supports were calcined in flowing air at 500 °C for three hours before use to remove surface carbonates. Moreover, the calcined catalysts are air-stable and can be handled without special precautions. To prepare trimethylsilyl-capped ASA, hexamethyldisilazane (HMDS, Aldrich, >99.5%) was transferred under reduced pressure via the vapor phase onto the dehydrated support at room temperature for one hour. The reactor was then evacuated at 350 °C for 4 hours to remove unreacted HMDS and ammonia.

Unless stated otherwise, all product analyses were performed in open-air conditions. Solution-state NMR experiments were performed on a 600 MHz SB Varian VNMRS spectrometer. GC-MS analyses were performed on a Shimadzu GC-2010 Gas Chromatograph coupled to a QP2010 Mass Spectrometer. The GC is equipped with a 30 m × 0.25 mm Agilent DB-1 capillary column containing a dimethylpolysiloxane stationary phase (0.25 μm). Helium was used as the carrier gas. The temperature was held at 60 °C for 2 min, then ramped from 60 to 200 °C at 15 °C/min and held at 200 °C for 10 min, then ramped from 200 to 270 °C at 15 °C/min and held for 10 min. Chiral HPLC was performed on Shimadzu LC20 equipped with a Chiralcel OJ-H column and UV detection at 225 nm. The eluting solvent was *n*-

hexane/*i*PrOH/diethylamine = 100/1/0.1, flowing at 1.0 mL/min.

Batch reaction test. Aniline (1.00 mM in 15 mL THF) was combined with the desired solid catalyst (50 mg) in a stirred Parr reactor (model 4590, volume 25 mL) equipped with a sampling port and a Parr 4843 controller. The reactor was stirred at 300 rpm during and after heating to 180 °C for 2 hours. The reaction progress was monitored by GC-MS. After cooling to room temperature, the catalyst was separated by centrifugation. The final conversion and product yield were determined by ^{1}H NMR, using 1,3,5-trimethoxybenzene (added after the reaction) as an internal standard.

Flow reactions. The solid catalyst (500 mg, > 100 mesh) was packed tightly into the continuous flow reactor to give a bed 2-3 cm in length. The catalyst bed was supported on each end by fused granular quartz (4-20 mesh, Sigma) and glass wool. A back pressure of at least 300 psi was applied to ensure that at least some of the solvent (e.g., THF, vapor pressure 300 psi at 200 °C) remained liquid in the packed bed reactor. The reactor was wrapped with heat tape to achieve the desired reaction temperature.

During a typical flow reactor test, the catalyst bed was operated under an inert atmosphere to prevent amine oxidation. Neat solvent and reactant solutions were deoxygenated by bubbling with N_2 in a 100 mL Schlenk tube for 15 min, then degassed using ultrasound (Branson 3510, 40 Hz) for 20 min before use. The solvent was pumped at 2.0 mL/min through the catalyst bed at room temperature to equilibrate the pressure of the flow reactor. The back pressure was adjusted to 400 psi, and the reactor temperature was then raised to 180 °C. After the temperature and pressure stabilized (about 5 min), the amine solution was introduced via the pump inlet. A volume of solution equal to twice the total reactor volume was passed through the system prior to beginning sample collection. Aliquots were collected in vials at

the flow reactor outlet. The product yield was determined by ^{1}H NMR using 1,3,5-trimethoxybenzene (added after the reaction) as an internal standard. Isolated yields were measured by withdrawing 5 mL (measured precisely using a volumetric pipette) at room temperature, removing the solvent by rotary evaporation, and purifying the product by column chromatography.

2.3 Computational methods

Active site model. ASA, with a low Al content, is an amorphous mixed oxide whose surface heterogeneity has been the cause of considerable speculation concerning the nature of the Lewis and Brønsted acid sites.[65-66] Spectroscopic investigations have shown that Al substitutes isomorphously for Si in the oxide lattice, in which the Al can be 4-, 5-, or 6-coordinate. ASA has higher Brønsted acidity than SiO2 and Al2O3 due to terminal silanols whose deprotonation is stabilized by coordination with neighboring Al(III) sites. Nevertheless, these silanols are less acidic than the bridging hydroxyl groups (Al-OH-Si) in zeolites.[67-68] In this work, the ASA active site was represented by a cluster model containing a tetrahedrally-coordinated Al site and two neighboring silanol groups, Figure 1. Dangling bonds at Si at the cluster boundary are capped with H atoms. A methylammonium ion is included to maintain overall charge neutrality due to the negative charge on the cluster caused by the introduction of Al(III).

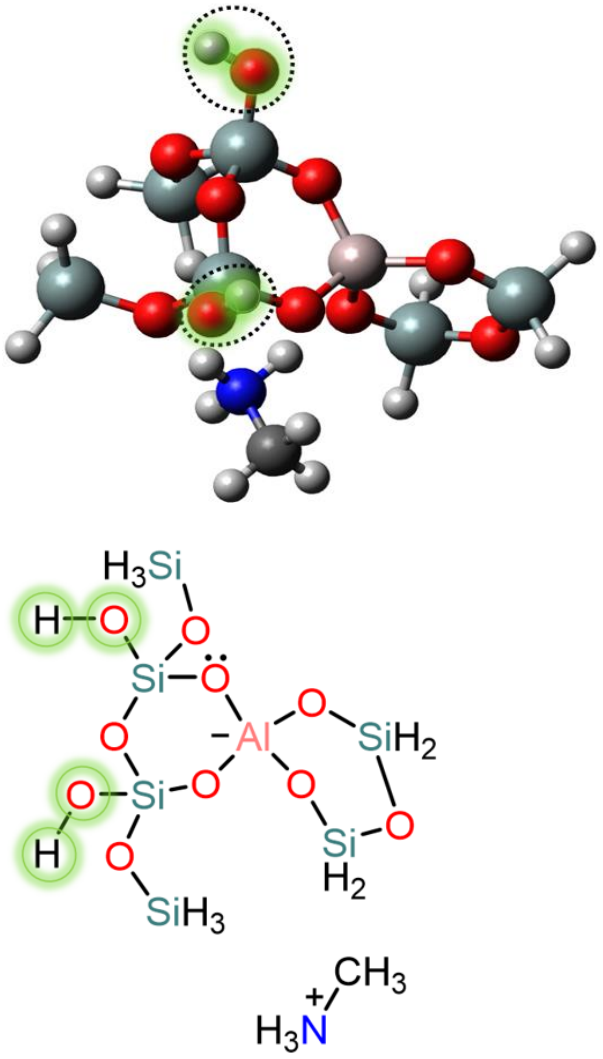

Figure 2.1 Cluster model representing an ASA active site, with one 4-coordinate Al (pink) and two neighboring SiOH groups (black dotted circles). A charge-neutralizing methylammonium cation is shown on the left-hand side of both the line drawing and the ball-and-stick model. Color scheme: H, white; O, red; Si, green; N, blue; C, grey; Al, pink.

Electronic structure calculations. Electronic structure calculations were performed using Gaussian 09, version d01. All atoms (Si, O, H, N, Al, and C) were modeled at the M062x/ 6-31g(d,p) theory level. Vibrational frequency analysis confirmed ground and intermediate

states by the absence of imaginary frequencies and transition states by the presence of a single imaginary frequency.

2.4 Results and discussion

Initial screening of solid acid catalysts: Azacycle formation was initially explored in the reaction between THF and benzylamine in flow conditions at 180 °C and 500 psi. Three readily available solid acids were selected for testing: γ-Al_2O_3, HY zeolite, and amorphous silica-alumina (ASA). γ-Al_2O_3 is Lewis acidic, while HY zeolite is a strong Brønsted acid. ASA has both Lewis and Brønsted acidity, although it is a weaker Brønsted acid than zeolite. The results are summarized in **Table 2.1**.

HY is considerably more active and selective compared to γ-Al_2O_3 on a mass basis, generating a 25% yield of *1*-benzylpyrrolidine at a flow rate of 0.04 mL/min, corresponding to a residence time of just 15 min (Table 1, entry 2). This result suggests the predominant importance of Brønsted acidity over Lewis acidity in the active sites. ASA gave a 70% yield of the pyrrolidone under the same conditions (Table 1, entry 3). For comparison, when the reaction was conducted in batch with ASA at the same temperature, a reaction time of 2 hours was required to obtain the product in 94 % yield.

Table 2.1 Optimization of reaction conditions for pyrrolidone formation [a]

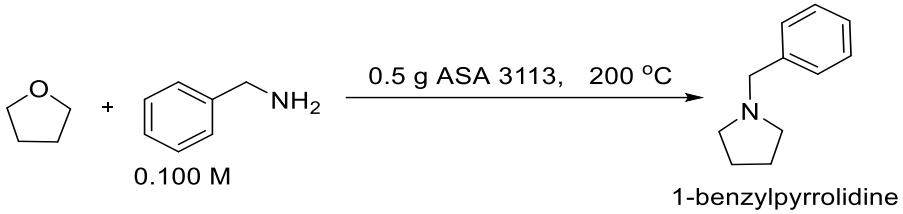

No.	Catalyst (g)	Pressure (psi)	Temp. (°C)	Flow rate (mL/min)	Residence Time (min)	Conv.(%) [b]	Yield (%) [b]
1	g-Al_2O_3	500	180	0.04	15	32	<5
2	HY zeolite	500	180	0.04	15	61	25
3	ASA	500	180	0.04	15	80	70
4	ASA	500	190	0.04	15	95	88
5	ASA	500	200	0.04	15	100	100
6	ASA	500	200	0.10	6	92	88
7	ASA	500	200	0.08	7.5	100	100
8	ASA	400	200	0.08	7.5	100	100
9	ASA	300	200	0.08	7.5	100	100
10	none	400	200	0.08	9.8	0	0

[a] Unless otherwise noted, continuous flow reactions were conducted using 0.100 M amine in THF, flowing through a packed catalyst bed (500 mg). [b] Determined by ^{1}H NMR.

When the reaction was conducted using ASA at a higher temperature (200 °C), the pyrrolidine was obtained in quantitative yield (Table 1, entry 5). At this temperature, higher flow rates (0.08 – 0.10 mL/min) and lower pressures (300 – 400 psi) had little effect on the reaction outcome (Table 1, entries 6-9). A control reaction conducted at 200 °C without

catalyst showed no product formation (Table 1, entry 10).

Temperature dependence. The activation energy for *N*-benzylpyrrolidone formation catalyzed by ASA was determined by varying the temperature from 180 to 210 °C while keeping the conversion low to ensure kinetic control without mass transport or equilibrium limitations. The Arrhenius plot in **Figure 2.2** shows the activation energy to be 62 kJ/mol. Given its modest barrier, the relatively high-temperature requirement for the reaction is likely a consequence of a small Arrhenius prefactor. This may reflect the consideration organization required in the transition state (see below).

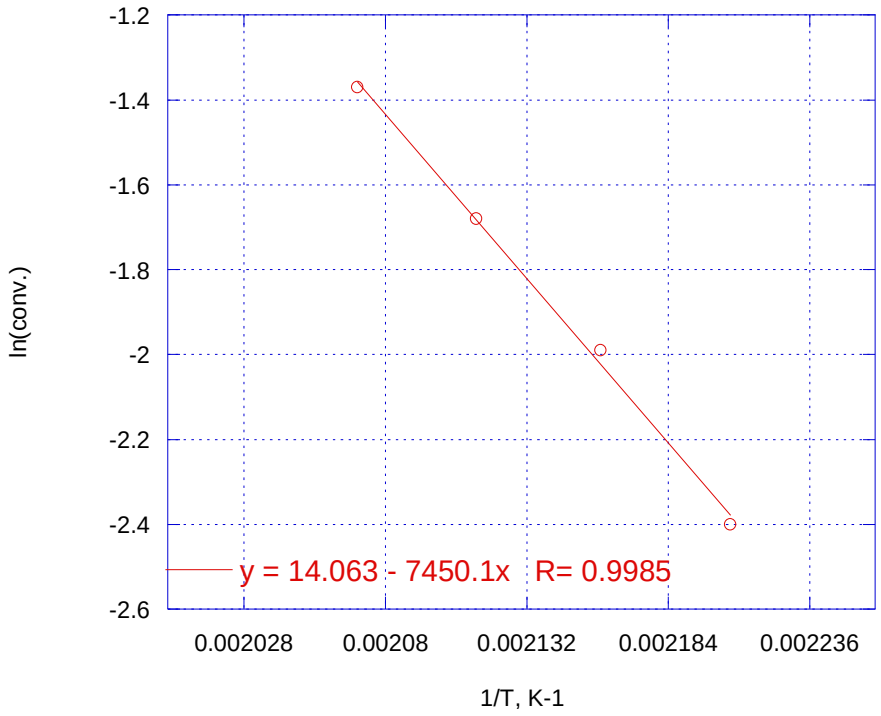

Figure 2.2 Arrhenius plot for *N*-benzylpyrrolidone formation from the reaction of benzylamine (0.100 M) with THF (also the solvent) in a packed-bed reactor containing ASA (0.250 g). Reaction conditions: flow rate 0.5 mL/min, 500 psi, 180-210 °C. The conversion of

benzylamine, measured by GC-MS using *n*-dodecane as the internal standard, was maintained at < X% to ensure kinetic control.

Substrate scope. The scope of direct azacycle formation from cyclic ethers was investigated using various amines and cyclic ethers in continuous flow conditions (**Scheme 2.2**). For the reaction of aniline with THF, *N*-phenylpyrrolidine (**1a**) was obtained in quantitative yield with a residence time of 15 min at 180 °C. (For comparison, conducting the reaction in batch at 180 °C gave the product in 94 % yield only after 2 hours.) A high yield (90 %) was also obtained using the same flow rate (0.04 mL/min) but at a lower temperature, 160 °C. Near-quantitative yields of *N*-aryl-substituted pyrrolidines were obtained using substituted arylamines bearing both electron-donating groups (Scheme 2, **1b**) and electron-withdrawing groups (Scheme 2.2, **1c**-**d**). The method is also compatible with less reactive aliphatic amines, although slightly higher temperatures are needed to achieve near-quantitative yields in short residence times (Scheme 2.2, **1e**-**j**). Notably, most previously reported methods are not effective with less reactive aliphatic amines at temperatures typically accessible in batch reactions which are limited by the normal boiling point of the solvent.

Scheme 2.2 Substrate Scope for Direct Synthesis of *N*-substituted Pyrrolidines and Piperidines Catalyzed by ASA in Continuous-Flow Conditions.[a]

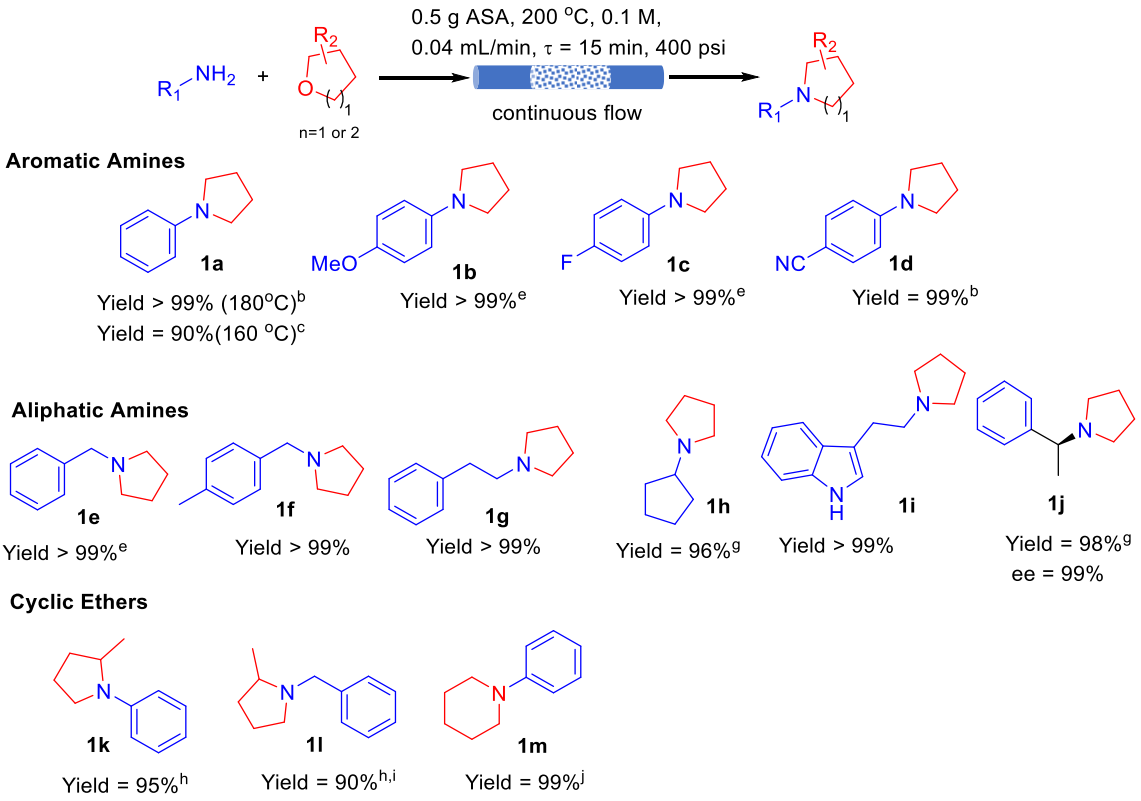

[a] Unless otherwise noted, reactions were conducted using 0.100 M amine in THF flowing at 0.04 mL/min at 200 °C with 500 mg catalyst in a packed-bed column at 400 psi. Yields were determined by ^{1}H NMR. [b] Flow rate 0.06 mL/min. [c] Flow rate 0.04 mL/min. [e] Flow rate 0.08 mL/min. [g] T = 220 °C. [h] The solvent was 2-MeTHF. [i] T = 230 °C. [j] The reaction was conducted using 0.100 M aniline, 2M pyran in toluene at 250 °C, and 600 psi with 1.00 g catalyst.

The method is also compatible with heteroaromatic indoles (products such as **1i**). Furthermore, the stereochemical integrity of the chiral substrate was maintained in product **1j**. Other cyclic ethers, including 2-MeTHF (**1k-l**) and tetrahydropyran (**1m**), also gave the corresponding azacycles in good yields (80 – 90 %), although higher temperatures and longer

residence times were needed.

Direct azacycle formation was also tested in synthesizing 1-(4-bromo-2-fluorobenzyl)pyrrolidine, an intermediate for the preparation of fluorocyclobutane-containing H3 antagonist [33] The reaction of 4-bromo-2-fluorobenzylamine in THF under the flow conditions optimized for the preparation of *N*-substituted piperidines afforded **1o** in 96% yield, **Scheme 2.3**. Thus, the method is clearly compatible with halide substituents.

Scheme 2.3 Continuous flow synthesis of key intermediate **1o** for H3 Antagonist

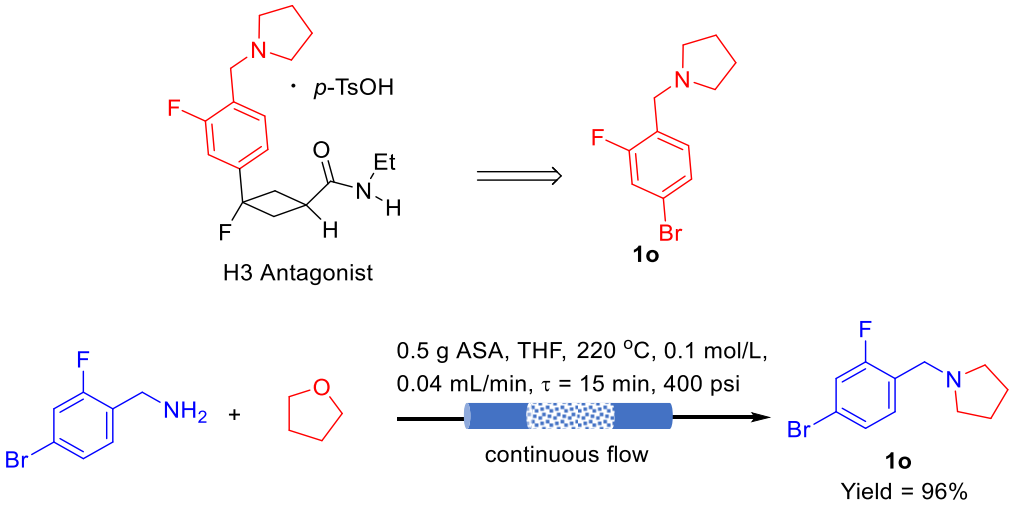

Gram-scale experiment. To demonstrate the application of the method to gram-scale synthesis, the reaction of aniline (0.300 M) in THF was conducted in the continuous flow reactor with 1.500 g ASA as the catalyst for a total duration of 68 h. After simple evaporation of the unreacted THF solvent, over 14 g *N*-phenylpyrrolidine was obtained, corresponding to a 99.5% isolated yield (**Scheme 2.4**). This amount represents a throughput of 1.0 mmol h^{-1} g_{cat}^{-1}, sustained over nearly 3 d. Considering the small scale of the packed bed reactor and the ready availability of ASA, the flow process has the potential to be highly productive and economical.

Scheme 2.4 Gram-scale synthesis of *N*-phenylpyrrolidine, catalyzed by ASA

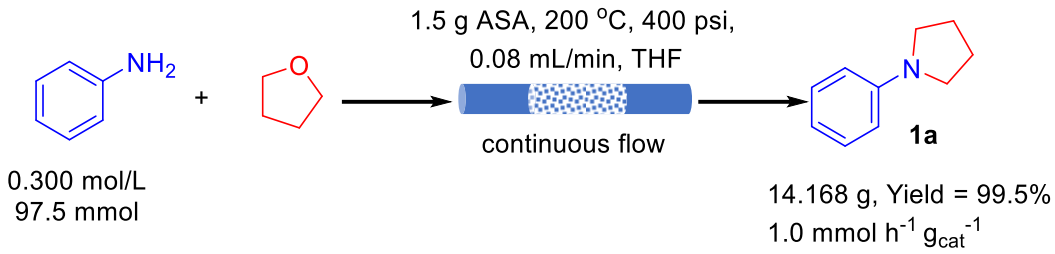

Mechanistic investigation of pyrrolidone formation. Two possible pathways for *N*-substituted pyrrolidine formation are shown in **Scheme 2.5**. In the non-concerted S_N1-type pathway (a), activation of THF by a Brønsted acid site associated with Al substitution in ASA gives carbocation character to the more highly substituted α-carbon, which is then captured by the amine to form the ring-opened intermediate **D**. In the concerted S_N2-type pathway (b), simultaneous bifunctional activation of the THF oxygen by a Brønsted acid site and of the amine by a Brønsted basic site leads to substitution at the less highly substituted α-carbon, forming the ring-opened intermediate **E**. An experiment with 2-methylTHF and aniline gave an intermediate with m/z = 179.26, detected by GC-MS. It was isolated by column chromatography, and its structure was established by comparison of its ^1H and ^{13}C NMR spectra to those for the known compound[69] to be that of *N*-phenyl-5-amino-2-pentanol (**E,** M^+ = calculated for $C_{11}H_{17}NO$ 179.13; found: 179.26). Furthermore,

this mechanistic proposal is in line with the previously reported reaction of aniline with 2-methyl THF catalyzed by g-Al_2O_3 [59], where the isolation of the intermediate methyl ether of E in the presence of dimethyl carbonate is consistent with azacycle formation by the S_N2 pathway. In contrast, the key intermediate D of the S_N1 pathway was not detected.

Scheme 2.5 Possible reaction pathways for solid acid-catalyzed *N*-phenylpyrrolidine formation

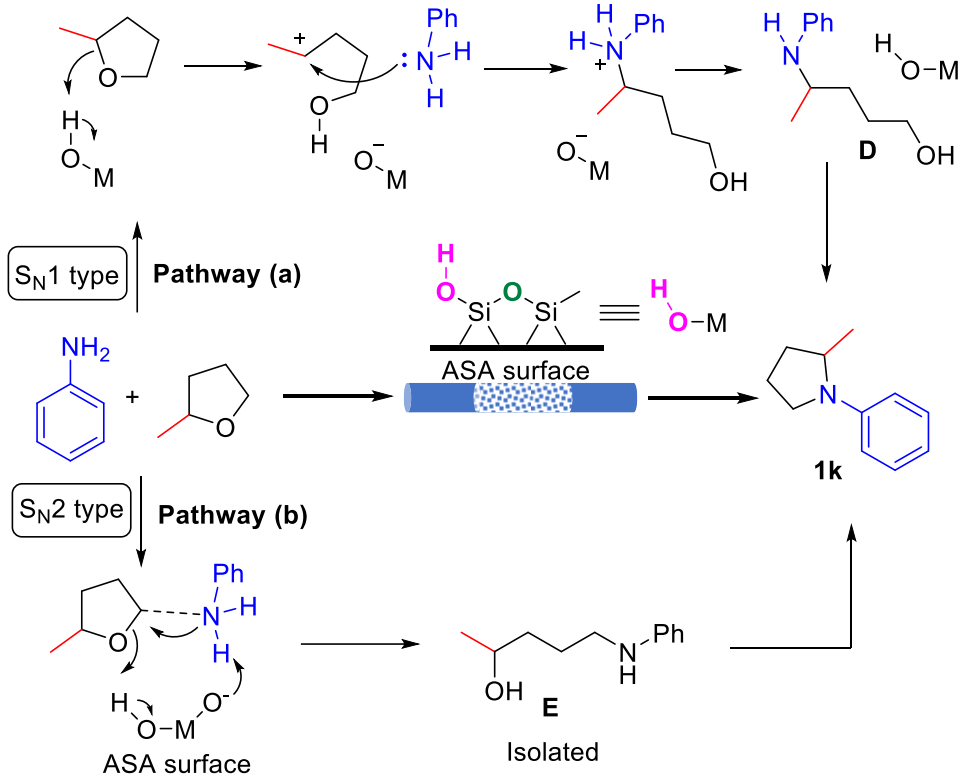

To investigate the role of Brønsted acid sites in the mechanism, the most acidic silanols of ASA were capped with trimethylsilyl groups via their reaction with hexamethyldisilazane (HMDS),[70] eq 2.1:

$$2\equiv SiOH + ((CH_3)_3Si)_2NH \rightarrow 2\equiv SiOSi(CH_3)_3 + NH_3 \qquad (2.1)$$

Dehydrated ASA shows a strong peak at 3747 cm^{-1} for the O-H stretching mode of the surface silanols, **Figure 2.3**. After silylation at 25 °C followed by removal of NH_3 by evacuation at 350 °C, the intensity of the silanol peak is partially attenuated, consistent with elimination of the stronger Brønsted acid sites (via the reaction of approx. 60 % of the silanols, as judged by the decrease in the integrated area of the bands in this region). This change is accompanied by the appearance of C-H stretching vibrations at 2965 and 2905 cm^{-1}, characteristic of trimethylsilyl groups. When tested under the same reaction conditions (0.1

M benzylamine in THF flowing at 0.20 mL/min, 0.500 g catalyst, 200 °C, 500 psi), the activity of HMDS-modified ASA was reduced by one-third (45 % conversion of benzylamine, compared to 69% for unmodified ASA); Hence the activity appears to be associated with the silanol groups.

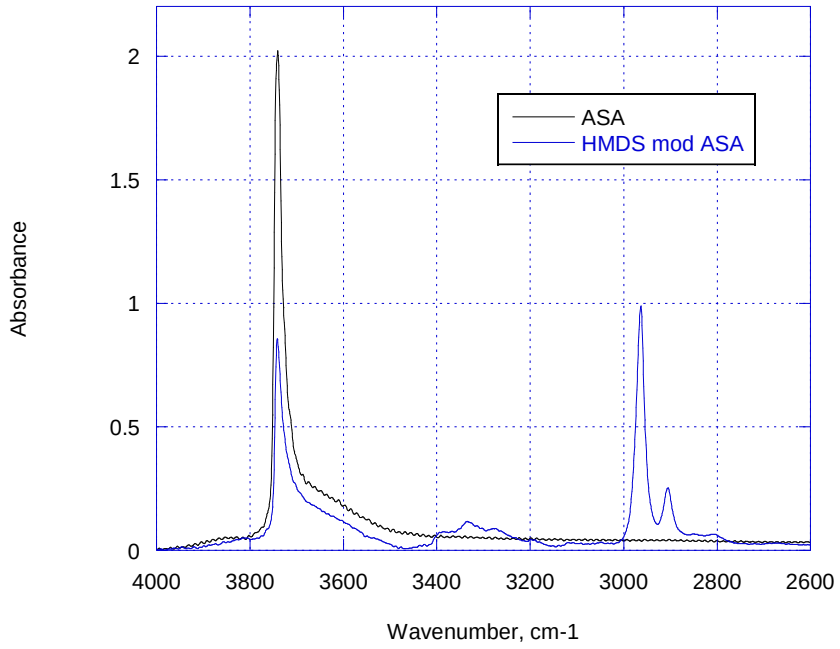

Figure 2.3. Comparison of transmission IR spectra for unmodified ASA (calcined at 500 °C and evacuated at 450 °C, black) and trimethylsilyl-capped ASA (treated with HMDS at 25 °C followed by evacuation at 350 °C to remove NH_3, blue).

The ring-opening step in the ASA-catalyzed amination of 2-methylTHF was investigated computationally with DFT, using methylamine as a model aliphatic amine. The small cluster model created to represent the active site is shown in **Figure 2.1**. It contains an Al atom substituted into a silica cluster adjacent to a vicinal pair of silanols. A methylammonium counteraction is present only to balance the charge. Prior to reaction, both the methylamine and the ether are stabilized by hydrogen bonding originating at the silanols, together worth X

kJ.mol (**Figure 2.4**). We were unable to isolate an S_N1 intermediate since these silanols are not acidic enough to protonate the ether: protonated 2-methylTHF transfers its proton back to the silanolate.

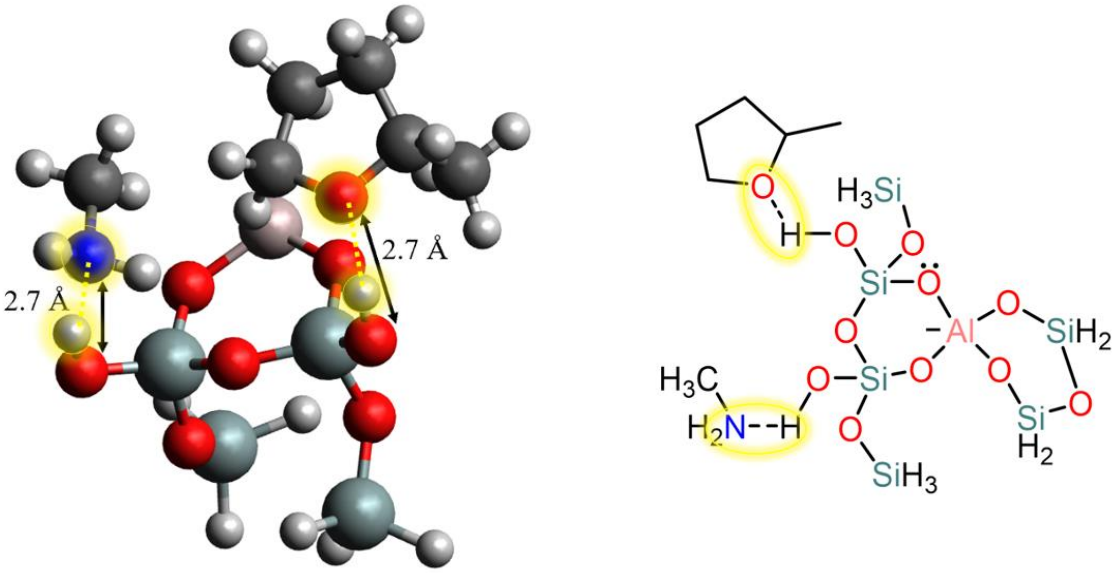

Figure 2.4 DFT-optimized geometry of the ASA cluster interacting with both 2-methylTHF and methylamine by H-bonding. For clarity, only a part of the cluster model is shown. Arrows mark the locations of the two H-bonds (O-H-O and N-H-O) between the reactants and the silanol groups of the active site. They are also depicted in the drawing on the right. Color scheme: H, white; O, red; Si, green; N, blue; C, grey; Al, pink.

Nucleophilic attack of the activated amine on the activated 2-methylTHF can, in principle, occur at either α-carbon of the ether ring and, in both cases, follows a concerted S_N2 mechanism. The transition state involves the simultaneous formation of a new C-N bond (1.98 Å) and breaking the C-O bond (1.97 Å), shown in **Figure 2.5** for reaction at the less substituted α-carbon. The amine is no longer H-bonded to a silanol but shifts to form a moderately strong H-bond (O-O distance 2.9 Å) with a siloxane bridge. The transition state is stabilized by a

strong H-bond (O-O distance 2.4 Å) between the silanol and the oxygen of 2-methylTHF, with the proton located halfway between the two O atoms. A considerable amount of organization is required to assemble this transition state, consistent with the small Arrhenius prefactor. In the product state, the proton is fully transferred to give *N*-phenyl-5-amino-2-pentanol (intermediate **E**). The latter undergoes rapid ring closure with little or no barrier.

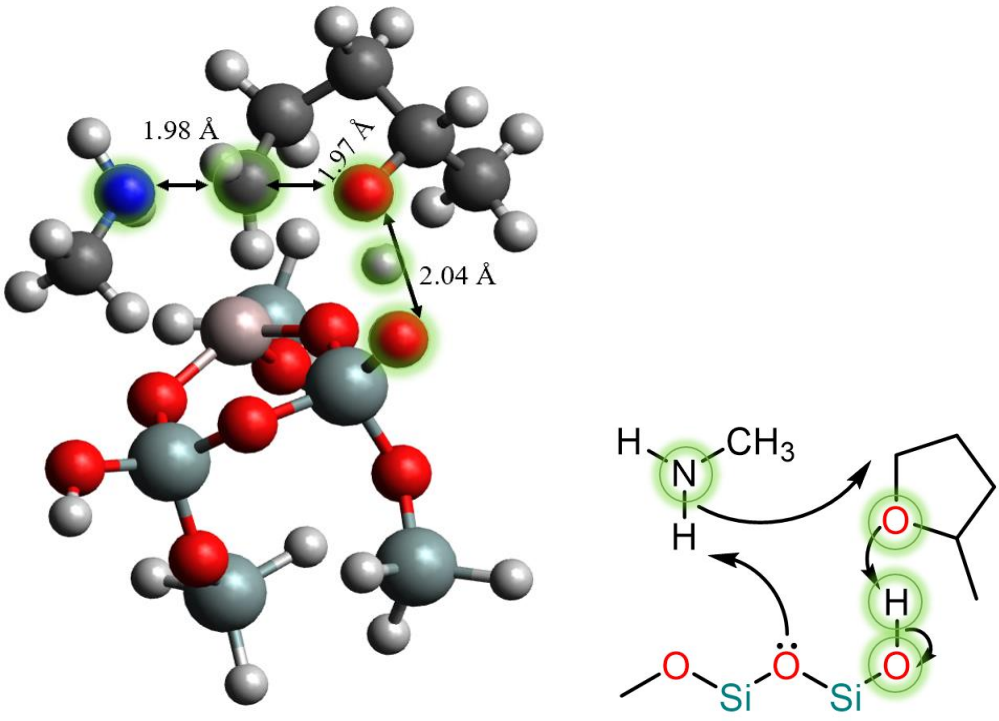

Figure 2.5 DFT-optimized transition state geometry showing the nucleophilic attack of methylamine on the less substituted a-carbon of 2-methylTHF. For clarity, only part of the cluster is shown. The key participating atoms are highlighted in green for both the computed structure and the schematic. Arrows indicate the locations of the nascent C-N bond, the breaking C-O bond, and the O-O hydrogen-bond. Color scheme: H, white; O, red; Si, green; N, blue; C, grey; Al, pink.

One of the transition states (corresponding to ASA-promoted nucleophilic attack of methylamine at the less substituted a-carbon of 2-methylTHF) is shown in in Figure 2.4. The

intrinsic barrier for this transition state is estimated to be 45 kJ/mol, while the apparent barrier (referenced to the isolated, gas-phase species) is about 11 kcal/mol due to the strong interactions of the reactants with the ASA active site (X kJ/mol). The barriers for the attack at the more substituted a-carbon of the ether are slightly higher, at 49 and 16 kcal/mol, respectively, due to steric interactions with the methyl group. The apparent barriers compare well with the experimentally-measured barrier of 64 kJ/mol (see above). For comparison, the uncatalyzed gas-phase reaction has a much higher intrinsic barrier, *ca*. 65 kcal/mol. Compared with the catalyzed reaction, the transition state for the uncatalyzed reaction is more product-like, with a significantly shorter nascent C-N bond and a more fully dissociated ether C-O bond

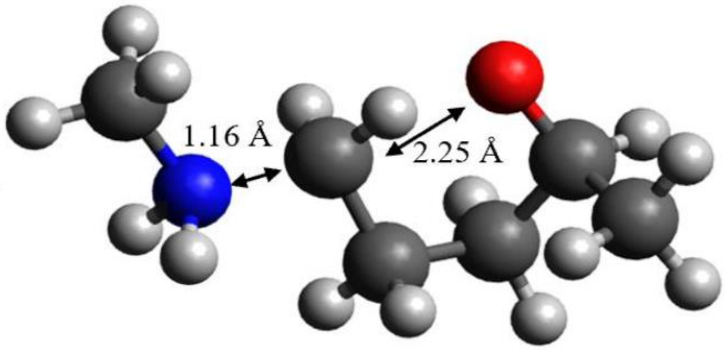

.

Figure 2.6 DFT-computed transition state geometry for the uncatalyzed nucleophilic attack of methylamine at the 5-position of 2MTHF, occurring in the gas phase. Arrows mark the locations of the nascent C-N bond and the breaking C-O bond. Color scheme: H, white; O, red; N, blue; C, grey.

Direct synthesis of aromatic azacycles from furans: Following our successful synthesis of saturated azacycles, we attempted to broaden the scope to include heterocycles. Pyrroles find wide applications in pharmaceuticals, materials science, and supramolecular chemistry.[71-74]

Moreover, renewable 2,5-dimethylfuran is readily obtained by hydrogenating cellulose-derived 5-hydroxymethylfurfural.[75-79] Batch reactions of furans with arylamines have been reported to be catalyzed by Brønsted acidic HY-zeolite[74] and Lewis acidic Hf-doped mesoporous SBA-15,[72] giving *N*-arylpyrroles after several hours at 150 °C. We explored the ability of ASA to catalyze the condensation of furans with amines to form functionalized pyrroles in continuous flow.

The flow conditions described above that were optimized for *N*-substituted pyrrolidine synthesis did not work well for pyrroles. Therefore, conditions were reoptimized using as the test case the direct reaction with aniline (**A)** and with 2,5-dimethylfuran (**B**) (see the SI). Under the best conditions found (0.120 **A** and 0.100 **B** in toluene, 500 mg catalyst, 0.04 mL/min at 180 °C and 600 psi), the expected product 2,5-dimethyl-1-phenyl-1H-pyrrole (**2a**) was obtained in > 99 % yield. Even when the concentrations of **A** and B were equimolar, the yield of **2a** was 95%. Para-substituted anilines with either electron-withdrawing groups (Scheme 2.6, **2b-2d**) or electron-donating groups (Scheme 2.6, **2e**) also gave pyrroles in high yield. Other furans, such as 2-methylfuran and furan, provided good yields to the corresponding pyrroles **2f** and **2g**. Reactions of the less reactive aliphatic amines need longer residence times (achieved using a higher catalyst loading) and higher temperatures. For example, a high yield (90%) of 1-(2-phenylethyl)-2,5-dimethyl-1H-pyrrole (**2h**) in the reaction of 2,5-dimethylfuran with phenethylamine required 250 °C.

Scheme 2.6. Substrate Scope for Direct Catalytic Synthesis of *N*-substituted Pyrroles Catalyzed by ASA in Continuous Flow Conditions[a]

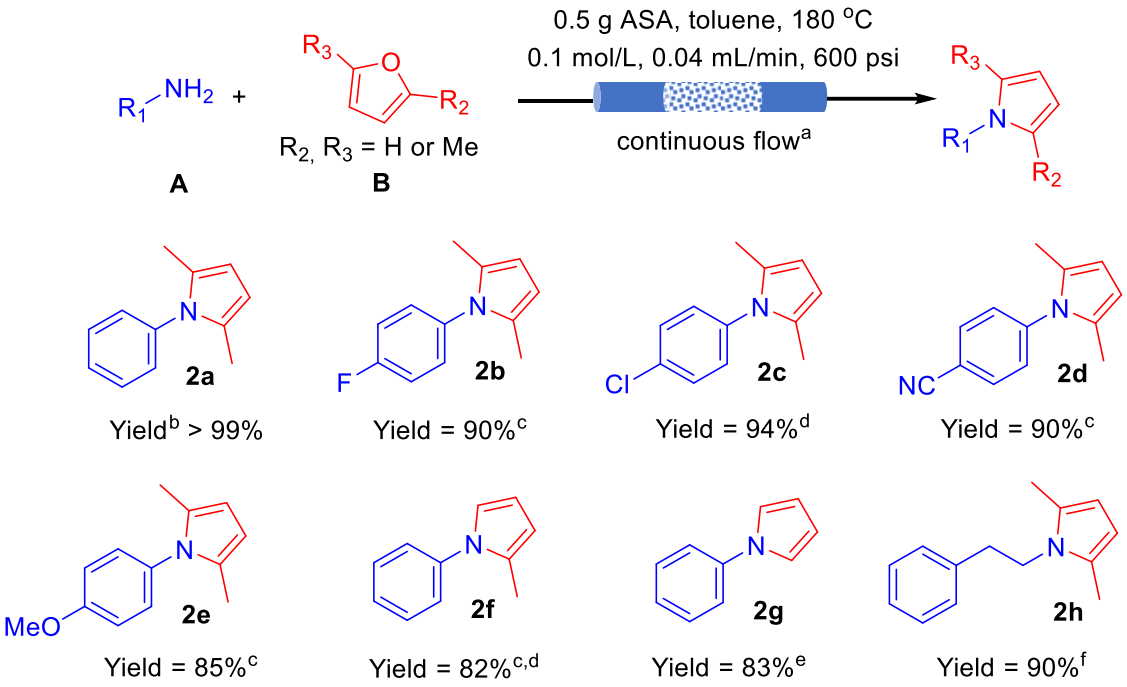

[a] Unless otherwise noted, continuous flow reactions were conducted using 0.120 M **A** and 0.100 M **B** in toluene, flowing at 0.04 mL/min at 180 °C, with 500 mg catalyst in a packed-bed reactor at 600 psi. [b] Yields reported are NMR yields, using 1,3,5-trimethoxybenzene as the internal standard. [c] T = 200 °C. [d] 1.00 g ASA catalyst was used. [e] T = 240 °C. [f] The reaction was conducted using 1.50 g of catalyst at 250 °C.

Mechanistic investigation of pyrrole formation. Previously, the reaction of 2,5-dimethylfuran with amines catalyzed by HY-zeolite was shown to generate 2,5-hexanedione as the key intermediate.[74] The dione is expected to undergo a Paal-Knorr reaction readily to give the *N*-substituted pyrrole. When a toluene solution of 2,5-dimethylfuran passed through the ASA catalyst bed at 180 °C in the absence of amine, traces of both 2,5-hexanedione (**G**, 3 mol%) and 3-methyl-2-cyclopenten-1-one (**H**, 7 mol%) were detected by GC-MS, **Scheme 2.7**. **G** is formed by Brønsted acid-catalyzed ring-opening of the furan, while **H** is plausibly derived from the intramolecular aldol condensation of **G**.[80] Furthermore, an independent

reaction of **G** with aniline provided the corresponding pyrrole in 85 % yield, comparable to the outcome of the direct reaction between 2,5-dimethylfuran and aniline. Based on these observations, we conclude that *N*-phenylpyrrole formation likely occurs via a typical Brønsted acid-catalyzed Paal−Knorr pathway with 2,5-hexanedione as an intermediate.

Scheme 2.7 Possible reaction pathway for solid acid-catalyzed *N*-phenylpyrrole formation.

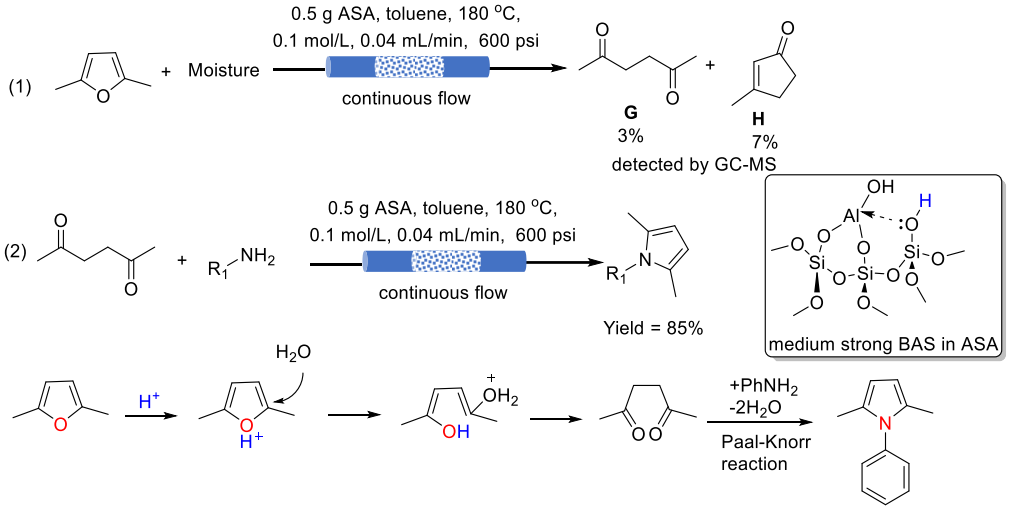

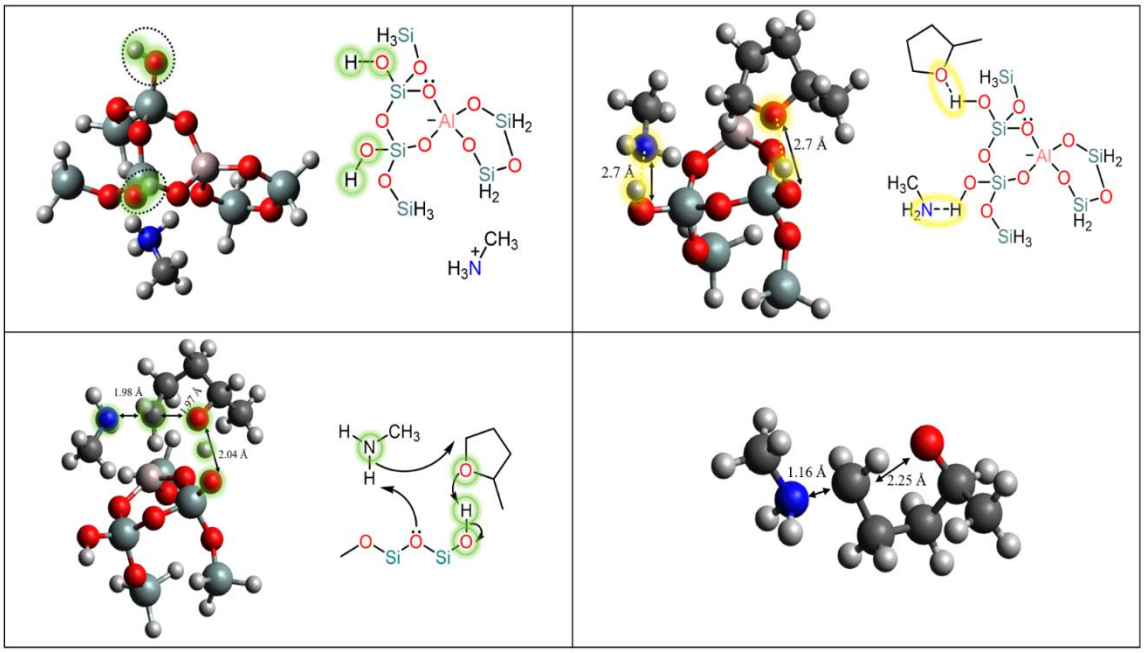

2.5 Conclusions

A simple and efficient continuous flow method was developed for the preparation of *N*-substituted azacycles in a packed-bed reactor. The catalyst, amorphous silica-alumina, is readily available and easy to handle. The general method is compatible with a variety of cyclic ethers and with aromatic amines, as well as more challenging aliphatic amines. Pyrrolidines, piperidines, and pyrroles were obtained in excellent yields (> 90 %) in several cases, and the method was demonstrated in the preparation of a key intermediate in the synthesis of an H3 antagonist. A gram-scale synthesis of *N*-phenylpyrrolidine was sustained over 68 h, providing > 14 g (nearly 100 mmol) pure product in over 99% yield, with isolation by simple solvent evaporation. For *N*-substituted pyrrolidones and piperidines, an S_N2 pathway is likely and was demonstrated by isolation of the ring-opened intermediate *N*-phenyl-5-amino-2-pentanol. In contrast, *N*-phenylpyrrole formation occurs via a typical Brønsted acid-catalyzed Paal−Knorr pathway, with 2,5-hexanedione as the ring-opened intermediate. This method could pave the way for the large-scale synthesis of *N*-substituted azacycles by reacting amines with simple cyclic ethers.

Acknowledgment

Pfizer Global R&D is gratefully acknowledged for the financial support of this work.

Contributions

This is a collaborative project completed with the help of Dr. Jing Wu, Costanza Leonardi, and Dr. Allison Wesley. I contributed to the experiments to study reproducibility by performing entry 6 of table 2.1. I contributed to determining the activation energy for N-benzylpyrrolidine by setting up experiments by varying the temperature from 180 to 210^{o}C

and calculating yields by NMR using 1,3,5-trimethoxybenzene as the internal standard. I participated in writing the introduction part of the paper and collected the references.

References

1. Gérardy, R.; Emmanuel, N.; Toupy, T.; Kassin, V.-E.; Tshibalonza, N. N.; Schmitz, M.; Monbaliu, J.-C. M., Continuous Flow Organic Chemistry: Successes and Pitfalls at the Interface with Current Societal Challenges. *Eur. J. Org. Chem.* **2018,** (20-21), 2301-2351.

2. Cambie, D.; Bottecchia, C.; Straathof, N. J. W.; Hessel, V.; Noel, T., Applications of Continuous-Flow Photochemistry in Organic Synthesis, Material Science, and Water Treatment. *Chem. Rev.* **2016,** *116* (17), 10276-10341.

3. Gilmore, K.; Seeberger, P. H., Continuous flow photochemistry. *Chem. Rec.* **2014,** *14* (3), 410-8.

4. Hartman, R. L., Flow chemistry remains an opportunity for chemists and chemical engineers. *Current Opinion in Chemical Engineering* **2020,** *29*, 42-50.

5. Britton, J.; Raston, C. L., Multi-step continuous-flow synthesis. *Chem. Soc. Rev.* **2017,** *46* (5), 1250-1271.

6. Colella, M.; Carlucci, C.; Luisi, R., Supported Catalysts for Continuous Flow Synthesis. *Top Curr Chem (Cham)* **2018,** *376* (6), 46.

7. Isbrandt, E. S.; Sullivan, R. J.; Newman, S. G., High Throughput Strategies for the Discovery and Optimization of Catalytic Reactions. *Angew Chem Int Ed Engl* **2019,** *58* (22), 7180-7191.

8. Pastre, J. C.; Browne, D. L.; Ley, S. V., Flow chemistry syntheses of natural products. *Chem. Soc. Rev.* **2013,** *42* (23), 8849-69.

9. Rogers, L.; Jensen, K. F., Continuous manufacturing – the Green Chemistry promise? *Green Chemistry* **2019,** *21* (13), 3481-3498.

10. Santoro, S.; Ferlin, F.; Ackermann, L.; Vaccaro, L., C-H functionalization reactions under flow conditions. *Chem Soc Rev* **2019,** *48* (10), 2767-2782.

11. Trobe, M.; Burke, M. D., The Molecular Industrial Revolution: Automated Synthesis of Small Molecules. *Angew Chem Int Ed Engl* **2018,** *57* (16), 4192-4214.

12. Britton, J.; Jamison, T. F., The assembly and use of continuous flow systems for chemical synthesis. *Nat. Protoc.* **2017,** *12* (11), 2423-2446.

13. Tanimu, A.; Jaenicke, S.; Alhooshani, K., Heterogeneous catalysis in continuous flow microreactors: A review of methods and applications. *Chem. Eng. J.* **2017,** *327*, 792-821.

14. Schneider, G., Automating drug discovery. *Nat. Rev. Drug Discovery* **2018,** *17* (2), 97-113.

15. Gioiello, A.; Piccinno, A.; Lozza, A. M.; Cerra, B., The Medicinal Chemistry in the Era of Machines and Automation: Recent Advances in Continuous Flow Technology. *J. Med. Chem.* **2020,** *63* (13), 6624-6647.

16. Tsubogo, T.; Oyamada, H.; Kobayashi, S., Multistep continuous-flow synthesis of (R)- and (S)-rolipram using heterogeneous catalysts. *Nature* **2015,** *520* (7547), 329-32.

17. Tanabe, K. H., W. F., Industrial application of solid acid-base catalysts *Applied Catalysis A: General* **1999**.

18. Wang, Y.; Zhang, C.; Li, S.; Liu, L., Iron-Catalyzed Synthesis of Pyrrole Derivatives and Related Five-Membered Azacycles. *European Journal of Organic Chemistry* **2021,** *2021* (27), 3837-3849.

19. Climent, M. J.; Corma, A.; Iborra, S., Heterogeneous Catalysts for the One-Pot Synthesis of Chemicals and Fine Chemicals. *Chem. Rev.* **2011,** *111* (2), 1072-1133.

20. Liang, J.; Liang, Z. B.; Zou, R. Q.; Zhao, Y. L., Heterogeneous Catalysis in Zeolites, Mesoporous Silica, and Metal-Organic Frameworks. *Adv. Mater.* **2017,** *29* (30).

21. Wu, J.; Zheng, C.; Li, B.; Hawkins, J. M.; Scott, S. L., Efficient, continuous N-Boc deprotection of amines using solid acid catalysts. *React. Chem. Eng.* **2021**.

22. Ciufolini, M. A.; Hermann, C. W.; Whitmire, K. H.; Byrne, N. E., Chemoenzymatic Preparation of Trans-2,6-Dialkylpiperidines and of Other Azacycle Building-Blocks - Total Synthesis of (+)-Desoxoprosopinine. *J. Am. Chem. Soc.* **1989,** *111* (9), 3473-3475.

23. Lu, X. H.; Peng, Y. Q.; Wang, C. L.; Yang, J.; Bao, X. L.; Dong, Q.; Zhao, W. L.; Tan, W. F.; Dong, X. C., Design, synthesis, and biological evaluation of optimized phthalazine derivatives as hedgehog signaling pathway inhibitors. *Eur. J. Med. Chem.* **2017,** *138*, 384-395.

24. Wang, C. L.; Zhu, M. F.; Lu, X. H.; Wang, H.; Zhao, W. L.; Zhang, X. W.; Dong, X. C., Synthesis and evaluation of novel dimethylpyridazine derivatives as hedgehog signaling pathway inhibitors. *Bioorg. Med. Chem.* **2018,** *26* (12), 3308-3320.

25. Hussein, Z.; Chu, S. Y.; Granneman, G. R., Enantioselective Determination of Dn-2327, a Novel Nonbenzodiazepine Anxiolytic, and or Its Active Metabolite in Human Plasma

and Urine Using High-Performance Liquid-Chromatography. *Journal of Chromatography-Biomedical Applications* **1993,** *613* (1), 113-120.

26. Bulumulla, C.; Gunawardhana, R.; Gamage, P. L.; Miller, J. T.; Kularatne, R. N.; Biewer, M. C.; Stefan, M. C., Pyrrole-Containing Semiconducting Materials: Synthesis and Applications in Organic Photovoltaics and Organic Field-Effect Transistors. *ACS Appl Mater Interfaces* **2020,** *12* (29), 32209-32232.

27. Estevez, V.; Villacampa, M.; Menendez, J. C., Multicomponent reactions for the synthesis of pyrroles. *Chem. Soc. Rev.* **2010,** *39* (11), 4402-4421.

28. Hubbard, H.; Lawitz, E., Glecaprevir plus pibrentasvir (ABT493+ABT-530) for the treatment of Hepatitis C. *Expert Review of Gastroenterology & Hepatology* **2018,** *12* (1), 9-17.

29. Popovici-Muller, J.; Lemieux, R. M.; Artin, E.; Saunders, J. O.; Salituro, F. G.; Travins, J.; Cianchetta, G.; Cai, Z. W.; Zhou, D.; Cui, D. W.; Chen, P.; Straley, K.; Tobin, E.; Wang, F.; David, M. D.; Penard-Lacronique, V.; Quivoron, C.; Saada, V.; De Botton, S.; Gross, S.; Dang, L.; Yang, H.; Utley, L.; Chen, Y.; Kim, H.; Jin, S. F.; Gu, Z. W.; Yao, G.; Luo, Z. Y.; Lv, X. B.; Fang, C.; Yan, L. P.; Olaharski, A.; Silverman, L.; Biller, S.; Su, S. S.; Yen, K., Discovery of AG-120 (Ivosidenib): A First-in-Class Mutant IDH1 Inhibitor for the Treatment of IDH1 Mutant Cancers. *Acs Medicinal Chemistry Letters* **2018,** *9* (4), 300-305.

30. Vangapandu, H. V.; Jain, N.; Gandhi, V., Duvelisib: a phosphoinositide-3 kinase/inhibitor for chronic lymphocytic leukemia. *Expert Opinion on Investigational Drugs* **2017,** *26* (5), 625-632.

31. Camidge, D. R.; Kim, H. R.; Ahn, M. J.; Yang, J. C. H.; Han, J. Y.; Lee, J. S.; Hochmair, M. J.; Li, J. Y. C.; Chang, G. C.; Lee, K. H.; Gridelli, C.; Delmonte, A.; Campelo, R. G.; Kim, D. W.; Bearz, A.; Griesinger, F.; Morabito, A.; Felip, E.; Califano, R.; Ghosh, S.; Spira, A.; Gettinger, S. N.; Tiseo, M.; Gupta, N.; Haney, J.; Kerstein, D.; Popat, S., Brigatinib versus Crizotinib in ALK-Positive Non-Small-Cell Lung Cancer. *N. Engl. J. Med.* **2018,** *379* (21), 2027-2039.

32. Perl, A. E.; Altman, J. K.; Cortes, J.; Smith, C.; Litzow, M.; Baer, M. R.; Claxton, D.; Erba, H. P.; Gill, S.; Goldberg, S.; Jurcic, J. G.; Larson, R. A.; Liu, C. F.; Ritchie, E.; Schiller, G.; Spira, A. I.; Strickland, S. A.; Tibes, R.; Ustun, C.; Wang, E. S.; Stuart, R.; Rollig, C.; Neubauer, A.; Martinelli, G.; Bahceci, E.; Levis, M., Selective inhibition of FLT3 by gilteritinib in relapsed or refractory acute myeloid leukaemia: a multicentre, first-in-human, open-label, phase 1-2 study. *Lancet Oncol.* **2017,** *18* (8), 1061-1075.

33. Hawkins, J. M.; Dubé, P.; Maloney, M. T.; Wei, L.; Ewing, M.; Chesnut, S. M.; Denette, J. R.; Lillie, B. M.; Vaidyanathan, R., Synthesis of an H3 Antagonist via Sequential One-Pot Additions of a Magnesium Ate Complex and an Amine to a 1,4-Ketoester followed by Carbonyl-Directed Fluoride Addition. *Org. Process Res. Dev.* **2012,** *16* (8), 1393-1403.

34. Christopher J. Collins, M. L. B. S., Facile Reduction of Tertiary Lactams to Cyclic Amines With 9-Borabicyclo[3.3.1]nonane (9-BBN). *Tetrahedron Letters* **1999,** *40*, 3673-3676.

35. Shim, S. C. H., K. T.; Park, W. H. , A new and facile synthesis of N-substituted pyrrolidine of amines with aqueous succinaldehyde using tetracarbonylhydridoferrate, HFe(CO)-4 as a highly selective reducing agent. *Tetrahedron* **1986,** (42), 259−263.

36. Watanabe, Y.; Shim, S. C.; Uchida, H.; Mitsudo, T.; Takegami, Y., Reducive Amination of Phthalaldehyde by Tetracarbonylhydridoferrate - Synthesis of 2-Arylisoindoles. *Tetrahedron* **1979,** *35* (11), 1433-1436.

37. Tran, V. H.; Kim, H. K., Facile tin(II)-catalyzed synthesis of N-heterocycles from dicarboxylic acids and arylamines. *Org Biomol Chem* **2022,** *20* (14), 2881-2888.

38. Craig, L. C.; Hixon, R. M., Synthesis of N-Phenylpyrrolidine and N-Hexahydrophenylpyrrolidine. *J. Am. Chem. Soc.* **1930,** *52* (2), 804-808.

39. Cui, X.; Dai, X.; Deng, Y.; Shi, F., Development of a general non-noble metal catalyst for the benign amination of alcohols with amines and ammonia. *Chemistry* **2013,** *19* (11), 3665-75.

40. Maeno, Z.; Torii, H.; Yamada, S.; Mitsudome, T.; Mizugaki, T.; Jitsukawa, K., Synthesis of tetraline derivatives through depolymerization of polyethers with aromatic compounds using a heterogeneous titanium-exchanged montmorillonite catalyst. *RSC Advances* **2016,** *6* (92), 89231-89233.

41. Rout, L.; Jammi, S.; Punniyamurthy, T., Novel CuO nanoparticle catalyzed C-N cross coupling of amines with iodobenzene. *Org. Lett.* **2007,** *9* (17), 3397-3399.

42. Khatri, P. K.; Jain, S. L., Glycerol ingrained copper: an efficient recyclable catalyst for the N-arylation of amines with aryl halides. *Tetrahedron Lett.* **2013,** *54* (21), 2740-2743.

43. Hou, T.; Zhang, C.; Wang, Y.; Liu, Z.; Zhang, Z.; Wang, F., Metal-free protocol for the synthesis of N -arylpyrrolidines catalyzed by hydrogen iodine. *Catal. Commun.* **2017,** *94*, 56-59.

44. Lin, Y.; Li, D.; Zhang, J.; Tang, Z.; Liu, L.; Huang, T.; Li, C.; Chen, T., I2/NaH2PO2-mediated deoxyamination of cyclic ethers for the synthesis of N-aryl-substituted azacycles. *New J Chem* **2021,** *45* (45), 21011-21014.

45. Hu, S.; Huo, Y.; Wang, Z., Boron trifluoride-mediated synthesis of N-aryl-substituted pyrrolidines from tetrahydrofuran and amines. *Chem. Heterocycl. Compd. (N. Y., NY, U. S.)* **2017,** *53* (12), 1365-1368.

46. Olsen, C. J.; Furst, A., N-Phenylpyrrolidine. *J. Am. Chem. Soc.* **1953,** *75* (12), 3026-3026.

47. Sun, Z.; Hu, S.; Huo, Y.; Wang, Z., Titanium tetrachloride-mediated synthesis of N-aryl-substituted azacycles from cyclic ethers. *RSC Advances* **2017,** *7* (8), 4363-4367.

48. Tran, V. H.; La, M. T.; Kang, S.; Kim, H. K., Practical direct synthesis of N-aryl-substituted azacycles from N-alkyl protected arylamines using TiCl4 and DBU. *Org Biomol Chem* **2020,** *18* (26), 5008-5016.

49. Korbad, B. L.; Lee, S. H., Synthesis of N-aryl substituted, five- and six-membered azacycles using aluminum-amide complexes. *Chem Commun (Camb)* **2014,** *50* (64), 8985-8.

50. La, M. T.; Kang, S.; Kim, H. K., Metal-Free Synthesis of N-Aryl-Substituted Azacycles from Cyclic Ethers Using POCl3. *J Org Chem* **2019,** *84* (11), 6689-6696.

51. Tran, V. H.; La, M. T.; Kim, H. K., Phosphoryl chloride-mediated solvent-free synthesis of N-aryl-substituted azacycles from arylamines and cyclic ethers. *Tetrahedron Lett.* **2019,** *60* (28), 1860-1863.

52. Zhang, Z.; Miao, C.; Xia, C.; Sun, W., Synergistic Acid-Catalyzed Synthesis of N-Aryl-Substituted Azacycles from Anilines and Cyclic Ethers. *Org Lett* **2016,** *18* (7), 1522-5.

53. Huo, Y.; Xu, Y.; Wang, Z. H., A DFT Study on the Mechanism of the FLP-access to N-Arylazacycles from Cyclic Ethers: Sequential Activation of Two C-O Bonds. *Chem. Lett.* **2017,** *46* (11), 1664-1667.

54. Hargis, D. C.; Shubkin, R. L., Gem-Cyclodialkylation - a Facile Synthetic Route to N-Substituted Heterocycles. *Tetrahedron Lett.* **1990,** *31* (21), 2991-2994.

55. Walkup, R. E.; Searles, S., Synthesis of Sterically Hindered 1-Arylpyrrolidines and 1-Arylpiperidines by Condensation of Primary Aromatic-Amines with Cyclic Ethers or Diols. *Tetrahedron* **1985,** *41* (1), 101-106.

56. Bourns, A. N.; Embleton, H. W.; Hansuld, M. K., The Reaction of Tetrahydropyran with Primary Aromatic Amines over Activated Alumina. *Canadian Journal of Chemistry-Revue Canadienne De Chimie* **1952,** *30* (1), 1-8.

57. Tsubogo, T.; Oyamada, H.; Kobayashi, S., Multistep continuous-flow synthesis of (R)- and (S)-rolipram using heterogeneous catalysts. *Nature* **2015,** *520* (7547), 329-332.

58. Walkup, R. E.; Searles, S., Synthesis of sterically hindered 1-arylpyrrolidines and 1-arylpiperidines by condensation of primary aromatic amines with cyclic ethers or diols. *Tetrahedron* **1985,** *41* (1), 101-106.

59. Amara, Z.; Streng, E. S.; Skilton, R. A.; Jin, J.; George, M. W.; Poliakoff, M., Automated Serendipity with Self-Optimizing Continuous-Flow Reactors. *European Journal of Organic Chemistry* **2015,** *2015* (28), 6141-6145.

60. Hargis, D. C.; Shubkin, R. L., gem-cyclodialkylation A facile synthetic route to N-substituted heterocycles. *Tetrahedron Letters* **1990,** *31* (21), 2991-2994.

61. Wu, J.; Zheng, C.; Li, B.; Hawkins, J. M.; Scott, S. L., Efficient, continuous N-Boc deprotection of amines using solid acid catalysts. *Reaction Chemistry & Engineering* **2021,** *6* (2), 279-288.

62. Mathieu, G.; Patel, H.; Lebel, H., Convenient Continuous Flow Synthesis of N-Methyl Secondary Amines from Alkyl Mesylates and Epoxides. *Organic Process Research & Development* **2020,** *24* (10), 2157-2168.

63. Zhang, J.; Wang, J., Atropoenantioselective Redox-Neutral Amination of Biaryl Compounds through Borrowing Hydrogen and Dynamic Kinetic Resolution. *Angew Chem Int Ed Engl* **2018,** *57* (2), 465-469.

64. Bains, A. K.; Kundu, A.; Yadav, S.; Adhikari, D., Borrowing Hydrogen-Mediated N-Alkylation Reactions by a Well-Defined Homogeneous Nickel Catalyst. *ACS Catalysis* **2019,** *9* (10), 9051-9059.

65. Crépeau, G.; Montouillout, V.; Vimont, A.; Mariey, L.; Cseri, T.; Maugé, F., Nature, Structure and Strength of the Acidic Sites of Amorphous Silica Alumina: An IR and NMR Study. *The Journal of Physical Chemistry B* **2006,** *110* (31), 15172-15185.

66. Hensen, E. J. M.; Poduval, D. G.; Degirmenci, V.; Ligthart, D. A. J. M.; Chen, W.; Maugé, F.; Rigutto, M. S.; Veen, J. A. R. v., Acidity Characterization of Amorphous Silica–Alumina. *The Journal of Physical Chemistry C* **2012,** *116* (40), 21416-21429.

67. Busca, G., Silica-alumina catalytic materials: A critical review. *Catalysis Today* **2020,** *357*, 621-629.

68. Goldsmith, B. R.; Peters, B.; Johnson, J. K.; Gates, B. C.; Scott, S. L., Beyond Ordered Materials: Understanding Catalytic Sites on Amorphous Solids. *ACS Catalysis* **2017,** *7* (11), 7543-7557.

69. Marichev, K. O.; Takacs, J. M., Ruthenium-Catalyzed Amination of Secondary Alcohols Using Borrowing Hydrogen Methodology. *ACS Catal.* **2016,** *6* (4), 2205-2210.

70. Moses, A. W.; Raab, C.; Nelson, R. C.; Leifeste, H. D.; Ramsahye, N. A.; Chattopadhyay, S.; Eckert, J.; Chmelka, B. F.; Scott, S. L., Spectroscopically Distinct Sites Present in Methyltrioxorhenium Grafted onto Silica−Alumina, and Their Abilities to Initiate Olefin Metathesis. *Journal of the American Chemical Society* **2007,** *129* (28), 8912-8920.

71. Song, S.; Fung Kin Yuen, V.; Di, L.; Sun, Q.; Zhou, K.; Yan, N., Integrating Biomass into the Organonitrogen Chemical Supply Chain: Production of Pyrrole and d-Proline from Furfural. *Angew. Chem. Int. Ed.* **2020**.

72. Huang, Y.-B.; Luo, Y.-J.; Rio Flores, A. D.; Li, L.-C.; Wang, F., N-Aryl Pyrrole Synthesis from Biomass-Derived Furans and Arylamine over Lewis Acidic Hf-Doped Mesoporous SBA-15 Catalyst. *ACS Sustainable Chemistry & Engineering* **2020,** *8* (32), 12161-12167.

73. Wang, Y.; Furukawa, S.; Fu, X.; Yan, N., Organonitrogen Chemicals from Oxygen-Containing Feedstock over Heterogeneous Catalysts. *ACS Catalysis* **2019,** *10* (1), 311-335.

74. Tao, L.; Wang, Z.-J.; Yan, T.-H.; Liu, Y.-M.; He, H.-Y.; Cao, Y., Direct Synthesis of Pyrroles via Heterogeneous Catalytic Condensation of Anilines with Bioderived Furans. *ACS Catal.* **2017,** *7* (2), 959-964.

75. Hu, L.; Lin, L.; Liu, S., Chemoselective Hydrogenation of Biomass-Derived 5-Hydroxymethylfurfural into the Liquid Biofuel 2,5-Dimethylfuran. *Ind. Eng. Chem. Res.* **2014,** *53* (24), 9969-9978.

76. Leitner, W.; Klankermayer, J.; Pischinger, S.; Pitsch, H.; Kohse-Hoinghaus, K., Advanced Biofuels and Beyond: Chemistry Solutions for Propulsion and Production. *Angew. Chem. Int. Ed.* **2017,** *56* (20), 5412-5452.

77. Nishimura, S.; Ikeda, N.; Ebitani, K., Selective hydrogenation of biomass-derived 5-hydroxymethylfurfural (HMF) to 2,5-dimethylfuran (DMF) under atmospheric

hydrogen pressure over carbon supported PdAu bimetallic catalyst. *Catal. Today* **2014,** *232*, 89-98.

78. Zu, Y.; Yang, P.; Wang, J.; Liu, X.; Ren, J.; Lu, G.; Wang, Y., Efficient production of the liquid fuel 2,5-dimethylfuran from 5-hydroxymethylfurfural over Ru/Co3O4 catalyst. *Applied Catalysis B: Environmental* **2014,** *146*, 244-248.

79. Corma, A.; Iborra, S.; Velty, A., Chemical routes for the transformation of biomass into chemicals. *Chem. Rev.* **2007,** *107* (6), 2411-2502.

80. Sacia, E. R.; Deaner, M. H.; Louie, Y. L.; Bell, A. T., Synthesis of biomass-derived methylcyclopentane as a gasoline additive via aldol condensation/hydrodeoxygenation of 2,5-hexanedione. *Green Chem.* **2015,** *17* (4), 2393-2397.

Appendix 2

Table A2.1. Optimization of reaction conditions for azacycle synthesis

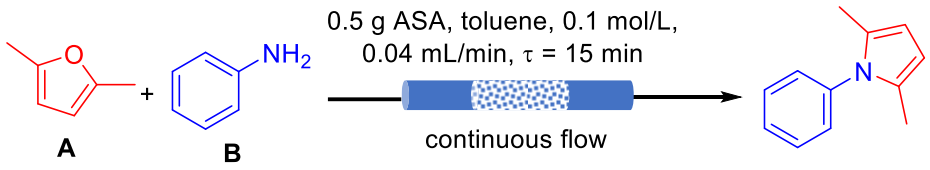

Entry [a]	Pressure (psi)	Temp. (°C)	A/B	Yield (%) [b]
1	400	230	1.0/1.0	78
2	400	240	1.0/1.0	79
3	500	240	1.2/1.0	91
4	600	240	1.2/1.0	94
5	600	200	1.2/1.0	>99
6	600	180	1.2/1.0	>99
7	600	160	1.2/1.0	74
8	600	170	1.2/1.0	76
9	600	180	1.0/1.0	95

[a] Unless otherwise noted, continuous flow reactions were conducted using 0.100 M of aniline, and 0.120 M 2,5-dimethylfuran in toluene, flowing at 0.04 mL/min at 200 °C through a bed of 500 mg catalyst packed in a tubular reactor. [b] NMR yield.

Characterization data for typical product

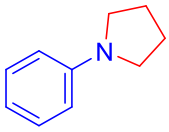

1a was prepared in a continuous flow reactor using 0.100 mol/L of aniline in THF flowing at 0.06 mL/min at 180 °C with 0.500 g ASA 3113 catalyst in a packed-bed column at 400 psi. The product was obtained as a yellow oil (>99% yield). ^{1}H NMR (600 MHz, Chloroform-*d*) δ 7.22 – 7.14 (m, 2H), 6.65 – 6.60 (m, 1H), 6.56 – 6.50 (m, 2H), 3.23 – 3.19 (m, 4H), 1.96 – 1.88 (m, 4H).^{13}C NMR (151 MHz, cdcl$_3$) δ 147.92, 129.04, 115.33, 111.61, 47.50, 25.41.

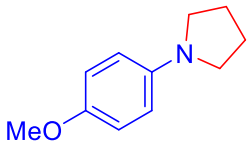

1b was prepared in a continuous flow reactor using 0.100 mol/L of 4-methoxyaniline in THF flowing at 0.08 mL/min at 200 °C with 0.500 g ASA 3113 catalyst in a packed-bed column at 400 psi. The product was obtained as a yellow oil (>99% yield). ^{1}H NMR (600 MHz, Chloroform-*d*) δ 6.86 – 6.80 (m, 2H), 6.55 – 6.49 (m, 2H), 3.74 (s, 3H), 3.23 – 3.19 (m, 4H), 1.99 – 1.94 (m, 4H). 13C NMR (151 MHz, cdcl3) δ 150.91, 143.35, 115.13, 112.73, 56.11, 48.36, 25.49.

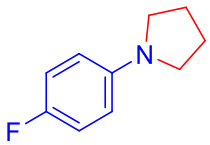

1c was prepared in a continuous flow reactor using 0.100 mol/L of 4-fluoroaniline in THF flowing at 0.08 mL/min at 200 °C with 0.500 g ASA 3113 catalyst in a packed-bed column at 400 psi. The product was obtained as a yellow oil (>99% yield). ^{1}H NMR (600 MHz, Chloroform-*d*) δ 6.90 (m, 2H), 6.42 (m, 2H), 3.17 (m, 5H), 1.95 (m,

4H).^{13}C NMR (151 MHz, Chloroform-*d*) δ 154.81 (d, *J* = 233.2 Hz), 144.83, 115.40 (d, *J* = 22.0 Hz), 112.05 (d, *J* = 7.1 Hz), 48.05, 25.46.

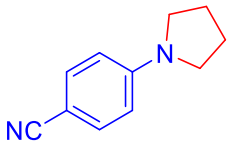

1d was prepared in a continuous flow reactor using 0.100 mol/L of 4-aminobenzonitrile in THF flowing at 0.06 mL/min at 200 °C with 0.500 g ASA 3113 catalyst in a packed-bed column at 400 psi. The product was obtained as a yellow oil (>99% yield).

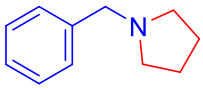

1e was prepared in a continuous flow reactor using 0.100 mol/L of benzylamine in THF flowing at 0.06 mL/min at 200 °C with 0.500 g ASA 3113 catalyst in a packed-bed column at 400 psi. The product was obtained as a yellow oil (>99% yield).

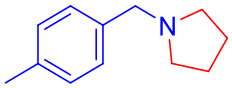

1f was prepared in a continuous flow reactor using 0.100 mol/L of p-tolylmethanamine in THF flowing at 0.04 mL/min at 200 °C with 0.500 g ASA 3113 catalyst in a packed-bed column at 400 psi. The product was obtained as a yellow oil (>99% yield). 1H NMR (600 MHz, Chloroform-d) δ 7.21 (d, J = 8.0 Hz, 2H), 7.12 – 7.09 (m, 2H), 3.56 (s, 2H), 2.51 – 2.46 (m, 4H), 2.32 (s, 4H), 1.80 – 1.72 (m, 4H). 13C NMR (151 MHz, cdcl3) δ 136.32, 136.30, 128.85, 128.84, 77.28, 77.07, 76.86, 60.41, 54.08, 23.42, 21.08, 0.00.

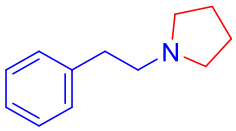

1g was prepared in a continuous flow reactor using 0.100 mol/L of 2-phenylethan-1-amine in THF flowing at 0.04 mL/min at 200 °C with 0.500 g ASA 3113 catalyst in a packed-bed column at 400 psi. The product was obtained as a yellow oil (>99% yield). ^{1}H NMR (600 MHz, Chloroform-*d*) δ 7.28 – 7.23 (m, 2H), 7.21 – 7.14 (m, 3H), 2.85 – 2.80 (m, 2H), 2.70 – 2.66 (m, 2H), 2.58 – 2.51 (m, 4H), 1.82 – 1.75 (m, 4H).^{13}C NMR (151 MHz, cdcl$_3$) δ 140.49, 128.58, 128.30, 125.94, 58.36, 54.19, 35.85, 23.46.

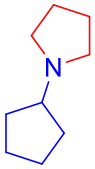

1h was prepared in a continuous flow reactor using 0.100 mol/L of cyclopentanamine in THF flowing at 0.04 mL/min at 200 °C with 0.500 g ASA 3113 catalyst in a packed-bed column at 400 psi. The product was obtained as a yellow oil (96% yield). ^{1}H NMR (600 MHz, Chloroform-*d*) δ 2.54 – 2.48 (m, 4H), 2.38 (tt, *J* = 8.7, 7.0 Hz, 1H), 1.86 – 1.79 (m, 2H), 1.79 – 1.75 (m, 4H), 1.73 – 1.65 (m, 2H), 1.60 – 1.50 (m, 2H), 1.49 – 1.42 (m, 2H). ^{13}C NMR (151 MHz, cdcl$_3$) 67.18, 53.68, 32.31, 24.21, 23.40.

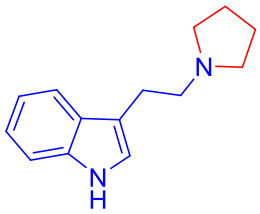

1i was prepared in a continuous flow reactor using 0.100 mol/L of 2-(3H-indol-3-yl)ethan-1-amine in THF flowing at 0.04 mL/min at 200 °C with 0.500 g ASA 3113 catalyst in a packed-bed column at 400 psi. The product was obtained as a yellow oil (>99% yield). ^{1}H NMR (600 MHz, Chloroform-*d*) δ 9.10 (s, 1H), 7.58 (d, *J* = 7.8 Hz, 1H), 7.19 (d, *J* = 8.0 Hz, 1H), 7.12 (t, *J* = 7.5 Hz, 1H), 7.09 – 7.04 (m, 1H), 6.82 (d, *J* = 2.1

Hz, 1H), 3.02 – 2.96 (m, 2H), 2.83 – 2.78 (m, 2H), 2.68 – 2.54 (m, 4H), 1.78 (dt, *J* = 6.4, 3.1 Hz, 4H). ^{13}C NMR (151 MHz, cdcl$_3$) δ 136.39, 127.38, 121.79, 121.51, 118.78, 118.64, 113.75, 111.18, 57.26, 54.08, 24.99, 23.47.

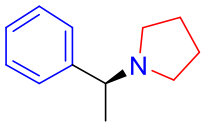

1j was prepared in a continuous flow reactor using 0.100 mol/L of (S)-1-phenylethan-1-amine in THF flowing at 0.04 mL/min at 220 °C with 0.500 g ASA 3113 catalyst in a packed-bed column at 400 psi. The product was obtained as a yellow oil (>99% yield, 99% ee). ^{1}H NMR (600 MHz, Chloroform-*d*) δ 7.35 – 7.32 (m, 2H), 7.29 (dd, *J* = 8.4, 6.8 Hz, 2H), 7.23 – 7.20 (m, 1H), 3.19 (q, *J* = 6.6 Hz, 1H), 2.55 (m, 2H), 2.41 – 2.33 (m, 2H), 1.82 – 1.69 (m, 4H), 1.40 (d, *J* = 6.6 Hz, 3H). ^{13}C NMR (151 MHz, cdcl$_3$) δ 145.54, 128.24, 127.21, 126.83, 66.00, 52.95, 23.41, 23.12. Enantiomeric excess was determined by HPLC: Chiralcel® Chiral OJ-H column, Hexane/*i*PrOH/DEA = 100/1/0.1, 1.0 mL/min, λ = 225 nm; t_R(major) = 4.363 min, t_R(minor) = 4.178 min.

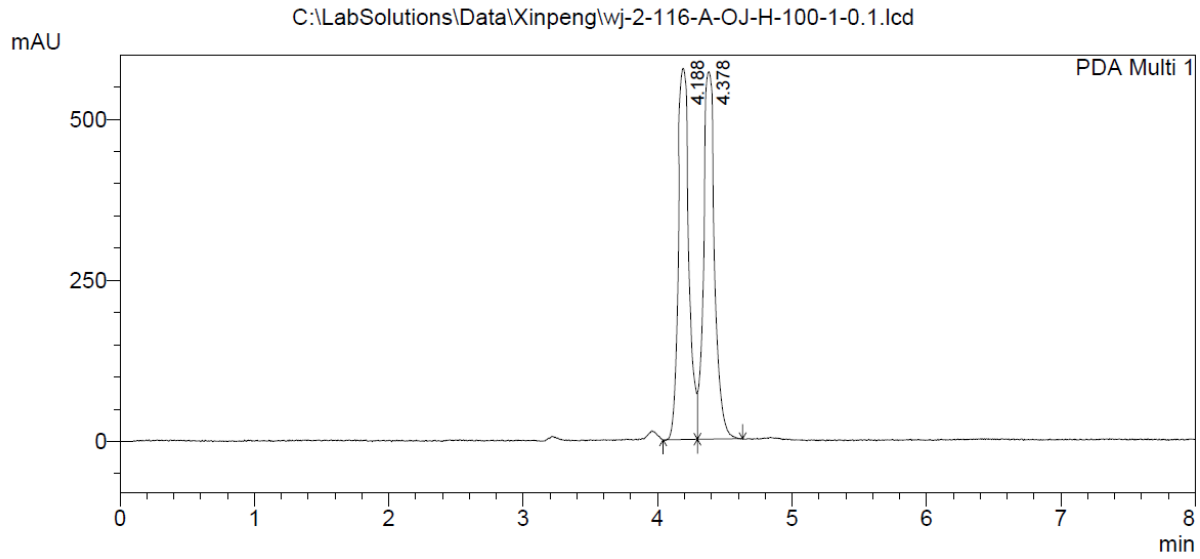

1 PDA Multi 1/225nm 4nm

PeakTable

PDA Ch1 225nm 4nm

Peak#	Ret. Time	Area	Height	Area %	Height %
1	4.188	3190893	575988	49.214	50.267
2	4.378	3292801	569875	50.786	49.733
Total		6483694	1145862	100.000	100.000

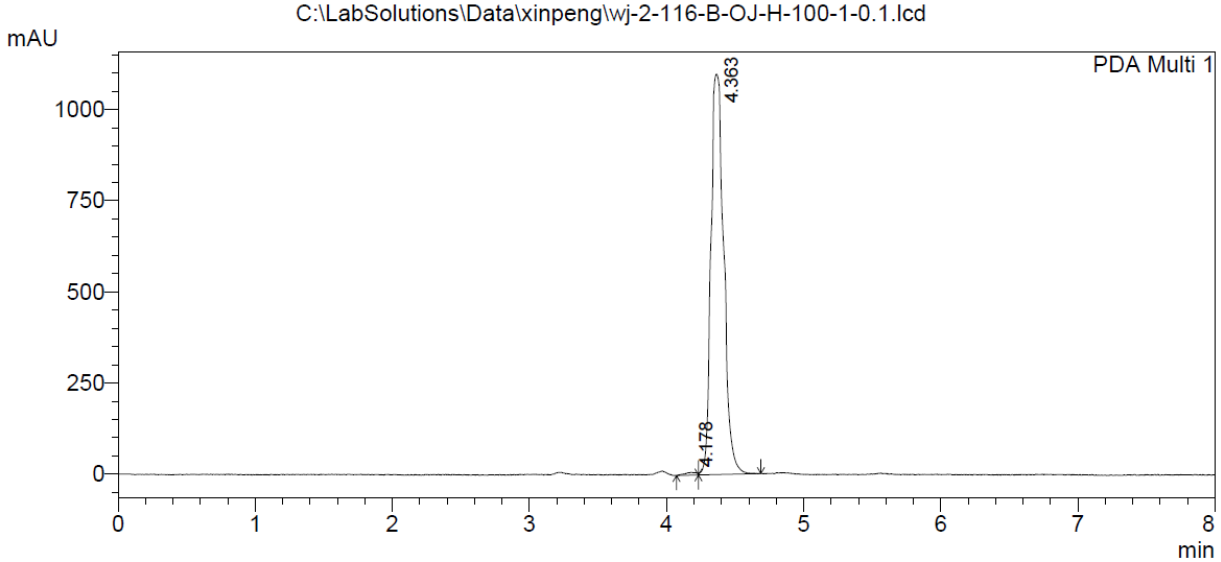

1 PDA Multi 1/225nm 4nm

PeakTable

PDA Ch1 225nm 4nm

Peak#	Ret. Time	Area	Height	Area %	Height %
1	4.178	45766	7399	0.638	0.669
2	4.363	7132695	1097805	99.362	99.331
Total		7178461	1105204	100.000	100.000

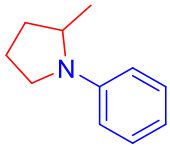

1k was prepared in a continuous flow reactor using 0.100 mol/L of aniline in 2-Me-THF flowing at 0.04 mL/min at 200 °C with 0.500 g ASA 3113 catalyst in a packed-bed column at 400 psi. The product was obtained as a yellow oil (95% yield). ^{1}H NMR (600 MHz, Chloroform-*d*) δ 7.22 – 7.17 (m, 2H), 6.64 – 6.60 (m, 1H), 6.56 (dt, *J* = 8.0, 1.1 Hz, 2H), 3.88 – 3.81 (m, 1H), 3.39 (ddd, *J* = 9.1, 7.4, 2.6 Hz, 1H), 3.13 (td, *J* = 9.0, 7.0 Hz, 1H), 2.08 – 1.99 (m, 2H), 1.97 – 1.91 (m, 1H), 1.66 (m, 1H), 1.15 (d, *J* = 6.3 Hz, 3H). ^{13}C NMR (151 MHz, cdcl$_3$) δ 147.20, 129.12, 115.14, 111.76, 53.55, 48.12, 33.11, 23.28, 19.34.

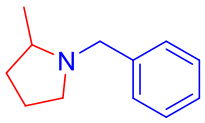

1l was prepared in a continuous flow reactor using 0.100 mol/L of benzylamine in 2-Me-THF flowing at 0.04 mL/min at 230 °C with 0.500 g ASA 3113 catalyst in a packed-bed column at 400 psi. The product was obtained as a yellow oil (90% yield). ^{1}H NMR (600 MHz, Chloroform-*d*) δ 7.34 – 7.26 (m, 4H), 7.23 – 7.20 (m, 1H), 4.01 (d, *J* = 12.8 Hz, 1H), 3.13 (d, *J* = 12.9 Hz, 1H), 2.89 (ddd, *J* = 9.0, 8.1, 2.5 Hz, 1H), 2.38 (ddd, *J* = 8.6, 7.2, 5.9 Hz, 1H), 2.09 (q, *J* = 9.0 Hz, 1H), 1.97 – 1.88 (m, 1H), 1.75 – 1.57 (m, 3H), 1.48 – 1.41 (m, 1H), 1.16 (d, *J* = 6.0 Hz, 3H). ^{13}C NMR (151 MHz, cdcl$_3$) δ 139.52, 129.04, 128.10, 126.72, 59.58, 58.33, 54.02, 32.74, 21.49, 19.14.

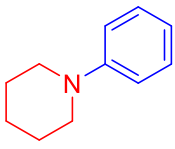

1m was prepared in a continuous flow reactor using 0.100 mol/L of aniline in toluene (pyran/aniline = 2.0/1.0 Equiv.) flowing at 0.04 mL/min at 250 °C with 1.00 g

ASA 3113 catalyst in a packed-bed column at 600 psi. The product was obtained as a yellow oil (99% yield). 1H NMR (600 MHz, Methanol-d4) δ 7.20 (dd, J = 8.7, 7.2 Hz, 2H), 6.96 (d, J = 8.1 Hz, 2H), 6.81 (t, J = 7.3 Hz, 1H), 3.16 – 3.06 (m, 4H), 1.70 (p, J = 5.7 Hz, 4H), 1.60 – 1.52 (m, 2H). 13C NMR (151 MHz, cd3od) δ 152.30, 128.52, 119.67, 116.95, 51.08, 25.49, 23.90.

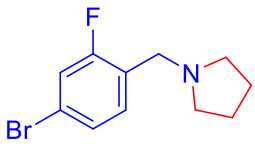

1o was prepared in a continuous flow reactor using 0.100 mol/L of 4-bromo-2-fluoroaniline in THF flowing at 0.04 mL/min at 220 °C with 0.500 g ASA 3113 catalyst in a packed-bed column at 400 psi. The product was obtained as yellow oil (96% yield) 1H NMR (600 MHz, Chloroform-d) δ 7.24 (t, J = 7.9 Hz, 1H), 7.19 (dd, J = 8.2, 2.0 Hz, 1H), 7.15 (dd, J = 9.3, 1.9 Hz, 1H), 3.58 (d, J = 1.5 Hz, 2H), 2.48 (m, 4H), 1.76 – 1.69 (m, 4H). 13C NMR (151 MHz, Chloroform-d) δ 160.76 (d, J = 250.8 Hz), 132.31 (d, J = 5.4 Hz), 127.14 (d, J = 3.5 Hz), 125.23 (d, J = 14.8 Hz), 120.65 (d, J = 9.7 Hz), 118.74 (d, J = 25.5 Hz), 53.87, 52.16, 23.45.

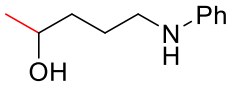

Intermediate **E**: 1H NMR (500 MHz, Chloroform-d) δ 7.21 – 7.15 (m, 2H), 6.73 (m, 1H), 6.68 – 6.63 (m, 2H), 3.85 (m, 1H), 3.15 (m, 2H), 2.87 (s, 1H), 1.73 (m, 2H), 1.60 – 1.53 (m, 2H), 1.21 (d, J = 6.2 Hz, 3H). 13C NMR (126 MHz, cdcl3) δ 148.00, 129.47, 118.10, 113.53, 68.05, 44.69, 36.97, 25.99, 23.89.

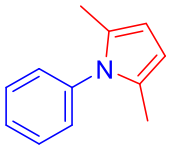

2a was prepared in a continuous flow reactor using 0.100 mol/L of aniline in toluene, 2,5-dimethylfuran/aniline = 1.2, flowing at 0.04 mL/min at 180 °C, with 0.500 g catalyst in a packed-bed reactor at 600 psi (>99% yield). 1H NMR (600 MHz, Chloroform-d) δ 7.42 – 7.38 (m, 2H), 7.36 – 7.32 (m, 1H), 7.19 – 7.16 (m, 2H), 5.89 (s, 2H), 2.01 (s, 6H). 13C NMR (151 MHz, CDCl3) δ 139.01, 128.99, 128.62, 128.21, 127.55, 105.72, 12.96 ppm.

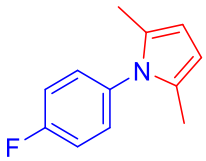

2b was prepared in a continuous flow reactor using 0.100 mol/L of 4-fluoroaniline in toluene, 2,5-dimethylfuran/amine = 1.2, flowing at 0.04 mL/min at 200 °C, with 0.500 g catalyst in a packed-bed reactor at 600 psi (90% yield). 1H NMR (600 MHz, Methanol-d4) δ 7.16 m, 4H), 5.79 (s, 2H), 1.95 (s, 6H). 13C NMR (151 MHz, cd3od) δ 161.90 (d, J = 246.1 Hz), 135.22 (d, J = 3.0 Hz), 129.87 (d, J = 8.7 Hz), 128.08, 115.51 (d, J = 22.8 Hz), 105.50, 11.63 ppm.

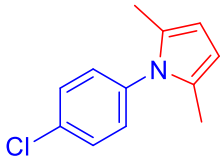

2c was prepared in a continuous flow reactor using 0.100 mol/L of 4-chloroaniline in toluene, 2,5-dimethylfuran/amine = 1.2, flowing at 0.04 mL/min at 180 °C, with 1.00 g catalyst in a packed-bed reactor at 600 psi (94% yield). 1H NMR (600 MHz, Methanol-d4) δ 7.41 (d, J = 8.6 Hz, 2H), 7.07 (d, J = 8.5 Hz, 2H), 5.80 (s, 2H), 1.94 (s, 6H), 13C NMR (151 MHz, CD3OD) δ 140.52, 128.79, 126.49, 125.32, 120.75, 107.87, 107.66, 11.66..

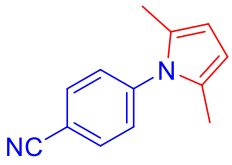

2d was prepared in a continuous flow reactor using 0.100 mol/L of 4-aminobenzonitrile in toluene, 2,5-dimethylfuran/amine = 1.2, flowing at 0.04 mL/min at 200 °C, with 0.500 g catalyst in a packed-bed reactor at 600 psi (90% yield). 1H NMR (600 MHz, Methanol-d4) δ 7.87 – 7.82 (m, 2H), 7.39 – 7.35 (m, 2H), 5.84 (s, 2H), 2.00 (s, 6H). 13C NMR (151 MHz, cd3od) δ 143.25, 132.97, 128.96, 127.90, 117.81, 111.00, 106.71, 11.70.

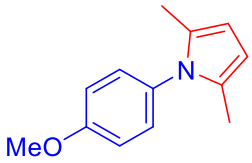

2e was prepared in a continuous flow reactor using 0.100 mol/L of 4-methoxyaniline in toluene, 2,5-dimethylfuran/aniline = 1.2, flowing at 0.04 mL/min at 200 °C, with 0.500 g catalyst in a packed-bed reactor at 600 psi (85% yield). 1H NMR (600 MHz, Chloroform-d δ 7.19 – 7.11 (m, 2H), 7.01 – 6.96 (m, 2H), 5.91 (s, 2H), 3.99 (s, 3H), 2.04 (s, 6H).13C NMR (151 MHz, CD3Cl3) δ 158.87, 131.77, 129.24, 129.06, 114.21, 105.26, 55.47, 12.97.

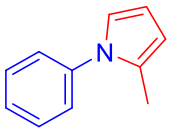

2f was prepared in a continuous flow reactor using 0.100 mol/L of aniline in toluene, 2-methylfuran/amine = 1.2, flowing at 0.04 mL/min at 200 °C, with 1.00 g catalyst in a packed-bed reactor at 600 psi (82% yield). 1H NMR (600 MHz, Methanol-d4) δ 7.38 (t, J = 7.9 Hz, 2H), 7.28 (t, J = 7.5 Hz, 1H), 7.25 – 7.20 (m, 2H), 6.67 (t, J = 2.3 Hz, 1H), 6.08 (s, 1H), 5.97 – 5.92 (m, 1H), 2.12 (s, 3H). 13C NMR (151 MHz, CD3OD) δ 140.52, 128.79, 126.49, 125.32, 120.75, 107.87, 107.66, 11.66.

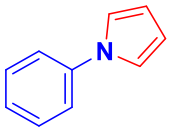

2g was prepared in a continuous flow reactor using 0.100 mol/L of aniline in toluene, furan/aniline = 1.2, flowing at 0.04 mL/min at 240 °C, with 0.500 g catalyst in a packed-bed reactor at 600 psi (83% yield). 1H NMR (600 MHz, Chloroform-d) δ 7.50 – 7.44 (m, 4H), 7.30 (m, 1H), 7.19 – 7.16 (m, 2H), 6.46 – 6.42 (m, 2H).

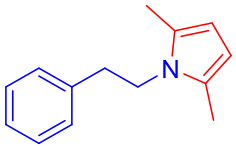

2h was prepared in a continuous flow reactor using 0.100 mol/L of 2-phenylethan-1-amine in toluene, 2,5-dimethylfuran/aniline = 1.2, flowing at 0.04 mL/min at 250 °C, with 1.50 g catalyst in a packed-bed reactor at 600 psi (90% yield). 1H NMR (600 MHz, Chloroform-d) δ 7.36 – 7.32 (m, 2H), 7.31 – 7.26 (m, 21), 7.15 – 7.12 (m, 2H), 4.00 (t, 2H), 2.93 (t, J = 7.2, 1.0 Hz, 2H), 2.20 (s, 6H). 13C NMR (151 MHz, CD3Cl3) δ 138.58, 128.88, 128.65, 127.40, 126.67, 105.21, 45.31, 37.58, 12.39 ppm.

NMR spectra (detected by the sample collected at the end of the flow reactor without purification)

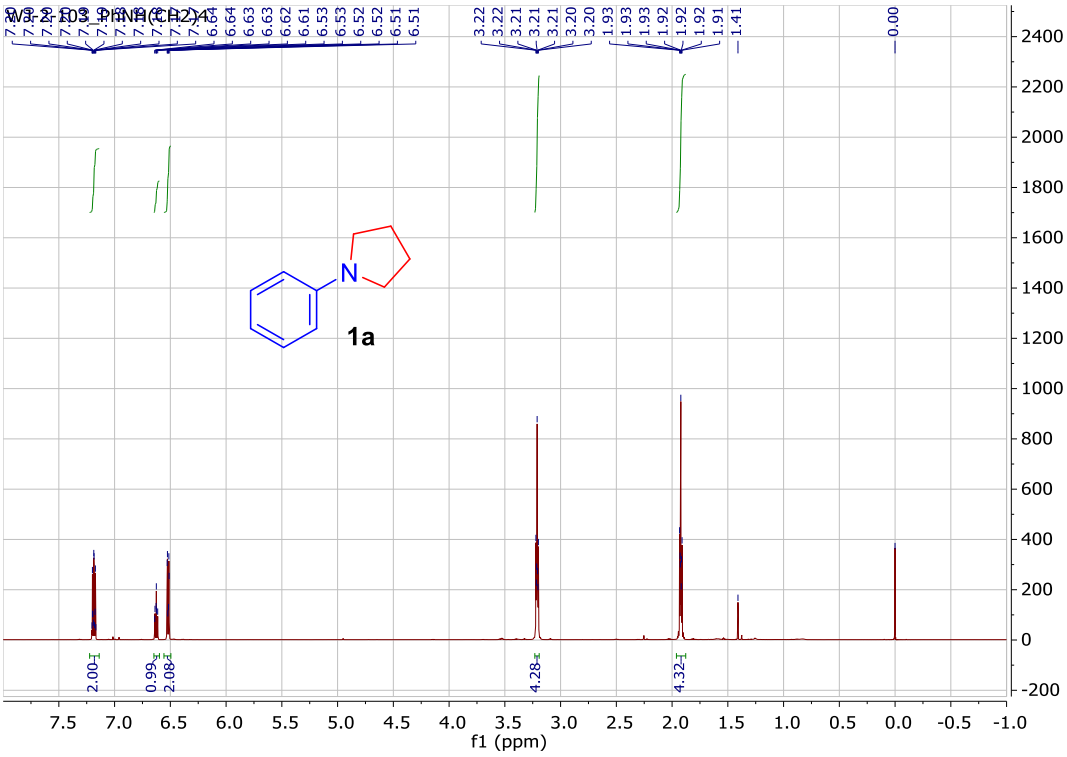
WJ-2-103_PhNH(CH2)4
1a
f1 (ppm)

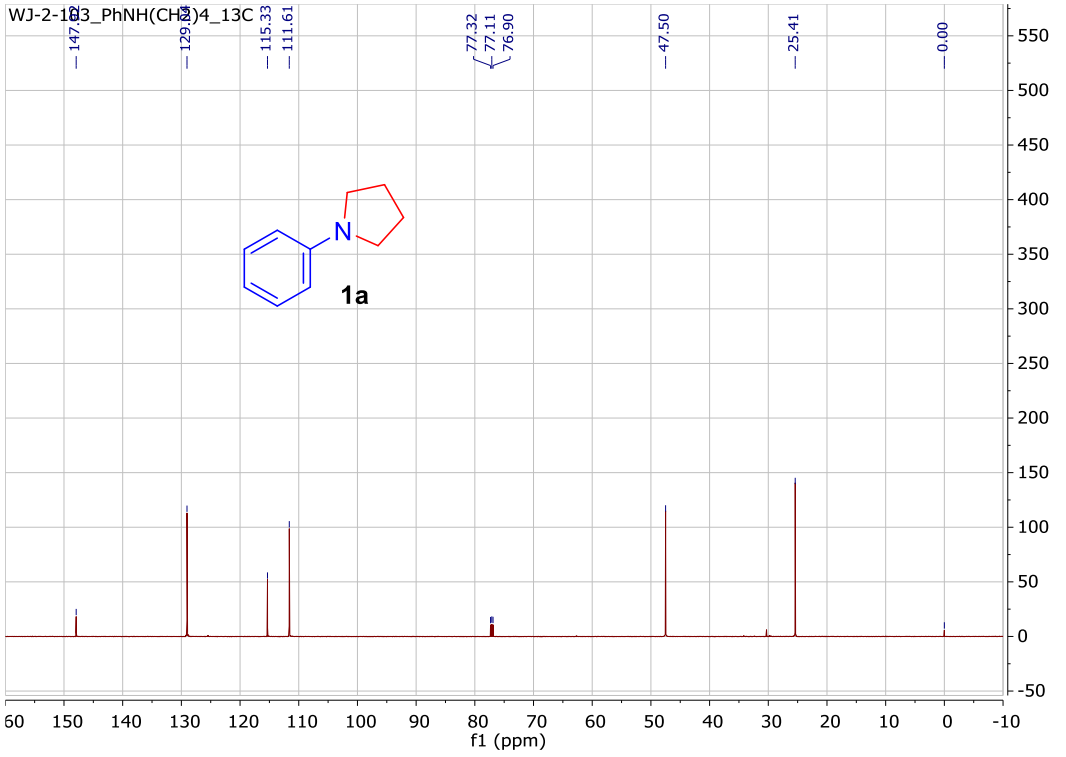
WJ-2-103_PhNH(CH2)4_13C
1a
f1 (ppm)

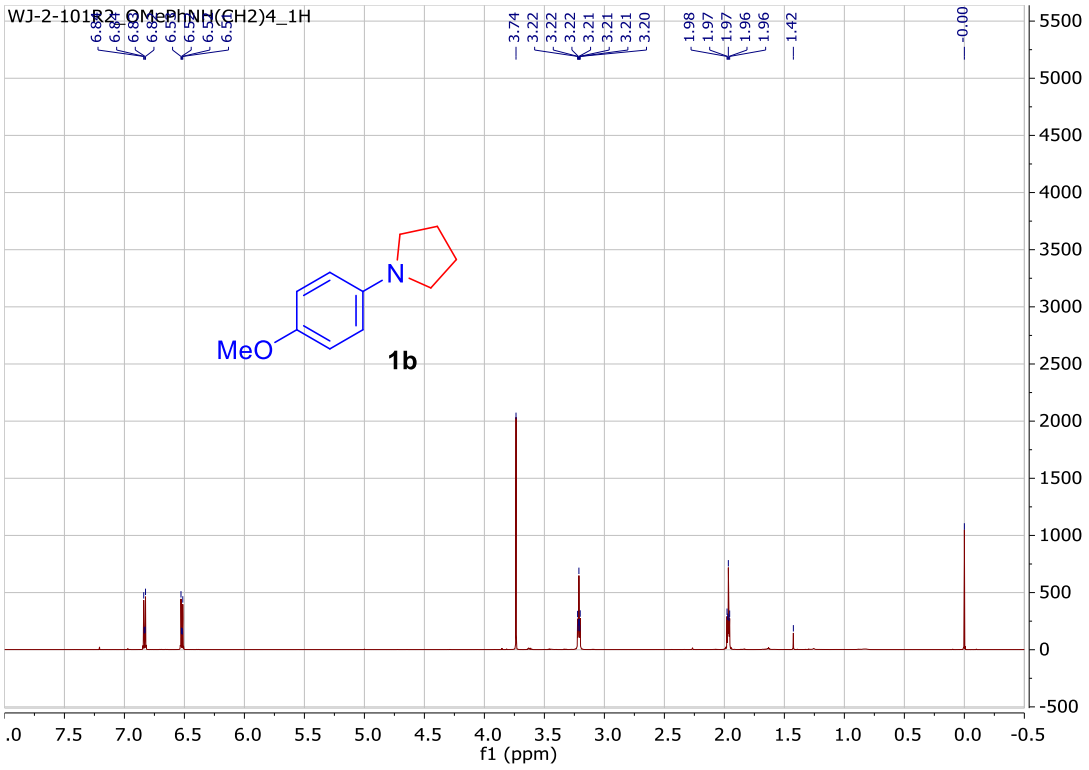
WJ-2-101R2_OMePhNH(CH2)4_1H
6.84
6.83
6.53
6.52
3.74
3.22
3.22
3.22
3.21
3.21
3.21
3.20
1.98
1.97
1.97
1.96
1.96
1.42
-0.00
N
MeO
1b
f1 (ppm)

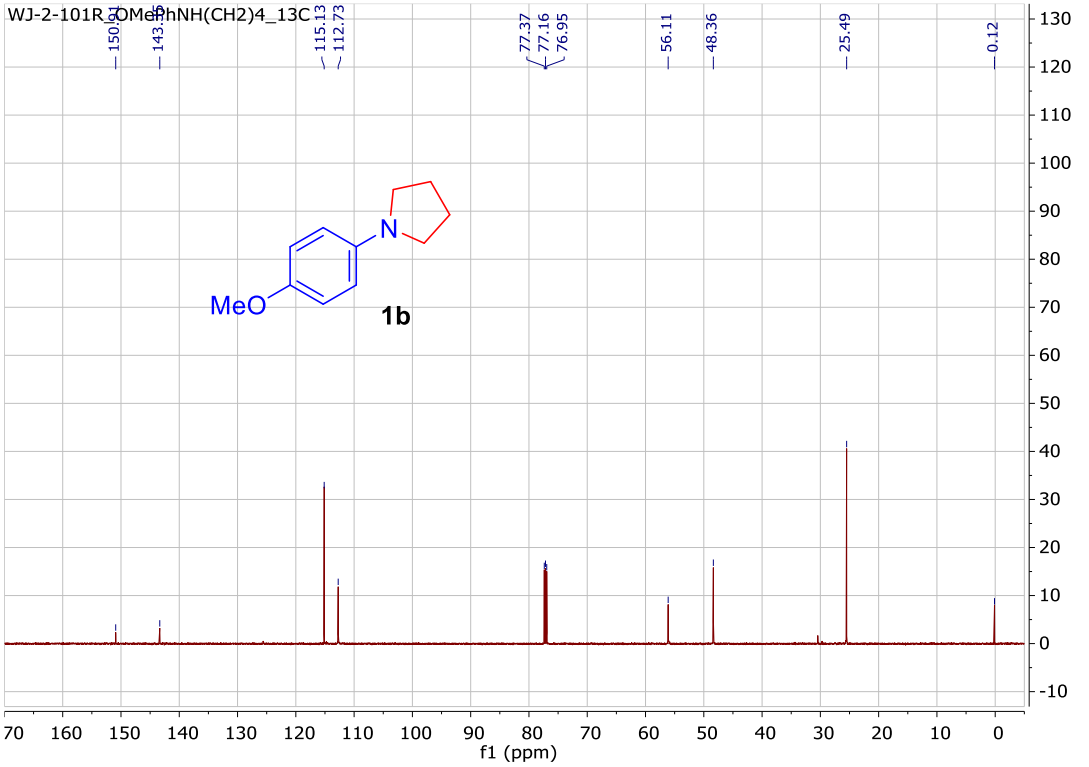
WJ-2-101R_OMePhNH(CH2)4_13C
150.01
143.80
115.13
112.73
77.37
77.16
76.95
56.11
48.36
25.49
0.12
N
MeO
1b
f1 (ppm)

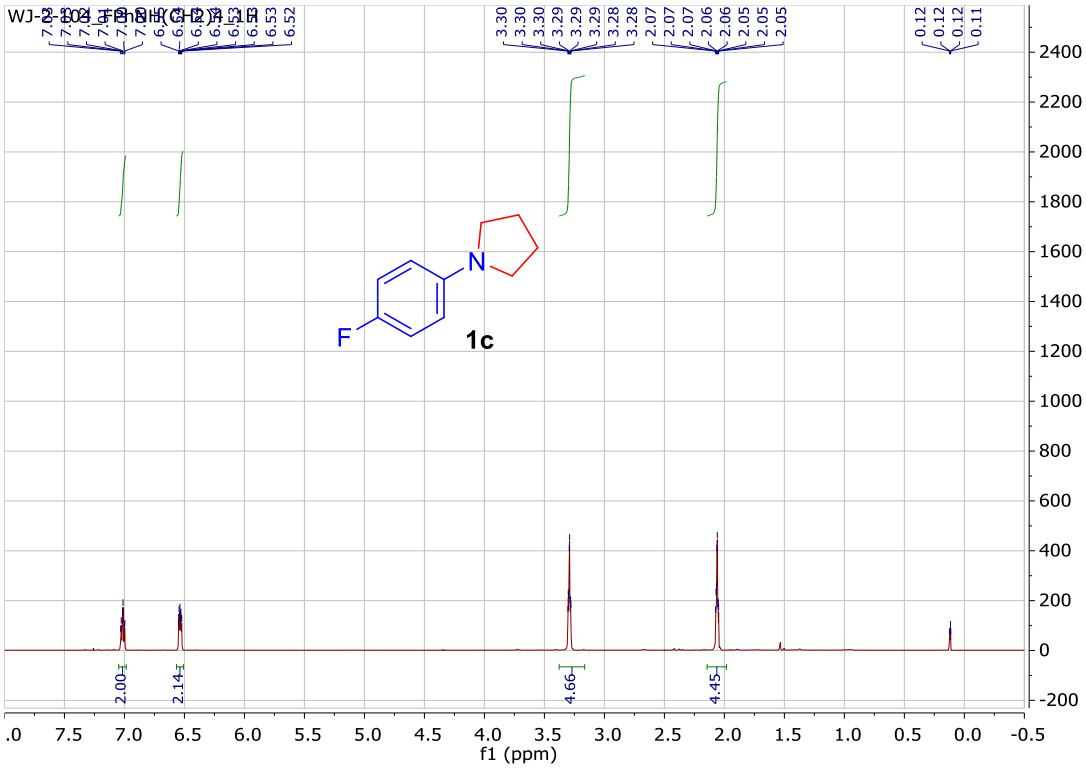
F
N
1c
f1 (ppm)

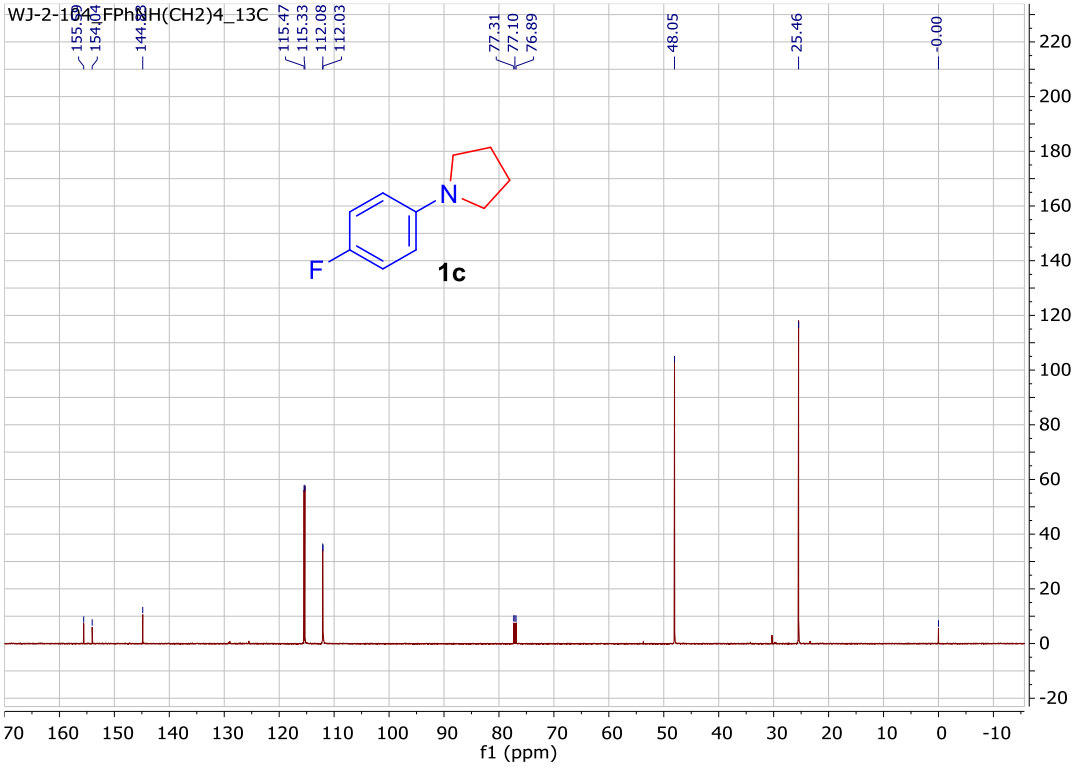
F
N
1c
f1 (ppm)

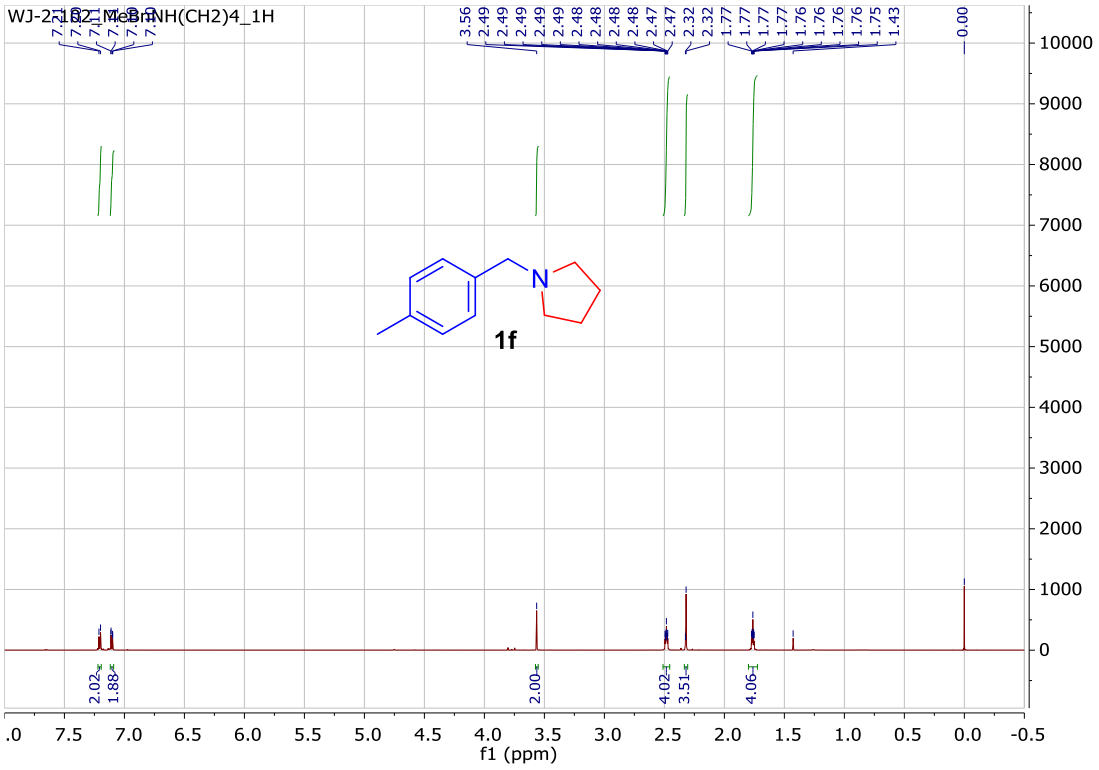
WJ-2-182_MeBnNH(CH2)4_1H
1f
f1 (ppm)

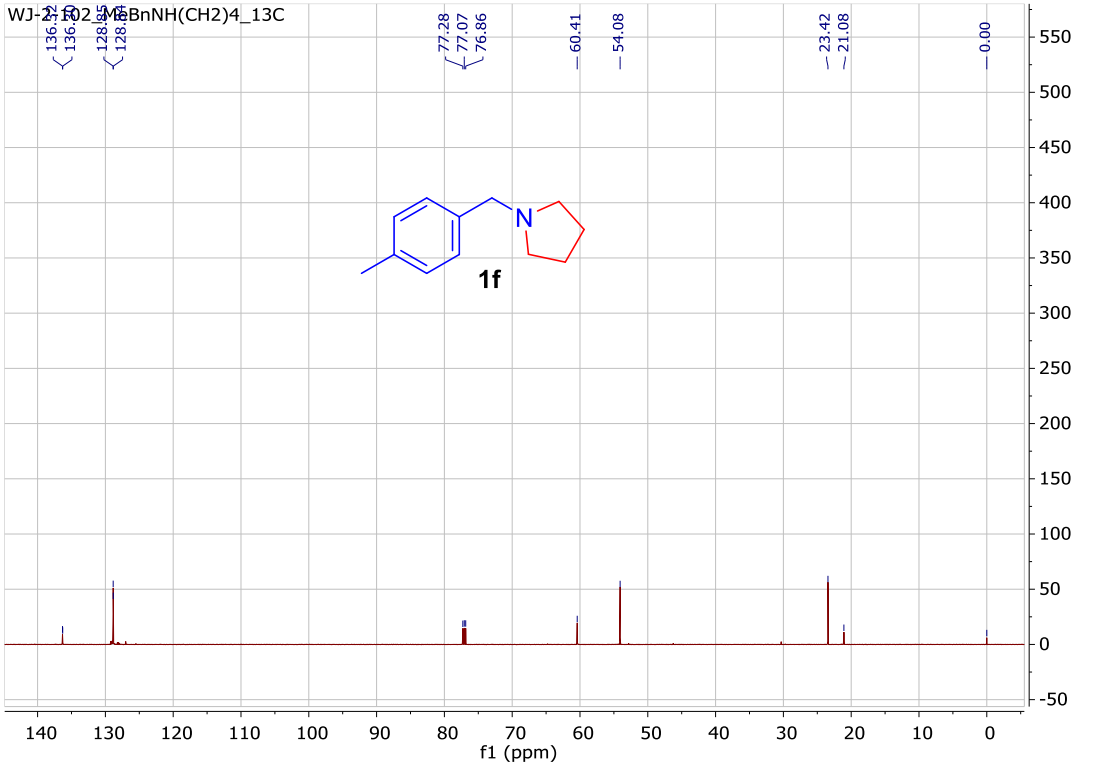
WJ-2-102_MeBnNH(CH2)4_13C
1f
f1 (ppm)

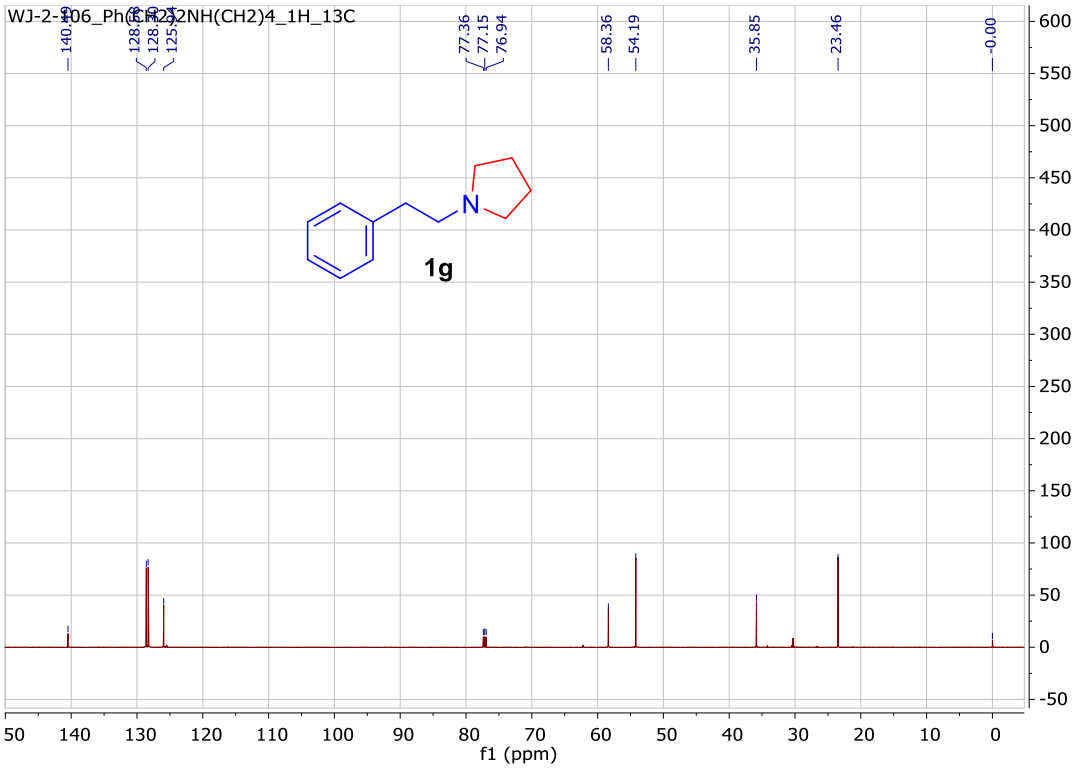
WJ-2-106_Ph(CH2)2NH(CH2)4_1H_13C
140.19
128.48
128.33
125.97
77.36
77.15
76.94
58.36
54.19
35.85
23.46
-0.00
1g
f1 (ppm)

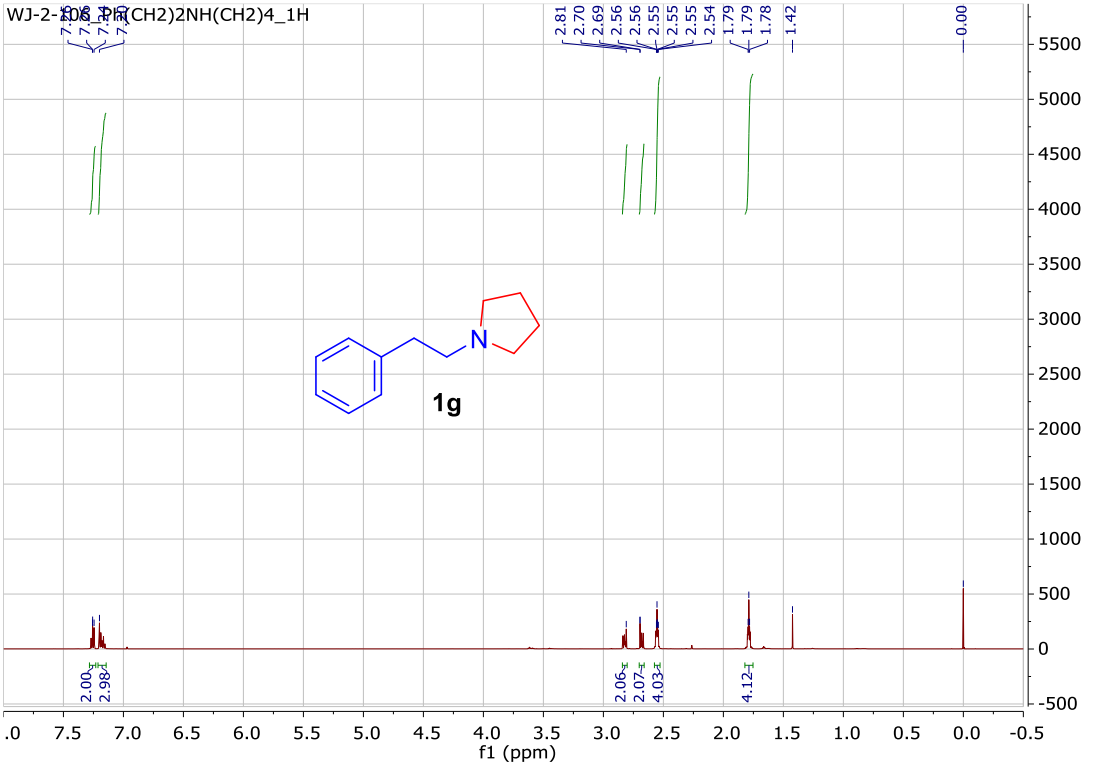
WJ-2-106_Ph(CH2)2NH(CH2)4_1H
2.81
2.70
2.69
2.56
2.56
2.55
2.55
2.55
2.54
1.79
1.79
1.78
1.42
0.00
2.00
2.98
2.06
2.07
4.03
4.12
1g
f1 (ppm)

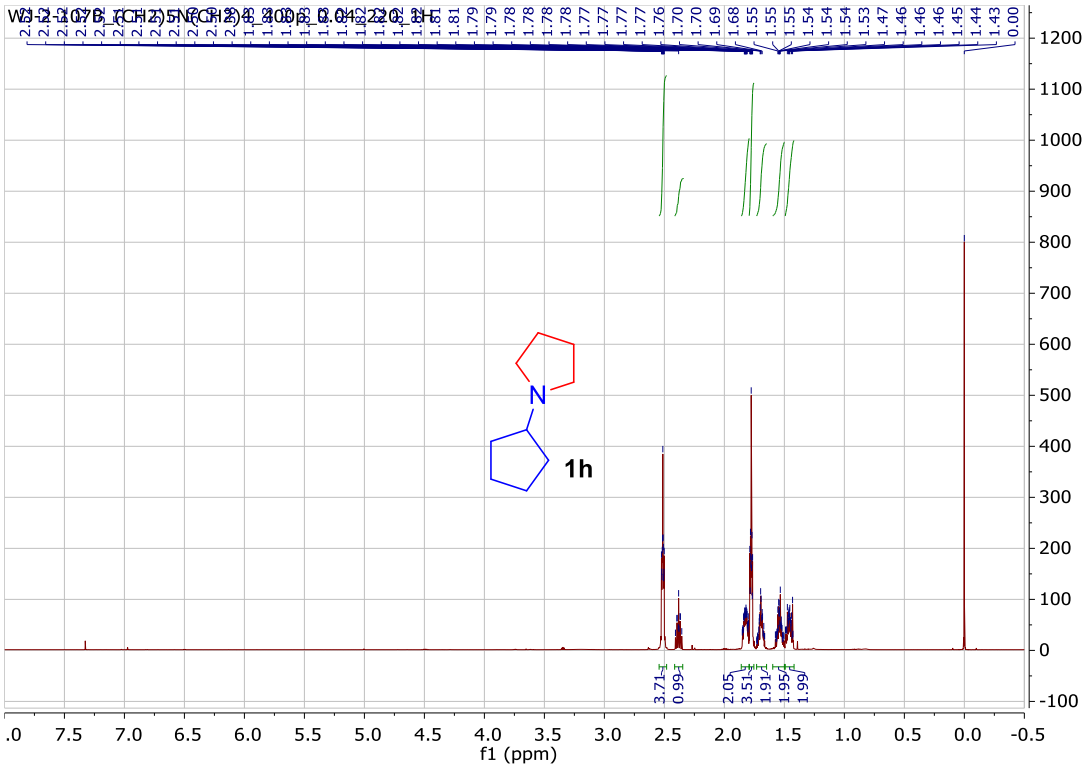
WJ-2-107B_(CH2)5N(CH2)4_400p_0.04_220_1H
1h
f1 (ppm)

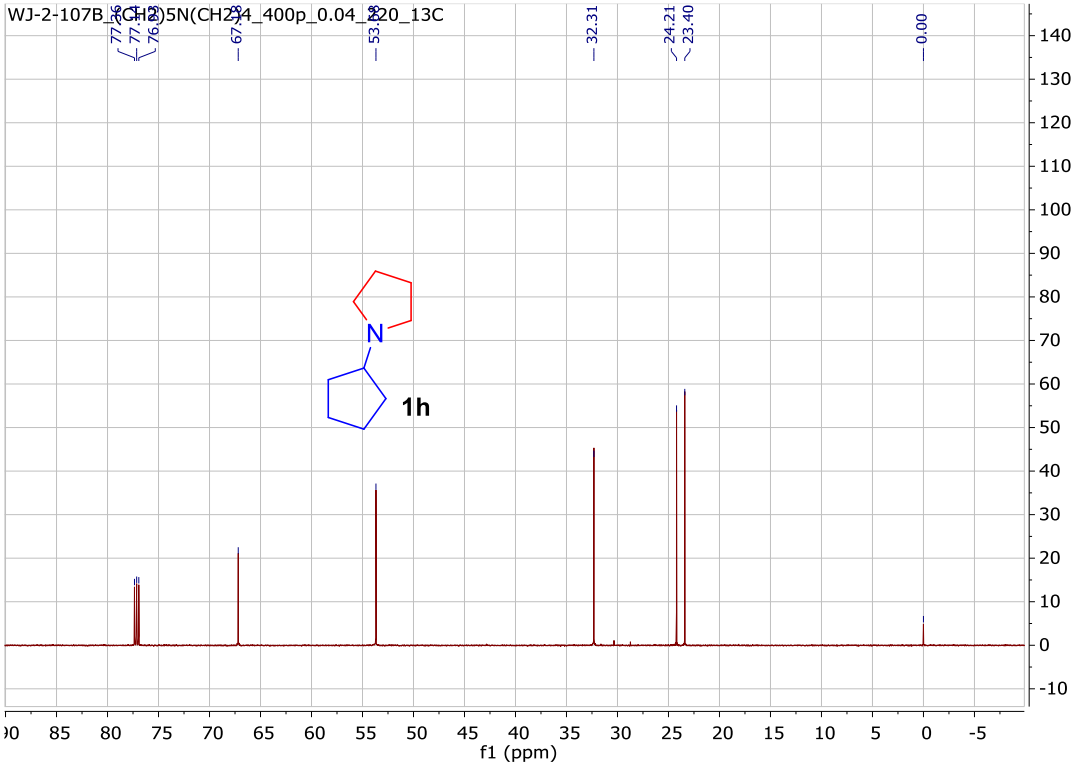
WJ-2-107B_(CH2)5N(CH2)4_400p_0.04_220_13C
77.16
77.41
76.91
67.28
53.88
32.31
24.21
23.40
0.00
1h
f1 (ppm)

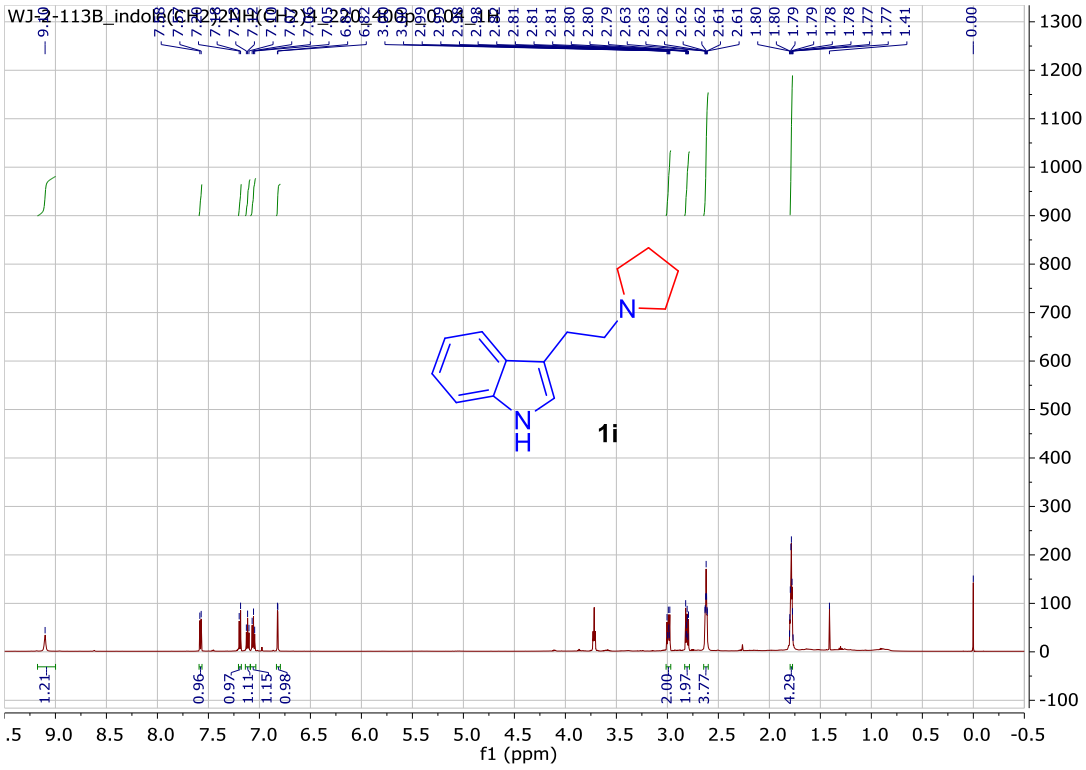
1i
f1 (ppm)

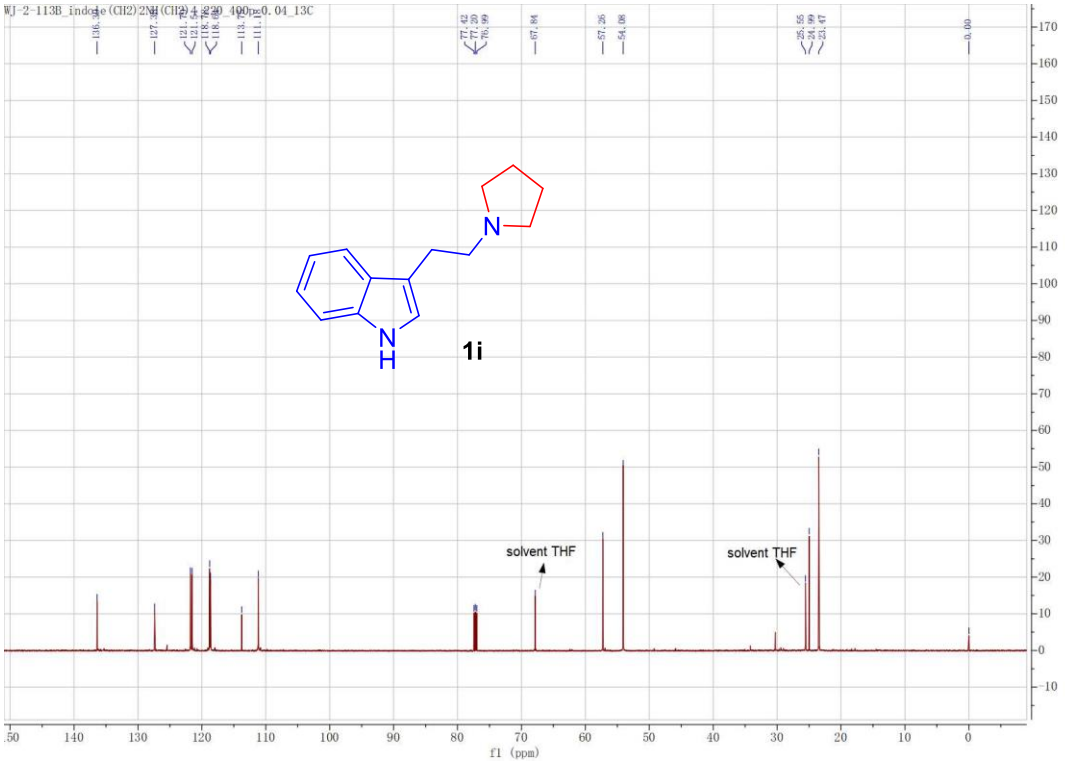
1i
solvent THF
solvent THF
f1 (ppm)

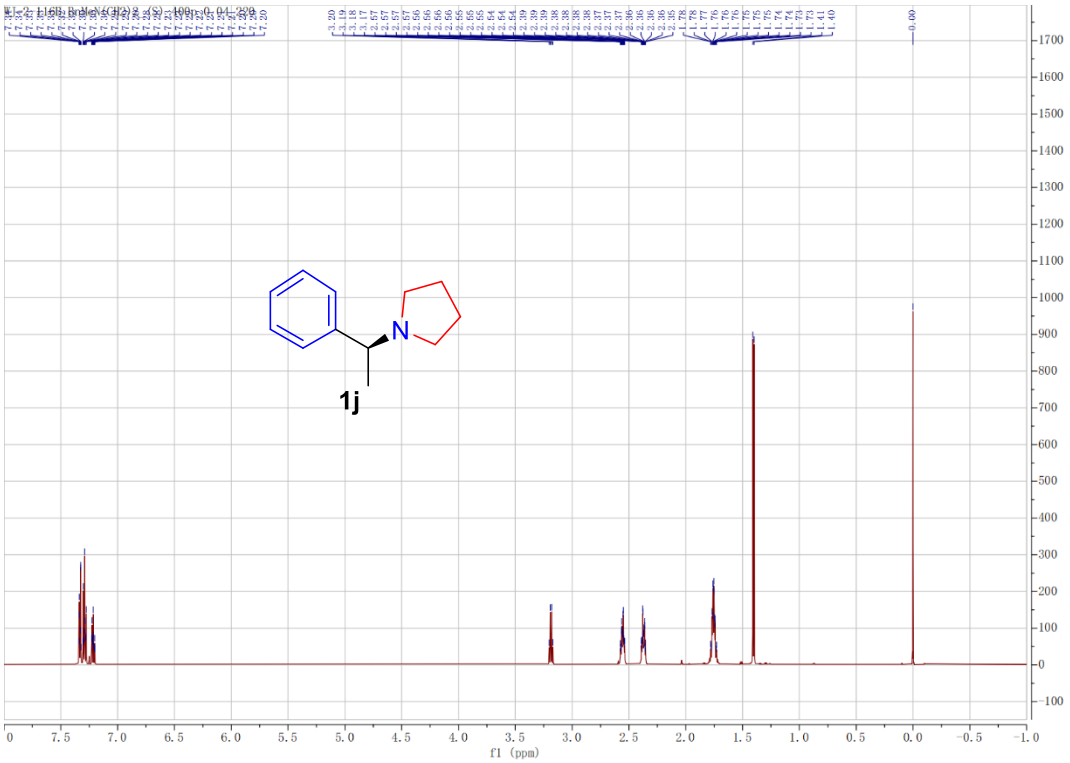
N
1j
f1 (ppm)

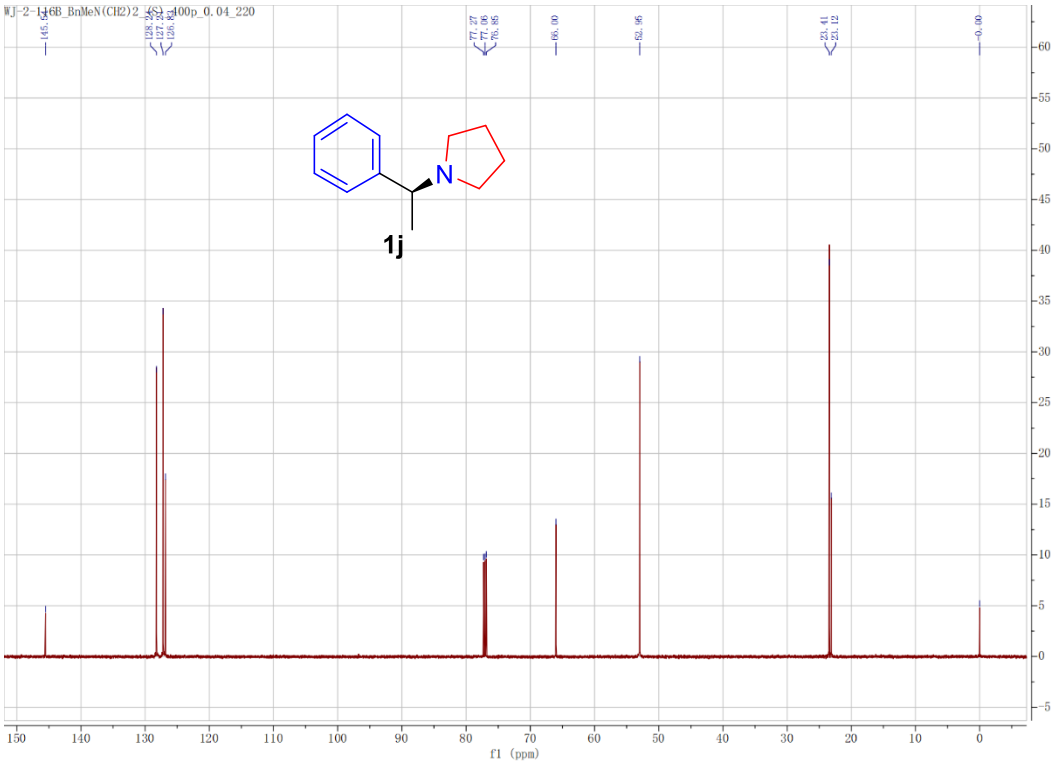
N
1j
f1 (ppm)

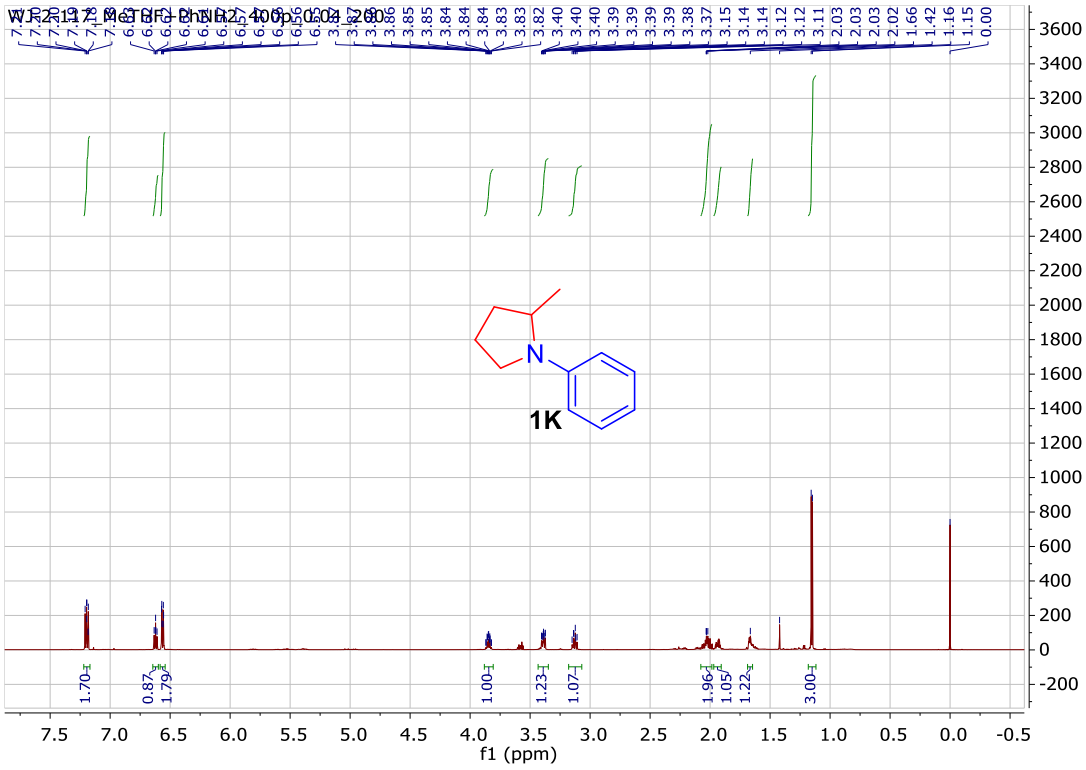
WJ-2-117_MeTHF+PhNH2_400p_0.04_200
1K
f1 (ppm)

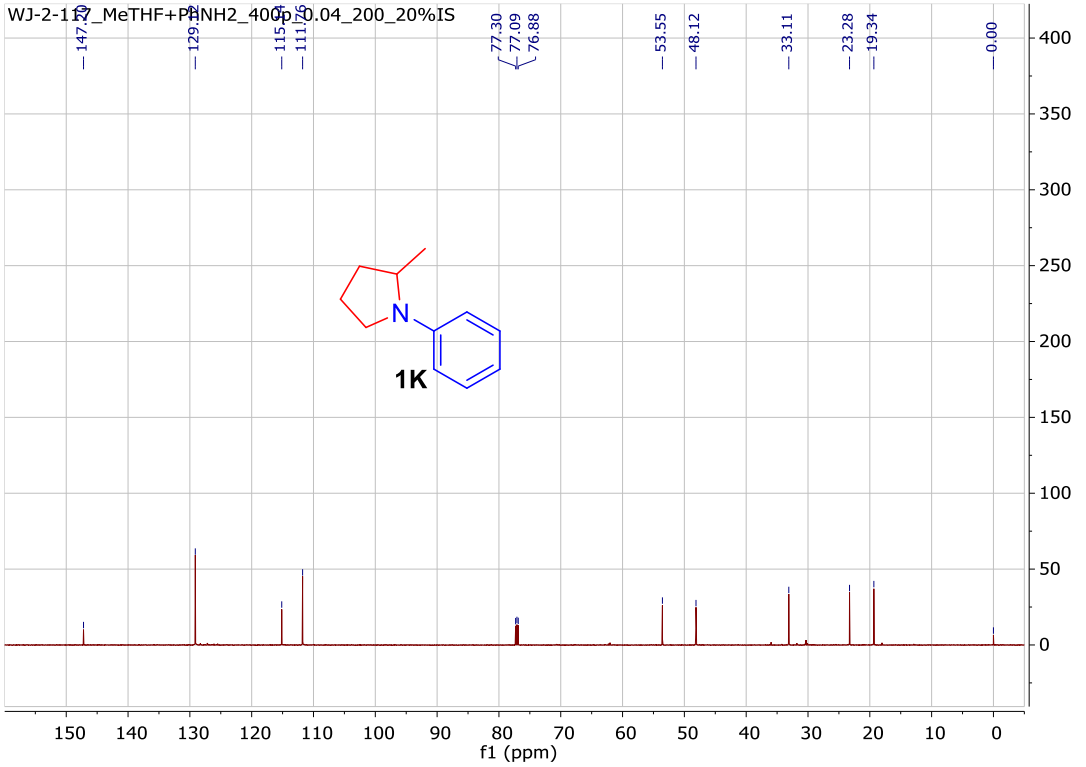
WJ-2-117_MeTHF+PhNH2_400p_0.04_200_20%IS
1K
f1 (ppm)

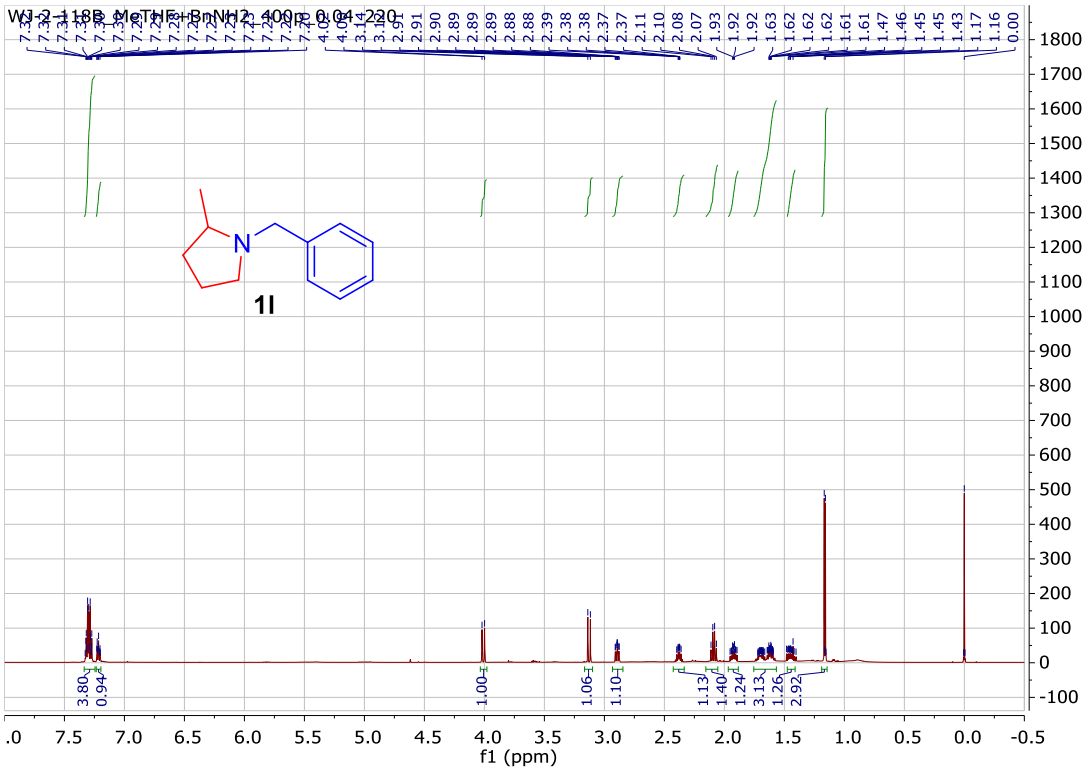
WJ-2-118B_MeTHF+BnNH2_400p_0.04_220
1l
f1 (ppm)

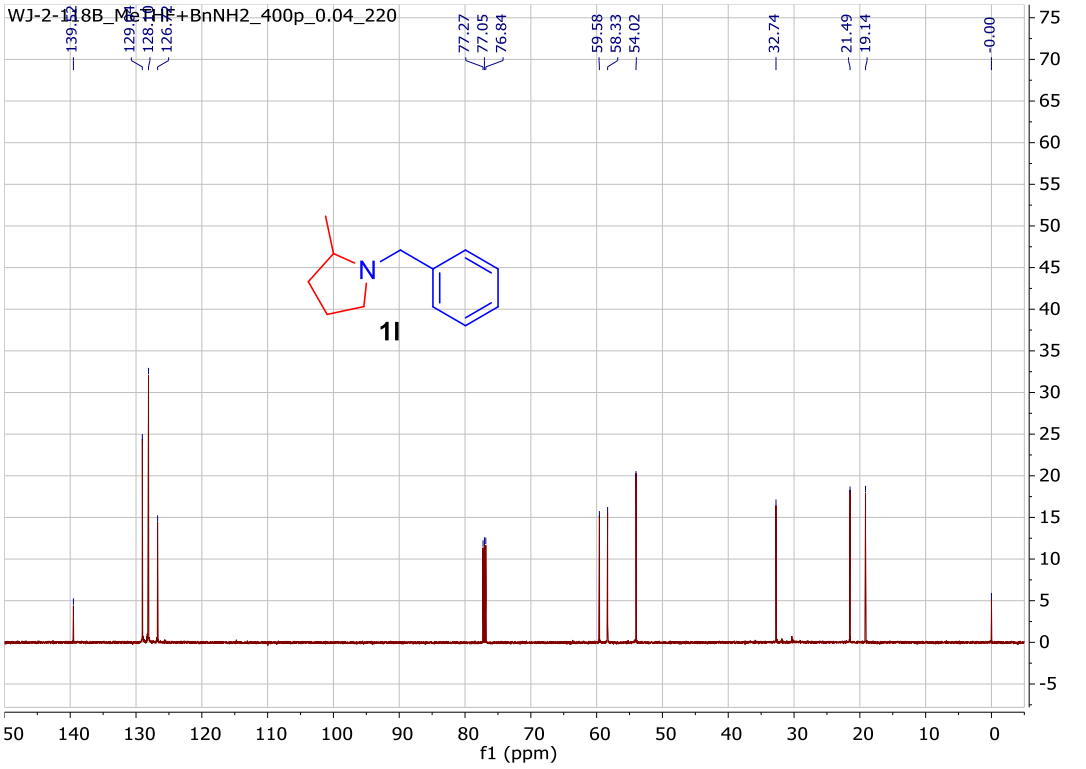
WJ-2-118B_MeTHF+BnNH2_400p_0.04_220
1l
f1 (ppm)

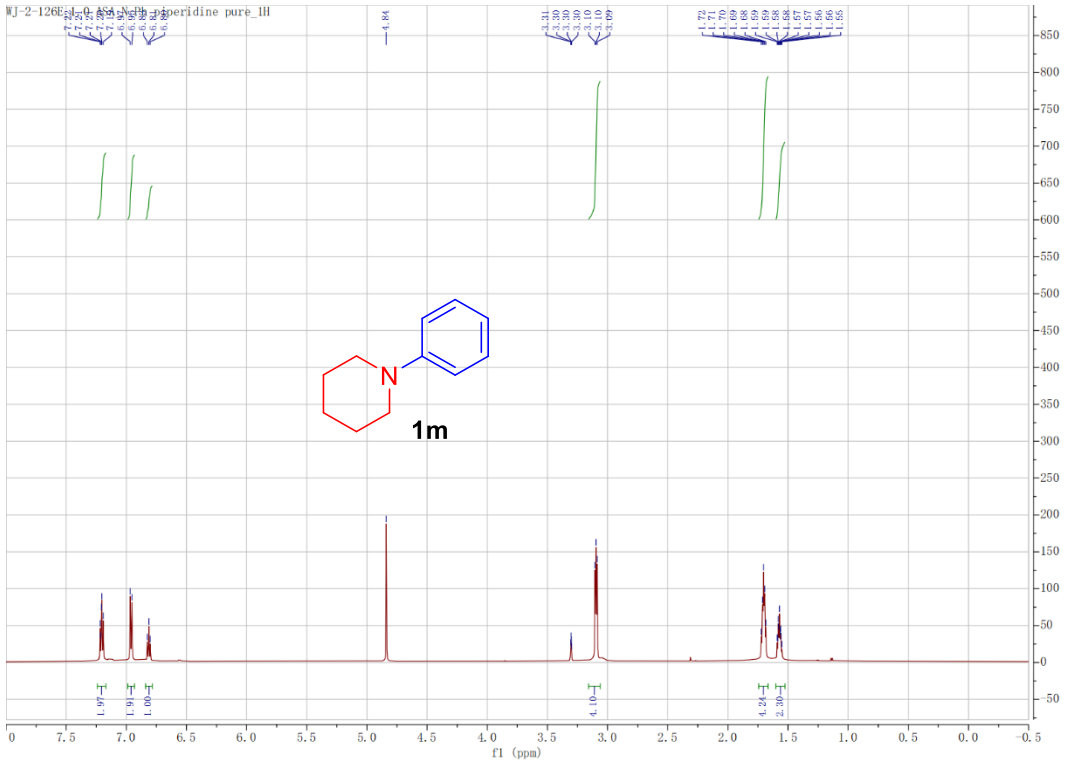
WJ-2-126E_1.0 ASA N-Ph piperidine pure_1H
1m
f1 (ppm)

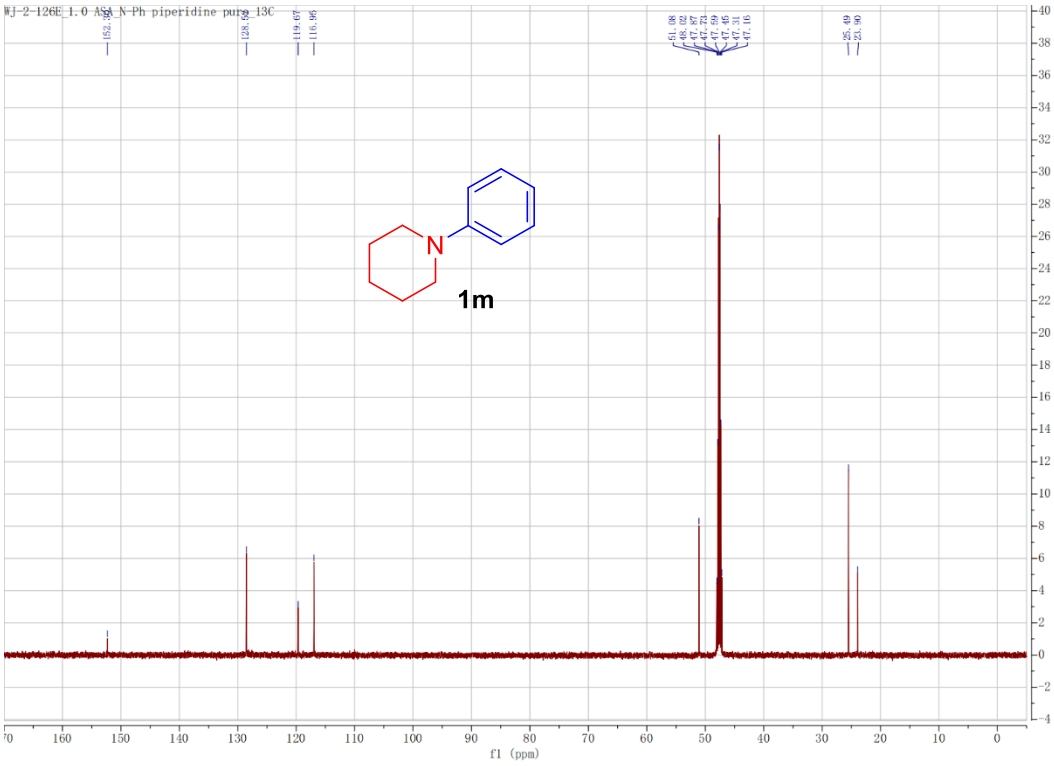
WJ-2-126E_1.0 ASA N-Ph piperidine pure_13C
1m
f1 (ppm)

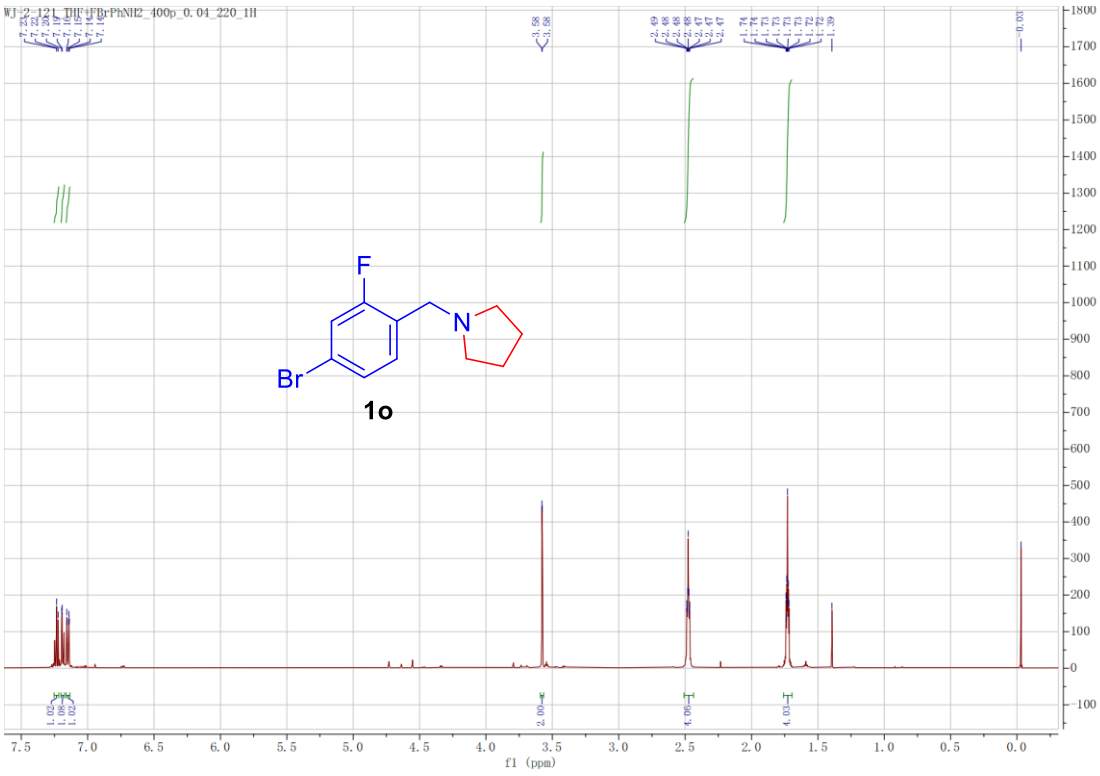
F
N
Br
1o
f1 (ppm)

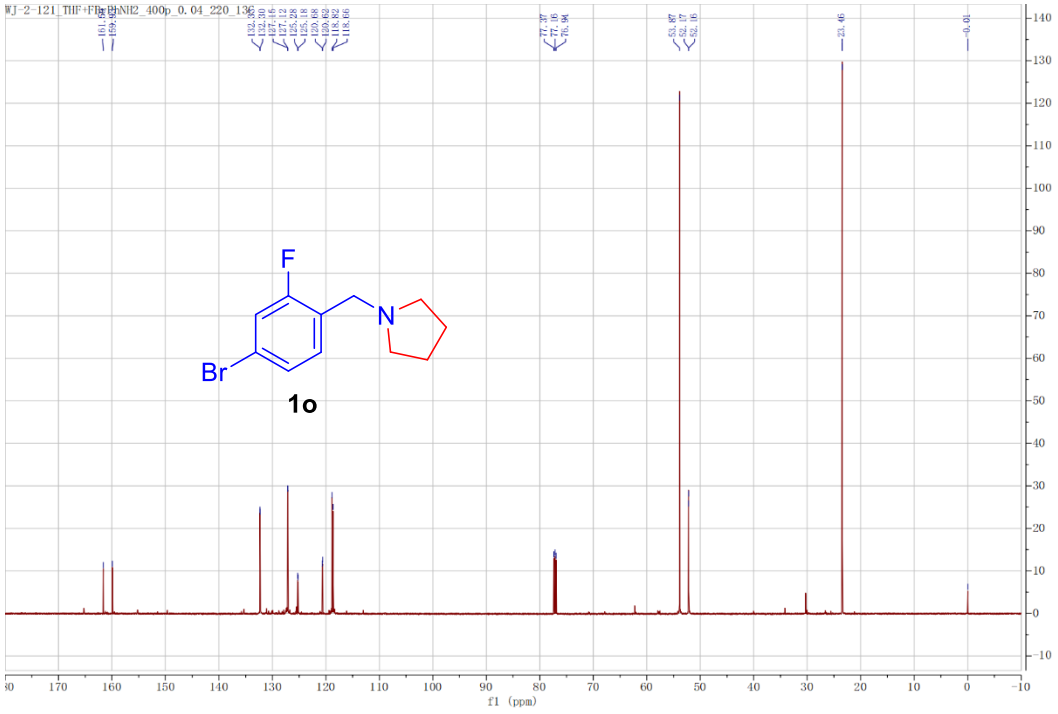
F
N
Br
1o
f1 (ppm)

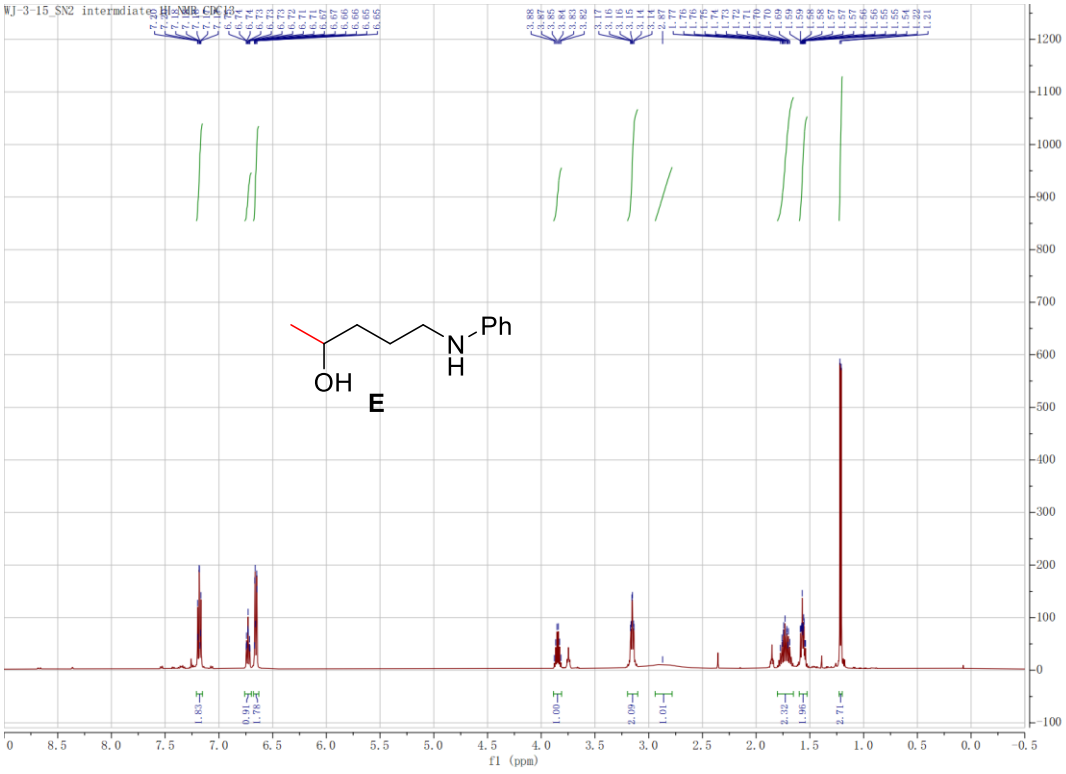
WJ-3-15_SN2 intermdiate_1H_NMR_CDCl3
Ph
N
H
OH
E
f1 (ppm)

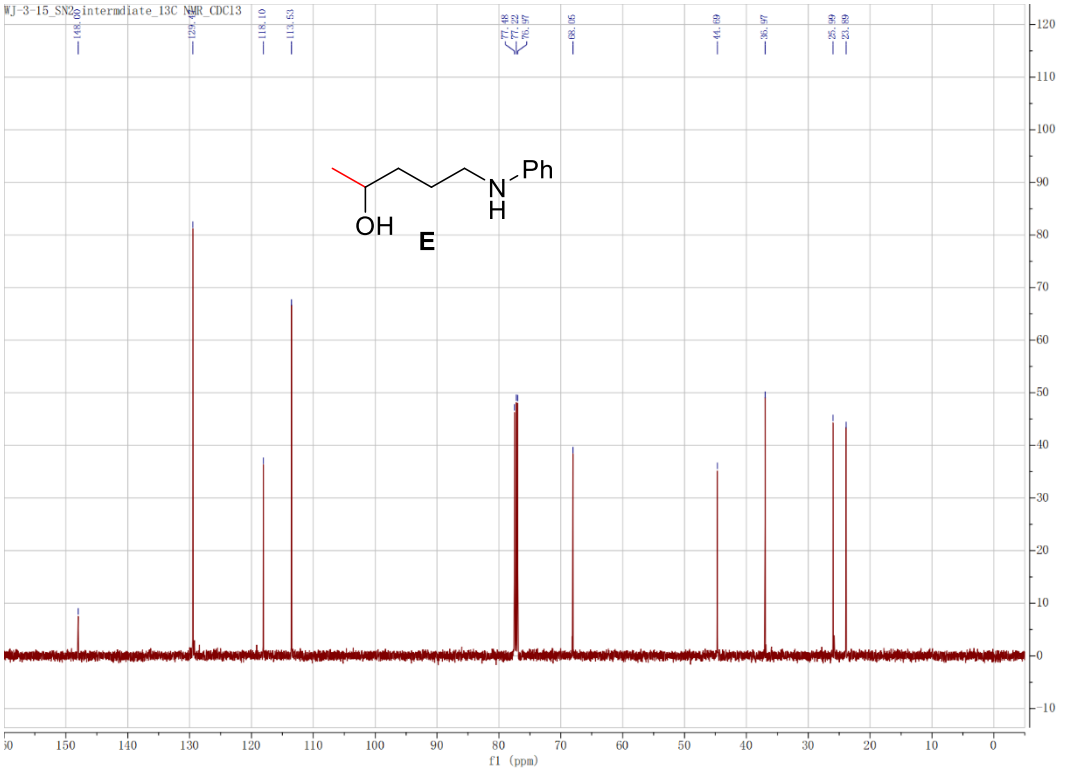
WJ-3-15_SN2 intermdiate_13C_NMR_CDCl3
Ph
N
H
OH
E
f1 (ppm)

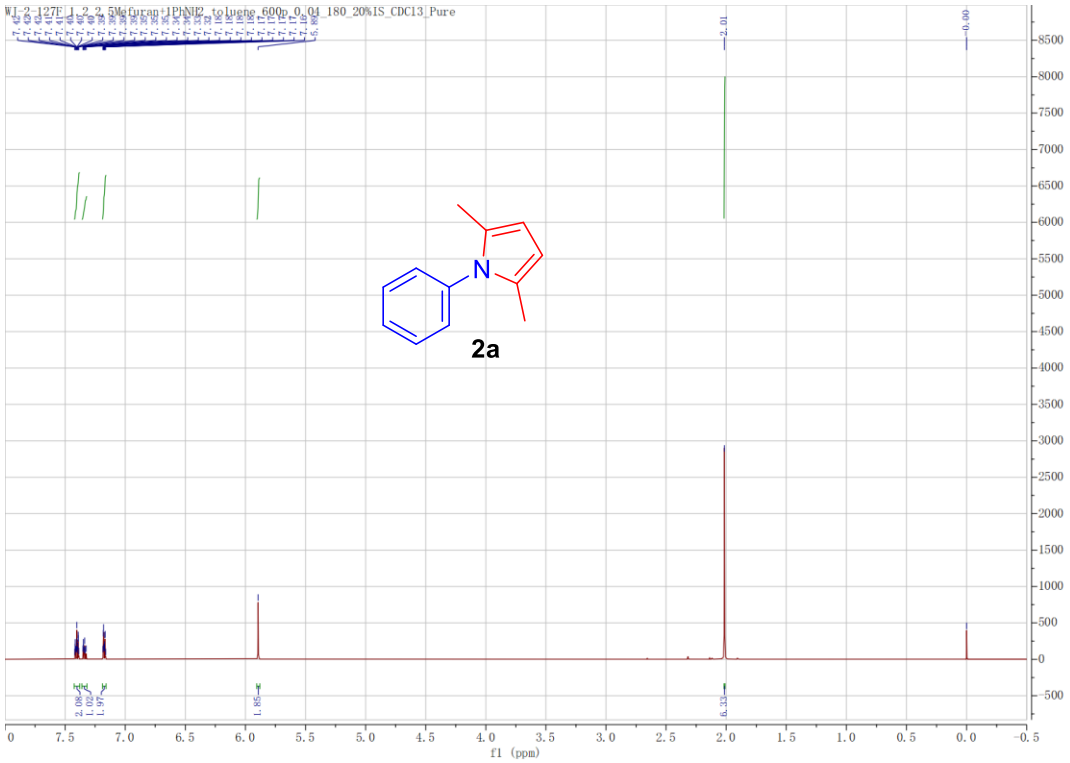
2a
f1 (ppm)

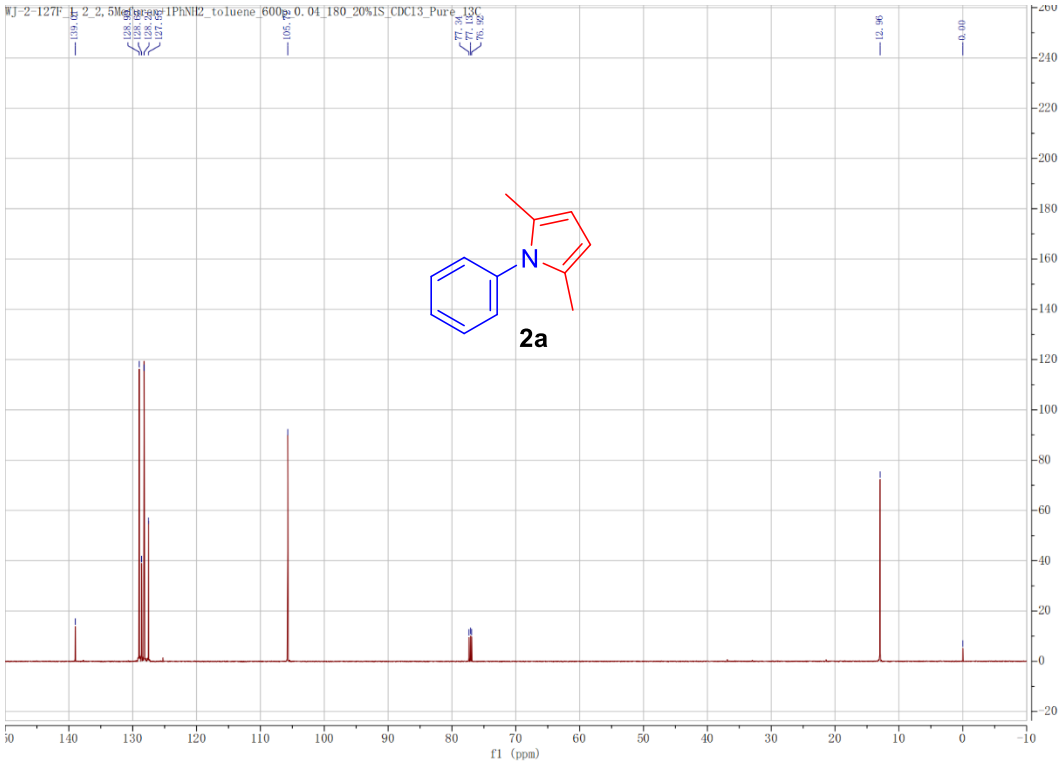
2a
f1 (ppm)

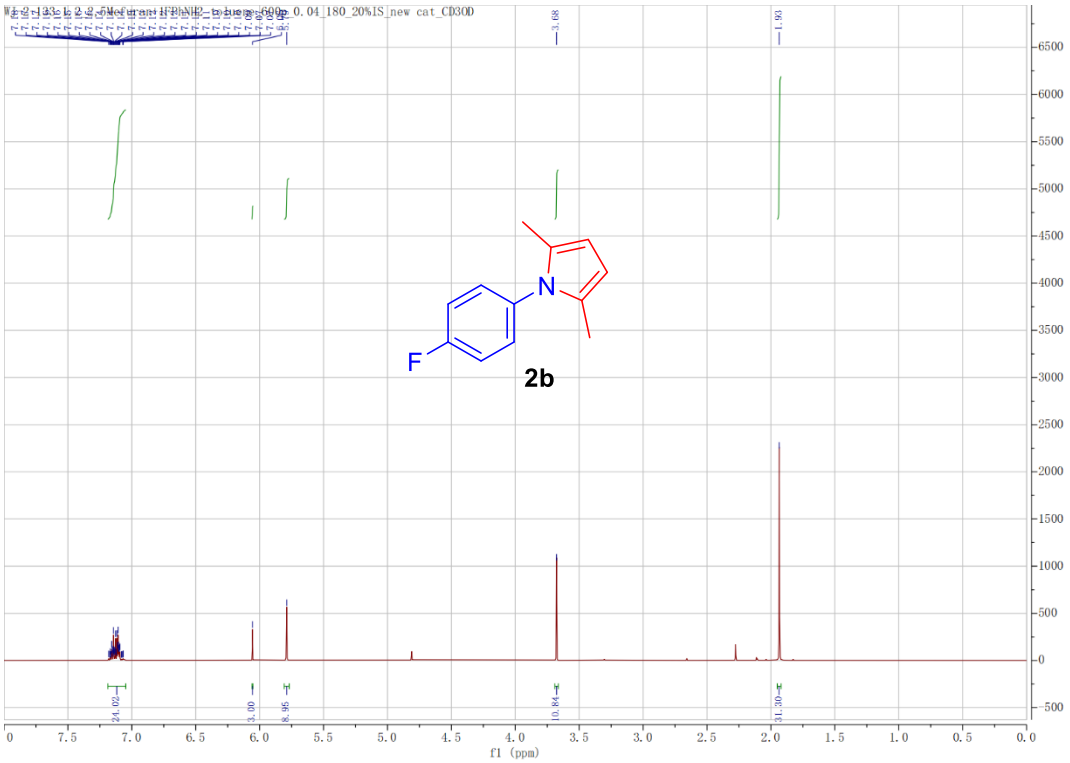
F
N
2b
f1 (ppm)

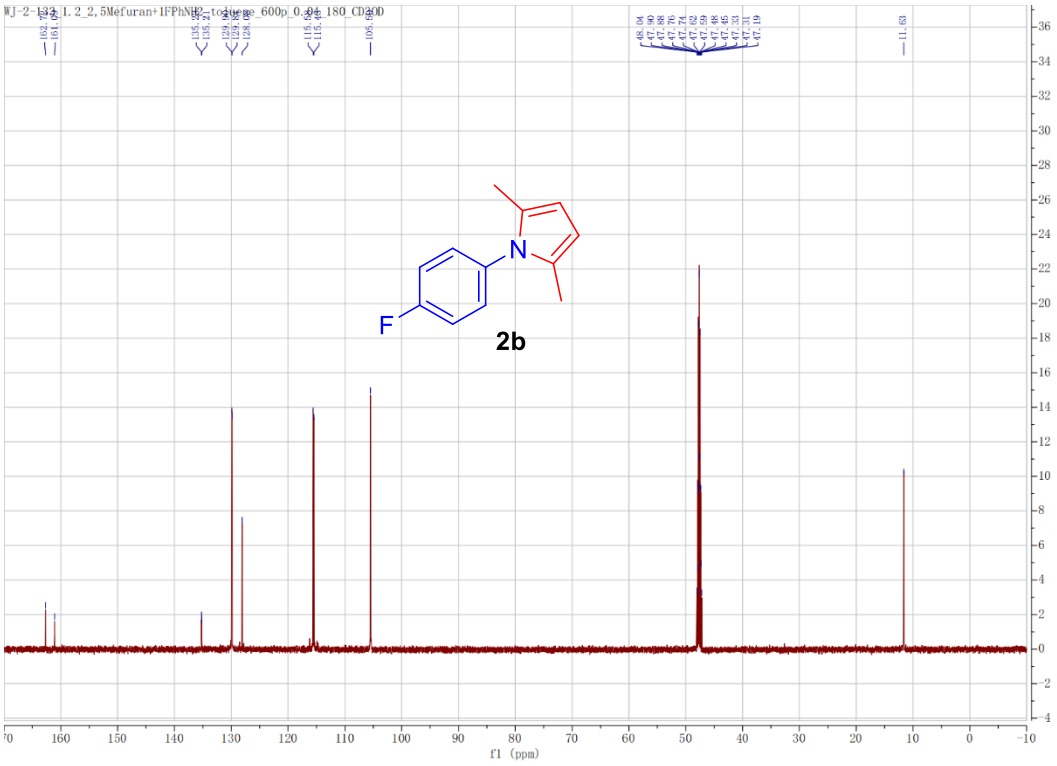
F
N
2b
f1 (ppm)

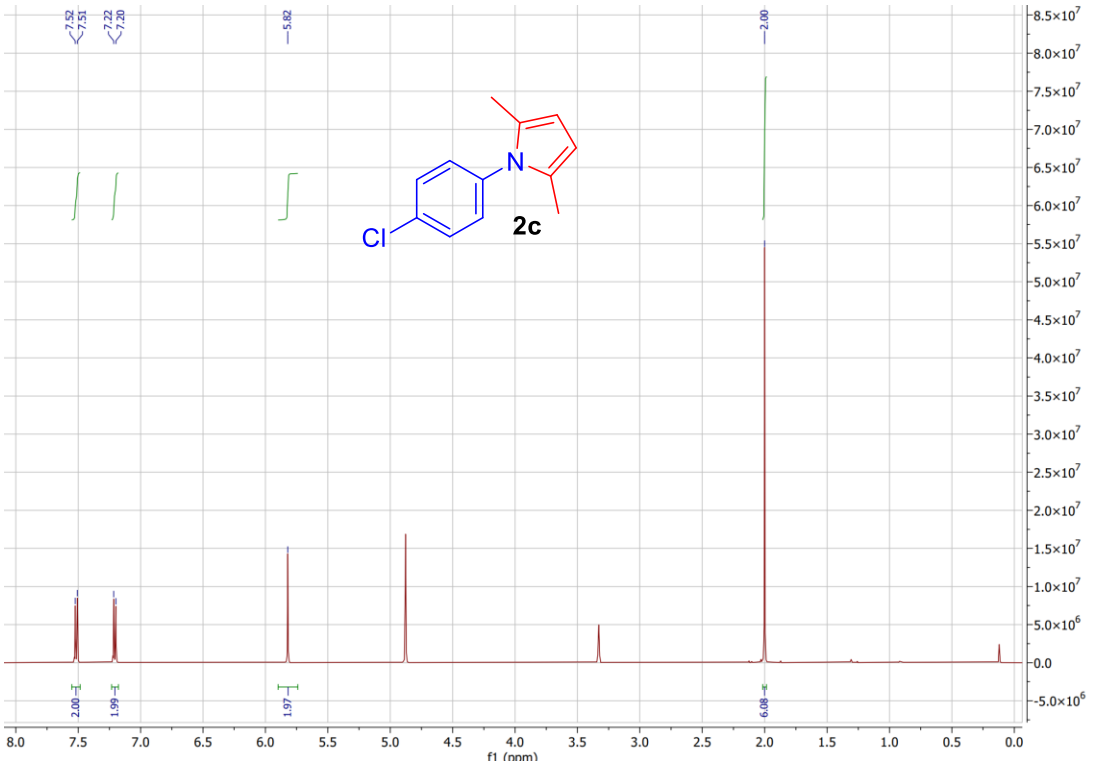
7.52
7.51
7.22
7.20
5.82
2.00
N
Cl
2c
2.00
1.99
1.97
6.08
f1 (ppm)

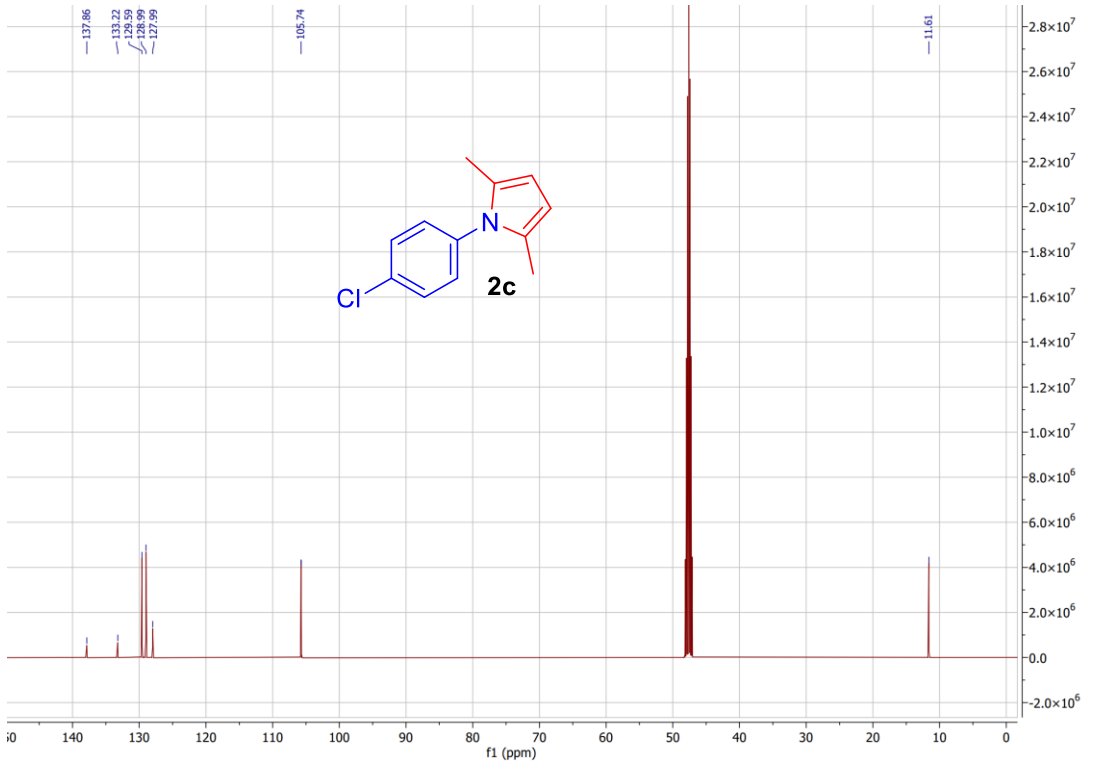
137.86
133.22
129.58
128.99
127.99
105.74
11.61
N
Cl
2c
f1 (ppm)

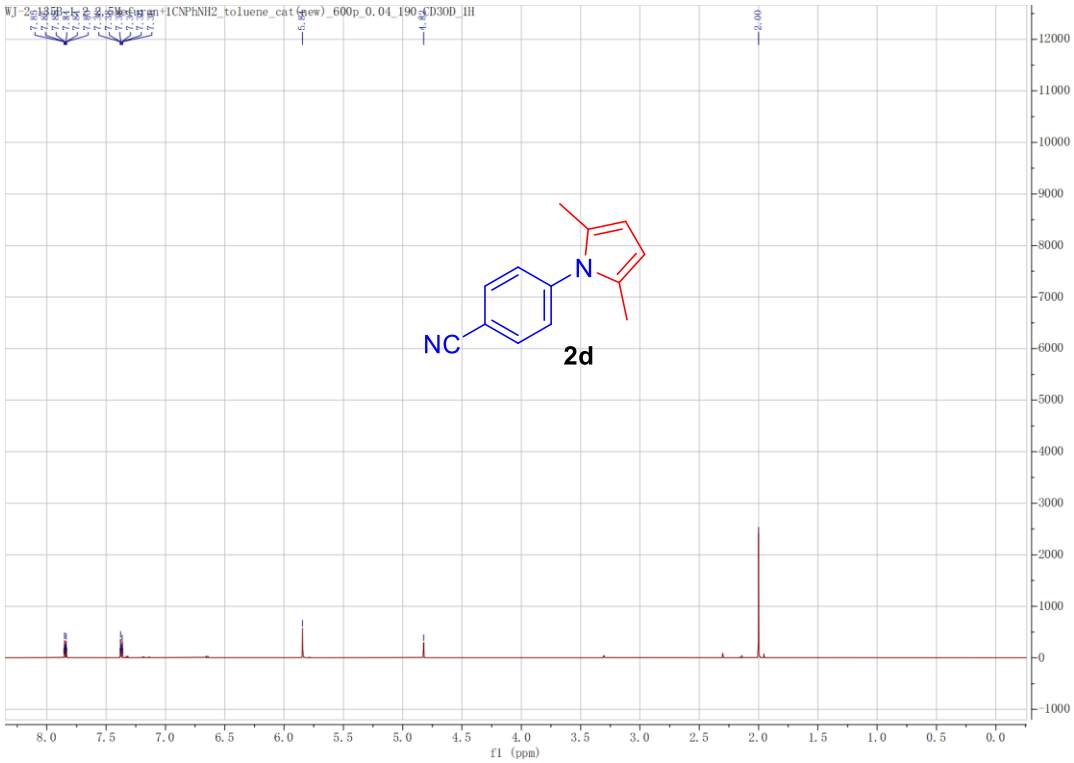
NC
N
2d
f1 (ppm)

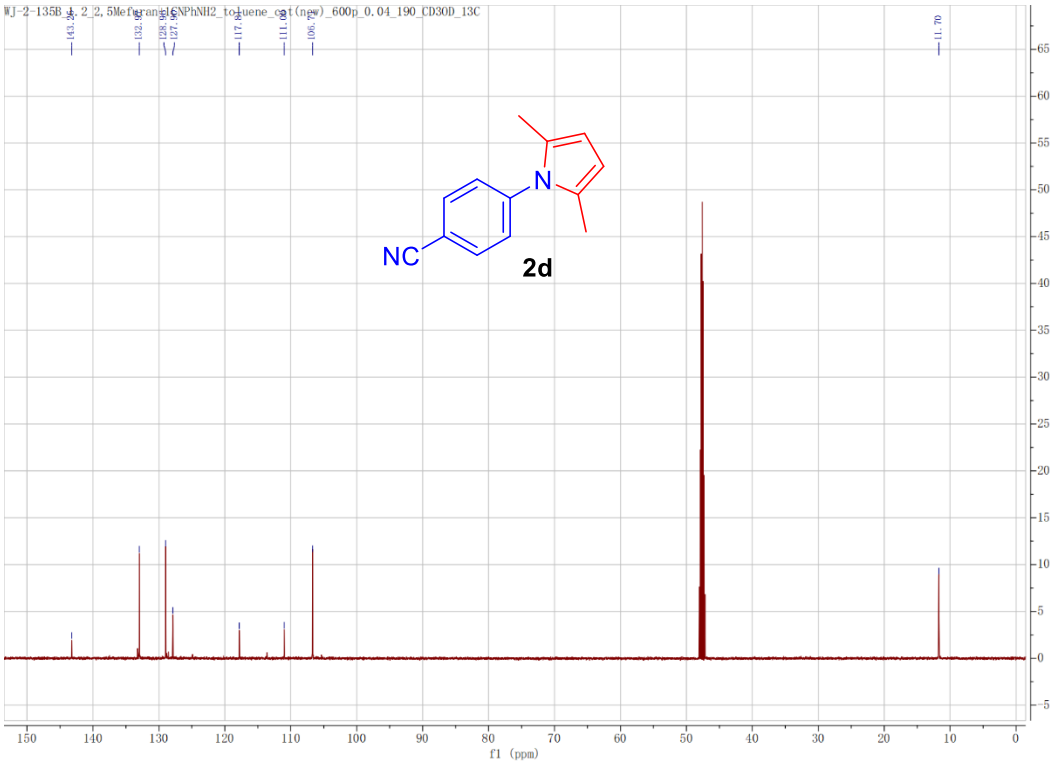
NC
N
2d
f1 (ppm)

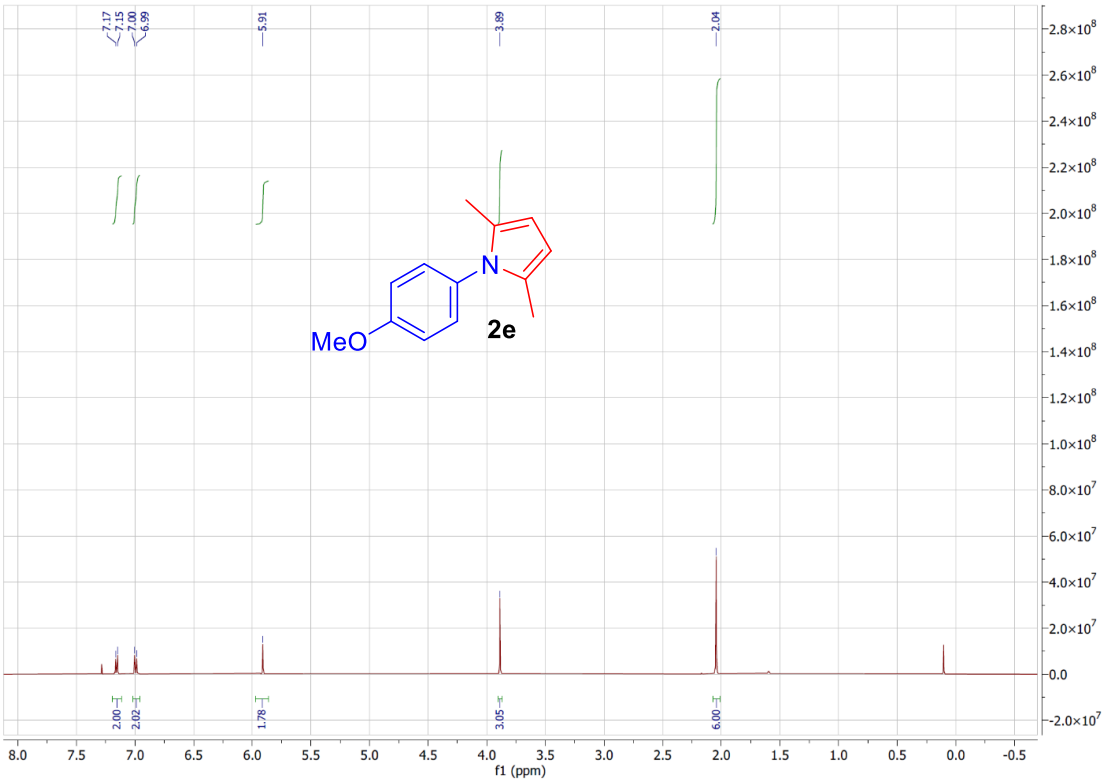
7.17
7.15
7.00
6.99
5.91
3.89
2.04
MeO
N
2e
2.00
2.02
1.78
3.05
6.00
f1 (ppm)

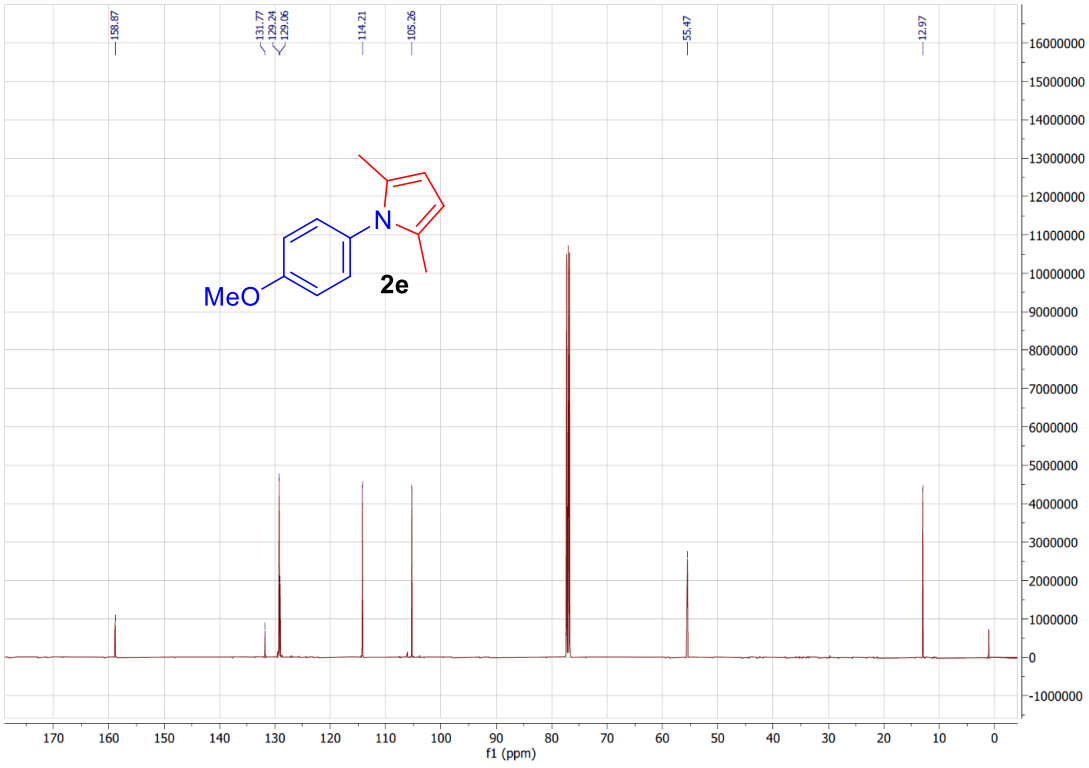
158.87
131.77
129.24
129.06
114.21
105.26
55.47
12.97
MeO
N
2e
f1 (ppm)

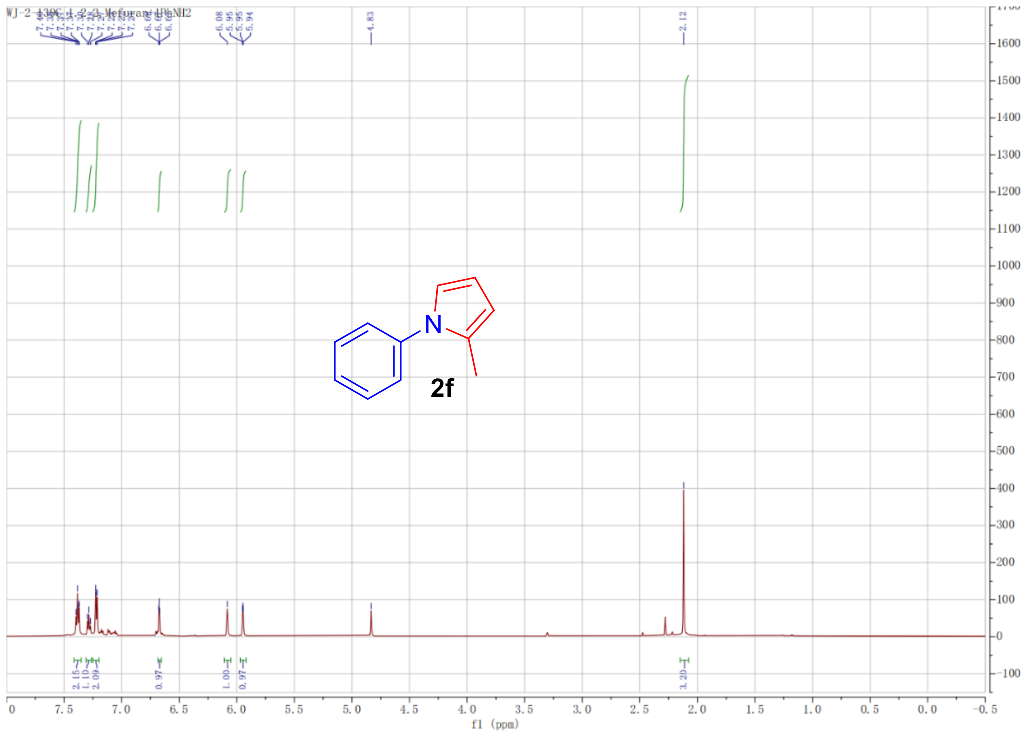
2f
f1 (ppm)

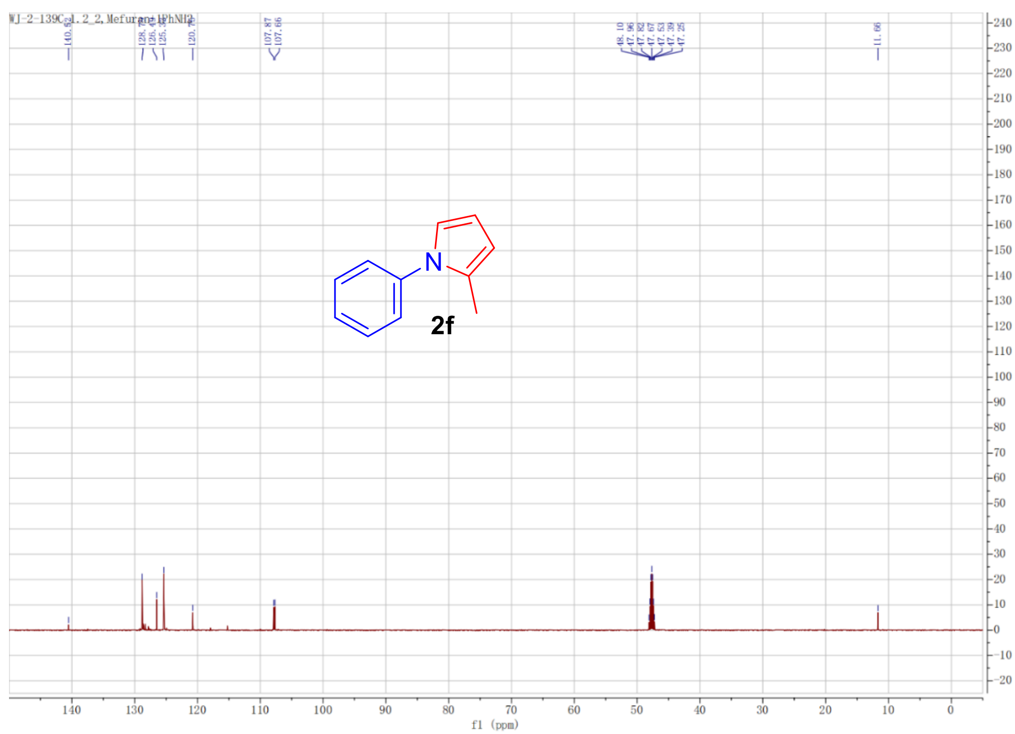
2f
f1 (ppm)

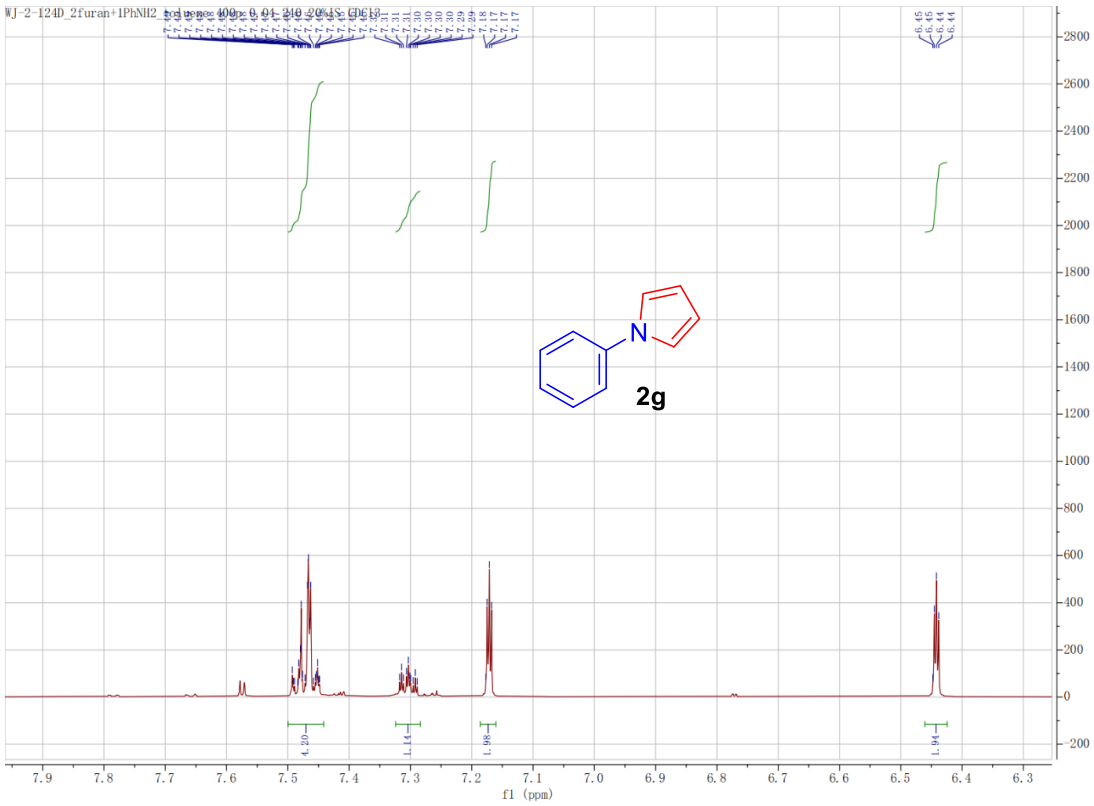
2g
f1 (ppm)

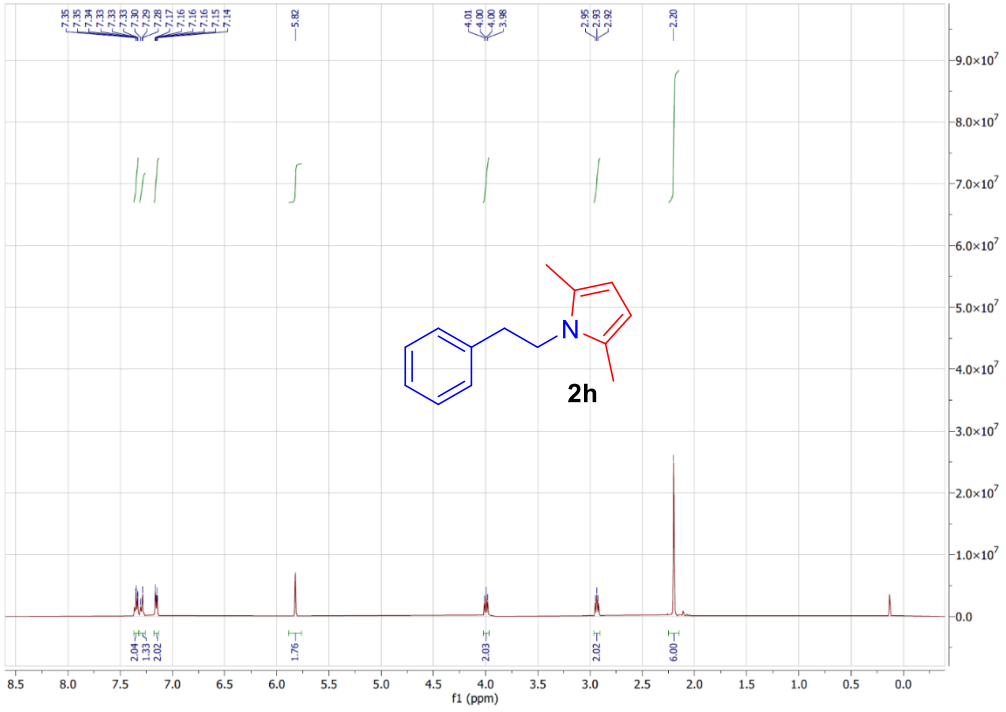
2h
f1 (ppm)

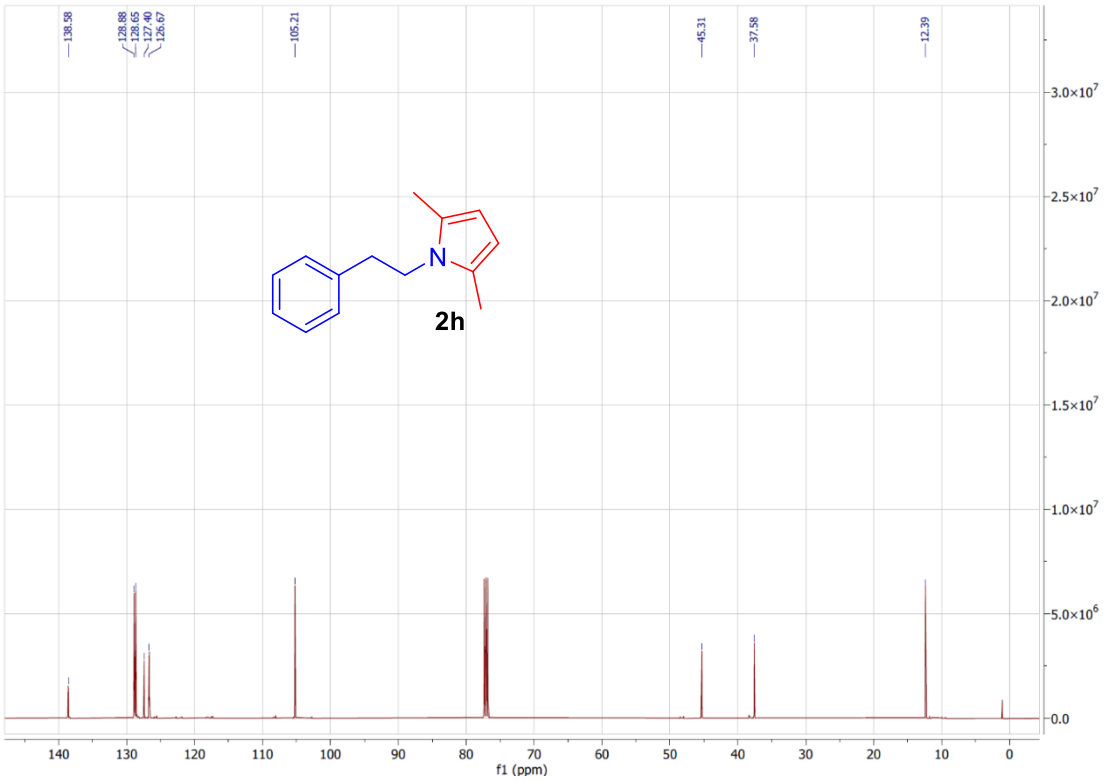
138.58
128.88
128.65
127.40
126.67
105.21
45.31
37.58
12.39
N
2h
3.0×10^7
2.5×10^7
2.0×10^7
1.5×10^7
1.0×10^7
5.0×10^6
0.0
140
130
120
110
100
90
80
70
60
50
40
30
20
10
0
f1 (ppm)

Chapter 3 Ester amidation in Flow

3.1 Introduction

Amides are ubiquitous functional groups in several natural products and are particularly important in pharmaceuticals.[1-4] Amide linkages are present in approximately one-quarter of the drugs on the market today and two-thirds of drug candidates.[5] Amide bond formation is one of the most important and frequently performed reactions in pharmaceutical research, development, and manufacturing.[6-7] However, efficient amide bond formation is still challenging.[5, 8] Conventional methods involve reactions of anhydrides or acyl chlorides with amines or using activated carboxylic acids in the presence of stoichiometric coupling reagents such as HATU or EDC. Both are accompanied by the generation of a lot of undesirable waste.[9-11]

An important example of the universality of amides and the complications of amidation reactions can be found in the oral SARS-CoV-2 inhibitor PF-07321332. This molecule contains 4 amide groups and a nitrile group accessed via dehydration of an amide. This molecule's reported synthesis involves using stoichiometric amounts of hazardous coupling agents, longer reaction times (~16 h), acutely toxic DMF as the reaction medium, and a tedious work-up procedure.[12] Developing more environmentally friendly and atom-economical amide bond formation methods remains a highly sought goal in academic research and industry.[6]

Recently, approaches involving the direct amidation of non-activated carboxylic acids and amines that generate only water as a byproduct have been investigated.[6, 13-15] They have the potential to reduce waste generation dramatically compared to traditional amide bond coupling pathways. However, elevated temperatures and intolerance towards the water, which is formed as a byproduct, are the limitations of the reported protocols. [6]Alternative routes to

form amides are also being investigated.[1, 16-17] Amidation of esters by free amines is promising because it requires simple, cheap, stable, and readily available methyl or ethyl esters and produces only volatile alcohol as a side-product. Indeed, the removal of the alcohol assists in driving the equilibrium-limited reaction to completion. Existing methods involving homogeneous catalysts include the activation of amines with strong bases,[18-23] activation of esters with Lewis acids such as Ni-IPr, $FeCl_3$, or $La(OTf)_3$,[24-27], and activation of the ester C-O bond through cross-coupling catalyzed by Ni, Pd, and Zn catalysts.[28-33] However, catalyst separation and recycling remain problematic.[29] Few heterogeneous catalysts have been reported to be effective to date.[34-35] Nb_2O_5,[36-40] OSU-6 (a type of mesoporous silica),[41,] and a Cu-Mn spinel,[42] have all been reported to show activity in the amidation of various esters by different amines. However, these Lewis/Bronsted acid catalysts also suffer from long reaction times, limited substrate scopes, or the need for molecular sieves, which add to the waste generated.

Continuous flow methods have emerged as a powerful and practical technology in organic synthesis, with several advantages over these batch methods.[43-58] They intensify reaction and process efficiency, improve safety and reproducibility, and are readily scaled up, all of which add to their appeal in pharmaceutical and fine chemical manufacturing.[59] Efficient heterogeneous catalysts used in packed-bed reactors for continuous flow processes have particular advantages for organic synthesis,[60] including the high local catalyst loading within the reactor and the ability to operate at temperatures above the solvent boiling point due to pressurization. The resulting process intensification allows the use of smaller reactors, thereby decreasing plant footprints and shortening start-up and shut-down times. Pressurization further allows the user to avoid high-boiling solvents, simplifying solvent removal, and since

the solid catalyst stays in the reactor, unit operations for catalyst removal are eliminated.[57-58]

Flow amidation with a homogeneous catalyst has been studied sporadically,[21, 63-66] but lacks many advantages of heterogeneous catalysts outlined above. Few heterogeneous amidation catalysts have been reported, and most do not demonstrate high enough intrinsic reactivity to allow for flow operation with reasonable residence times. To our knowledge, there is only one prior report on heterogeneous flow amidation involving a commercial ZrO_2 catalyst.[67] No residence time was reported; however, given the volume of the reactor and the flow rate, we estimate the residence time to be approx. 80 min. This study investigates various solid acids as catalysts for ester amidation in a continuous flow process. A simple, inexpensive, readily available amorphous silica-alumina achieves the direct amidation of esters with high efficiency and short residence times. Moreover, we demonstrate a novel pressure effect that drives conversion.

3.2 Experimental methods

General. Commercially available compounds were purchased from Sigma-Aldrich, Fisher, or Alfa Aesar and were used without further purification. Mesoporous SBA-15 (<150 μm particle size, 4 nm pore diameter, hexagonally-ordered mesopores) was obtained from Sigma. HBEA zeolite was prepared from NH_4^+-BEA (Alfa Aesar, 680 m^2/g, $SiO_2/Al_2O_3 = 25$). It was pressed, ground, and sieved to 80-100 mesh, then calcined in flowing air at 500 °C for 3 h. Two amorphous silica-aluminas (Davicat SIAL 3125, 552 m^2/g, pore volume 0.79 cm^3/g $SiO_2/Al_2O_3 = 75/25$, and Davicat SIAL 3113, 573 m^2/g, pore volume 0.76 cm^3/g, $SiO_2/Al_2O_3 = 85/15$) were provided by Grace-Davison (Columbia, MD). Both ASA catalysts were calcined in flowing air at 500 °C for 3 h before use.

Unless otherwise noted, all catalytic reactions and product analyses were performed in

the air. Solution-state NMR experiments were performed on a 600 MHz SB Varian VNMRS spectrometer. GC-MS analyses were performed on a Shimadzu GC-2010 Gas Chromatograph coupled to a QP2010 Mass Spectrometer. It is equipped with a 30 m × 0.25 mm Agilent DB-1 capillary column containing a dimethylpolysiloxane stationary phase (0.25 μm). He was used as the carrier gas. The temperature was held at 60 °C for 2 min, ramped from 60 to 200 °C at 15 °C/min, held at 200 °C for 10 min, ramped from 200 °C to 270 °C at 15 °C/min, and then held at 270 °C for 10 min.

Batch screening reactions. Typically, methyl benzoate (1.00 mmol, 0.136 g) and benzylamine (1.00 equivalents, 1.00 mmol, 0.107 g) were dissolved in 2 mL toluene containing *n*-dodecane (0.100 mmol, 22.7 μL) as an internal standard, and combined with 50 mg catalyst in a Schlenk tube equipped with a magnetic stir bar and a reflux condenser. The vessel was placed in a preheated oil bath at 120 °C for 6 h, and the reaction progress was monitored by either TLC or GC-MS. After cooling to room temperature, the catalyst was separated by centrifugation and washed by shaking with toluene. The washing liquid was recovered by centrifugation, combined with the organic phase, then the final conversion and product yield were determined by GC-MS or ^{1}H NMR. The product was purified by column chromatography.

Flow reactions. The continuous flow reactor was constructed using Swagelok stainless steel seamless tubing (316/316L, 0.18" i.d., ¼" o.d., 10" length) and standard valves, a back-pressure regulator (Equilibar) and a piston pump (MXT class, Chrom Tech). The reactor was heated to the desired temperature using heat tape before introducing the reactant. The solid catalyst (500 mg) was packed into the reactor to give a bed 2-3" in length. The catalyst bed was supported on each end by fused granular quartz (4-20 mesh, Sigma) and glass wool.

Prior to a typical experiment, toluene was sparged with N_2 in a Schlenk flask for 15 min and degassed with ultrasound for 20 min. The solvent was pumped at 2.0 mL/min to increase the pressure in the flow reactor. The back pressure regulator was adjusted to the desired set point of 50 to 500 psi, the flow rate was reduced to 0.04 mL/min, and the reactor temperature was raised to 170 °C. After stabilization of the flow system for about 5 min, the reactants were introduced via the pump inlet. The reactant mixture, consisting of a solution of methyl benzoate **A** (0.200 mol/L) and a slight excess of benzylamine **B** (0.240 mol/L, A/B = 1.2) in toluene, was also bubbled with N_2 in a volumetric bottle equipped with a septum for 15 min and degassed with ultrasound for 20 min before use.

The reactor and inlet/outlet tubing were purged with the substrate solution two times the system volume before sample collection began. Aliquots were collected in vials at the flow reactor outlet. The sample collection vials were heated at 50°C to dissolve any amide precipitate before analysis. The product yield was determined either by GC-MS using an internal standard (*n*-dodecane, 0.0200 mol/L, added with methyl benzoate and benzylamine in the feed solution) or by ^{1}H NMR using 1,3,5-trimethoxybenzene as the internal standard added to each sample after the reaction. The isolated yields were measured after obtaining the pure products by withdrawing 5 mL eluent from the reactor outlet (measured precisely using a volumetric pipette), removing the solvent by rotary evaporation, and purification by column chromatography.

Capping of Brønsted acid sites. To prepare trimethylsilyl-capped silica-alumina, Hexamethyldisilazane (HMDS, Aldrich, >99.5%) was transferred via the vapor phase under reduced pressure onto the dehydrated support for 1 hour. The reactor was then heated to 350 °C for 4 h under vacuum to remove unreacted HMDS and ammonia produced during the silanol

reaction.

3.3 Results and Discussion

Solid acid catalyst screening in batch. Several solid acid catalysts were first screened in the amidation of methyl benzoate with benzylamine under batch conditions (Table 3.1). SBA-15-type silica with ordered mesopores, amorphous silica-alumina (ASA) with non-ordered mesopores, and the large-pore zeolite HBEA all have surface silanol groups (weak Brønsted acid sites). Silica-alumina and HBEA also have strong Brønsted acid sites (BAS) associated with framework substitution of Si^{4+} by Al^{3+}. However, only ASA has significant Lewis acidity in the form of accessible, coordinatively-unsaturated Al^{3+} ions. Lewis acid sites are expected to be the active sites for ester amidation, according to Shimizu et. Al.[37] The batch results reported in Table 3.1 support this conclusion due to the high activity of the ASA catalysts. Compared to silica (entry 1) and HBEA (entry 2), the ASAs (entries 3 and 4) are more effective ester amidation catalysts. The ASA with the higher Si/Al ratio gave the best result, with 77% and 98% yields of *N*-benzylbenzamide after 3.5 and 6.0 h, respectively.

Table 3.1 Batch reactor screening of solid acids in amidation catalysis[a]

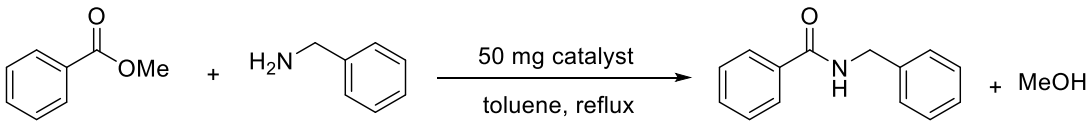

Entry	Catalyst	SiO_2/Al_2O_3	% Yield (3.5 h) [b]
1	SBA-15	∞	0
2	HBEA	25	35
3	ASA 3125 [c]	3	62
4	ASA 3113 [c]	6	77 (3.5 h) 98 (6.0 h)

[a] Reactions were conducted using equimolar methyl benzoate (1.0 mmol) and benzylamine (1.0 mmol), with 50 mg solid catalyst in 2 mL refluxing toluene at atmospheric pressure. [b] Yields were measured by GC-MS, using *n*-dodecane as an internal standard. [c] Calcined at 500 °C in the air prior to use.

Exploration of ASA amidation catalyst in continuous flow conditions. Initial experiments were conducted with ASA 3113 as the catalyst and toluene as the solvent. At 200 °C and 500 psi, with inlet concentrations of 0.050 and 0.10 M methyl benzoate and benzylamine, respectively, and a flow rate of 0.04 mL/min (corresponding to a residence time of 15 min) through a bed of 500 mg ASA, the yield of *N*-benzylbenzamide was 28 % (Table 3.2, entry 1). Since the rate law is expected to be mixed second-order (see below), the rate should depend strongly on the reactant concentrations. Increasing the methyl benzoate and benzylamine concentrations four-fold caused the yield increase to 68% (entry 2), although no further improvement in yield was observed with higher concentrations. The rate law was investigated further and is described below.

Table 3.2 Continuous flow amidation of methyl benzoate by benzylamine, catalyzed by ASA 3113[a]

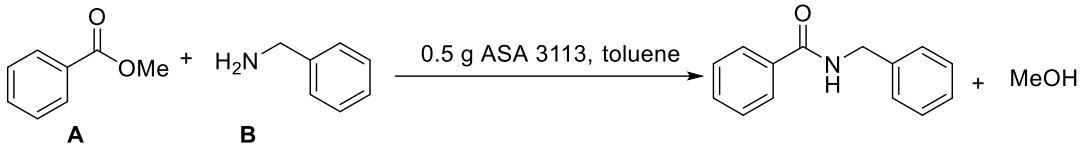

Entry	[**A**] (M)	[**B**] (M)	[**B**]/[**A**]	Temp (°C)	Pressure (psi)	Flow rate(mL/ min)	Res. Time[b] (min)	Conv [c] (%)	Yield [c] (%)
1	0.050	0.10	2.0	200	500	0.04	15	--	28
2	0.20	0.40	2.0	200	500	0.04	15	74	68
3	0.20	0.40	2.0	200	50	0.04	15	98	96
4	0.20	0.40	2.0	170	50	0.04	15	98	97
5	0.20	0.40	2.0	160	50	0.04	15	87	85
6	0.20	0.24	1.2	170	50	0.04	15	92	92
7	0.20	0.20	1.0	170	50	0.04	15	78	76
8[d]	0.20	0.24	1.2	180	50	0.1	23	84	78

[a] Unless otherwise noted, reactions were conducted in a packed-bed reactor with 0.500 g calcined ASA 3113 as the catalyst and toluene as solvent. [b] Residence time is calculated as the volume of the catalyst bed divided by volumetric flow rate [c] Conversion and yield were measured by GC-MS, using *n*-dodecane as internal standard. [d] The amount of ASA 3113 catalyst was increased to 1.00 g.

Surprisingly, when the reactor pressure was decreased from 500 to 50 psi, the yield increased dramatically to 96% (entry 3). The origin of the pressure effect in the catalyst bed was investigated and is described further below. The high yield was maintained at the lower pressure even when the temperature was reduced to 170 °C (entry 4), declining to 87 % only when the temperature was lowered further to 160 °C (entry 5). At 170 °C, the amide was recovered in high yield (92 %) even when the excess of amine was reduced from 2.0 to 1.2 Equiv. (entry 6). However, the yield declined slightly to 76 % when the excess amine was eliminated (i.e., the ester and amine were used in stoichiometric amounts, entry 7), suggesting that the reaction is equilibrium-limited (see below). The reaction was also attempted with a higher flow rate (0.1 mL/min) and a higher catalyst loading (1.00 g). At 180 °C, the amide was obtained in 78% yield (entry 8).

For the optimized reaction conditions represented by entry 6 in Table 3.2, the space-time yield of *N*-benzylbenzamide is 13.7 g h^{-1} dL^{-1}. For comparison, the previous report of heterogeneous flow amidation using an amorphous ZrO_2 catalyst gave a space-time yield for the same product of 3.8 g h^{-1} dL^{-1} under their optimized conditions (0.5 MPa, 160°C, 0.1 mL/min of 0.25M ester and 0.30M amine, 6 g catalyst).[67]

Substrate Scope. The optimized reaction conditions were used to study the substrate scope. A variety of amide products were successfully produced in 68 to 99% yields, Scheme 3.1. This protocol has been applied to various aromatic, aliphatic, Michael addition susceptible, and heterocyclic acids to achieve good to quantitative yields. Even though the reaction conditions were efficient for aliphatic and aromatic amines, it was not promising for amino alcohol and indole derivatives.

Scheme 3.1 Substrate scope for continuous flow amidation of various methyl esters with different amines, catalyzed by ASA[a]

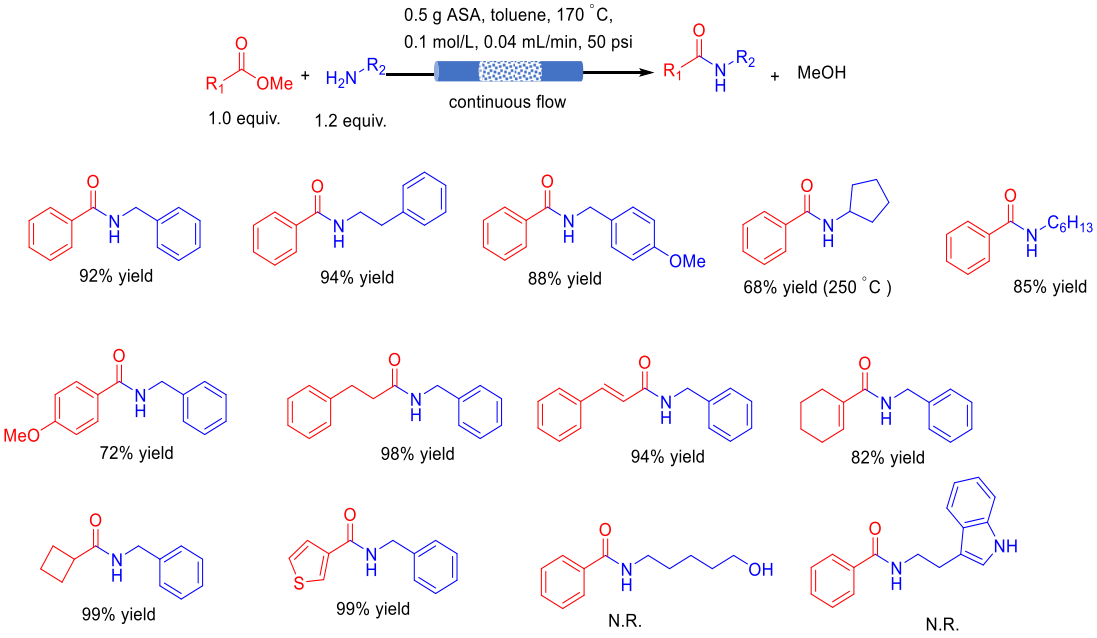

[a] Reported yields were determined by NMR

Kinetics and mechanism of amidation. To assess the rate law for ester amidation, kinetics measurements were conducted for the reaction of methyl benzoate and benzylamine in toluene at 170 °C and 50 psi under differential conditions. To minimize concentration gradients within the catalyst bed, the flow rate was increased to 0.3 mL/min, and the loading of the ASA catalyst was reduced to 250 mg. Both result in a low conversion (< 15 %), which ensures that the rate reflects intrinsic kinetics without mass transport or equilibrium limitations.

For a packed-bed reactor operated under differential conditions, the reaction rate *r* at steady-state operation is described in eq 3.1:

$$r = \frac{F_{in} - F_{out}}{W_{cat}} = \frac{C_{in} X Q_{in}}{W_{cat}} \qquad (3.1)$$

where F_{in} and F_{out} represent the molar flow rate of the limiting reagent in and out of the reactor, C_{in} denotes the concentration (M) of the limiting reagent (i.e., Methyl benzoate), X is the conversion of methyl benzoate, Q_{in} is the volumetric flow rate (L/min), and W_{cat} is the weight of the catalyst in grams. To determine the reaction orders, the rate was calculated from the outlet conversion when the inlet concentration of either methyl benzoate or benzylamine was varied while keeping the other inlet concentration constant. The results are reported in Table 3.3. When the concentration of methyl benzoate is halved, the rate decreases by almost half (entries 1-2). Likewise, when the concentration of benzylamine is halved, the rate decreases by a little over half (entries 1 and 3). When either concentration is doubled, the rate approximately doubles. Therefore, the reaction is first order with respect to both ester and amine, eq 3.2:

$$r = k\, m_{\text{cat}}\, [\mathbf{A}]\, [\mathbf{B}] \qquad (3.2)$$

where *k is the reaction rate constant,* [**A**] is the concentration of methyl benzoate (M), and [**B**] is the concentration of benzylamine (M). This mixed second-order rate law agrees with previous reports, including the type of catalyst and reactor). Therefore, the transition state contains one molecule of each reactant. At 170 °C, the second-order rate constant *k* is 5.58E-4 L^2 min^{-1} g^{-1} mol^{-1}

Table 3.3 Dependence of the amidation rate for the reaction[a] of methyl benzoate (**A**) with benzylamine (**B**) catalyzed by ASA on the inlet concentrations of the reactants

Entry	[**A**] (M)	[**B**] (M)	[**A**]/[**B**]	**A** Conv. (%)	Rate mmol/(min•g_{cat})	Relative Rate
1	0.20	0.24	1.0	7.8	0.019	1
2	0.10	0.24	0.5	10	0.012	0.6
3	0.20	0.12	2.0	3.3	0.0079	0.4
4	0.40	0.24	2.0	9.5	0.046	2.4
5	0.20	0.48	0.5	14.9	0.036	1.9

[a] Reactions of methyl benzoate with benzylamine with varying concentrations were conducted at 170 °C in a packed-bed reactor with 0.250 g ASA 3113 as the catalyst, and toluene as solvent, with a flow rate of 0.3 mL/min (residence time 15 min) and a pressure of 50 psi. [b] Conversion was measured by GC-MS, using *n*-dodecane as the internal standard.

To determine the activation energy required for the methyl benzoate amidation reaction over ASA catalyst, again, low conversion conditions were produced to ensure kinetic control without mass transport or equilibrium limitations. Therefore, 0.2M methyl benzoate and 0.24M benzylamine were passed through 250 mg ASA at 50 psi and 0.5 mL/min while varying the temperature. The reaction rates were calculated according to eq 3.1, and the reaction rate constants, k, were determined using eq. 3.2. The reaction temperature varied from 150 to 170 °C, and the inverse of temperature was plotted vs. the natural log of the reaction constant as described by the linear form of the Arrhenius equation as noted in eq 3.3 and seen in Figure 3.3. The activation energy for the ester amidation reaction over ASA catalyst was determined to be 40 kJ/mol.

$$ln(k) = -\frac{E_a}{R}\left[\frac{1}{T}\right] + ln(A) \quad (3.3)$$

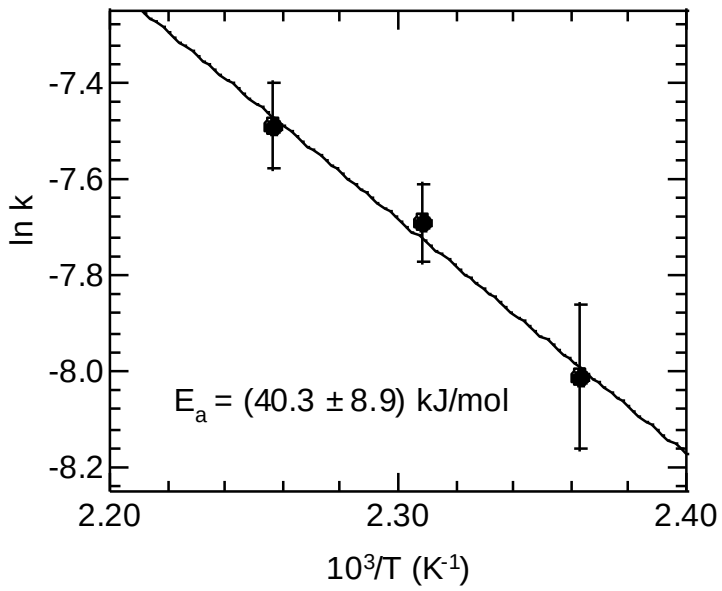

Figure 3.3. Arrhenius plot of 0.2 M methyl benzoate and 0.24 M benzylamine reacted in a packed-bed reactor with 0.250 g ASA 3113 as the catalyst, and toluene as solvent, with a flow rate of 0.5 mL/min (residence time 15 min) and a pressure of 50 psi, while varying temperature from 150-170 °C. The conversion was measured by GC-MS, using *n*-dodecane as an internal standard.

To investigate the nature of the active sites on ASA, the Brønsted acid sites were capped with trimethylsilyl groups, using hexamethyldisilazane (HMDS), eq 3.4, according to the procedure published previously[68].

$$2 \equiv SiOH + ((CH_3)_3Si)_2NH \rightarrow 2 \equiv SiOSi(CH_3)_3 + NH_3 \quad (3.4)$$

The IR spectrum of ASA 3113 calcined at 500 °C in air and then evacuated at 450 °C shows a strong peak at 3740 cm^{-1} for the O-H stretching mode of the surface silanols, Figure

3.4. No distinct lower frequency peak for bridging hydroxyls SiO(H)Al is seen in crystalline aluminosilicates. The Brønsted acidity of the amorphous material has been described as latent since the silanol coordinates to coordinatively-unsaturated Al sites only after its deprotonation.[68] After silylation and removal of the NH_3 by evacuation at 350 °C, the intensity of this peak is strongly attenuated, signaling the reaction of both weak and strong Brønsted acid sites. The appearance of two C-H stretching vibrations at 2965 and 2905 cm^{-1} characteristic of the trimethylsilyl group confirms the capping of 75% of the silanols.

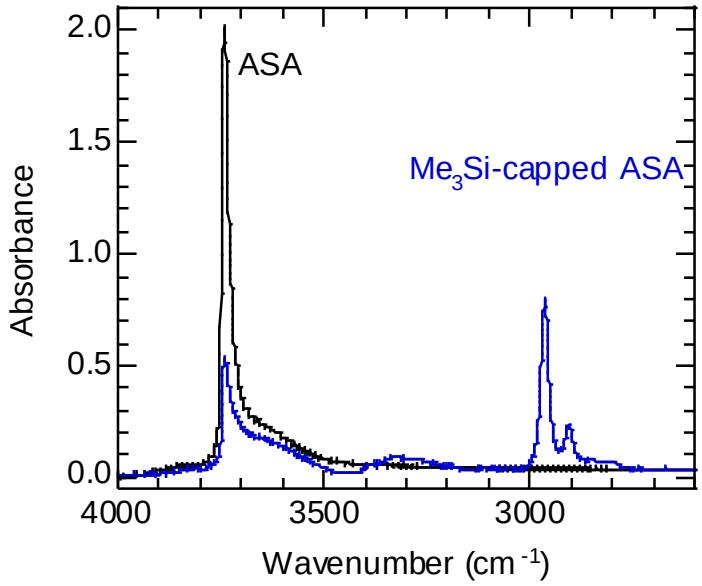

Figure 3.4. Comparison of transmission IR spectra for ASA calcined at 500 °C and evacuated at 450 °C (black) and trimethylsilyl-capped ASA (blue).

The HMDS-modified catalyst was tested under the same conditions (0.20 M methyl benzoate, 0.24 M benzylamine in toluene flowing at 0.10 mL/min, 1.00 g ASA, 180 °C, 50 psi). The ester conversions for the capped and uncapped catalyst are comparable at 79 and 84%. Similarly, the amide yields for the capped and uncapped catalysts are comparable at 79

and 78%. Therefore, the Brønsted acid sites of ASA do not play a significant role in the ester amidation reaction. Logically, the Lewis acid sites must be responsible for the activity.

Overcoming the equilibrium limit. Ester amidation is a reversible reaction; the catalytic conversion of amides to esters has also been reported.[70-74] The loss of low-boiling alcohols, which drives amidation to completion in open batch reactors, is not possible in continuous flow reactors. To investigate the effect of equilibrium on the amidation yield in the flow reactor, we conducted the methanolysis of *N*-benzylbenzamide in the presence of ASA. At 200 °C and 500 psi, a 13% yield of methyl benzoate was obtained (Scheme 3.2 a).

Scheme 3.2 Investigation of equilibration in the catalytic amidation

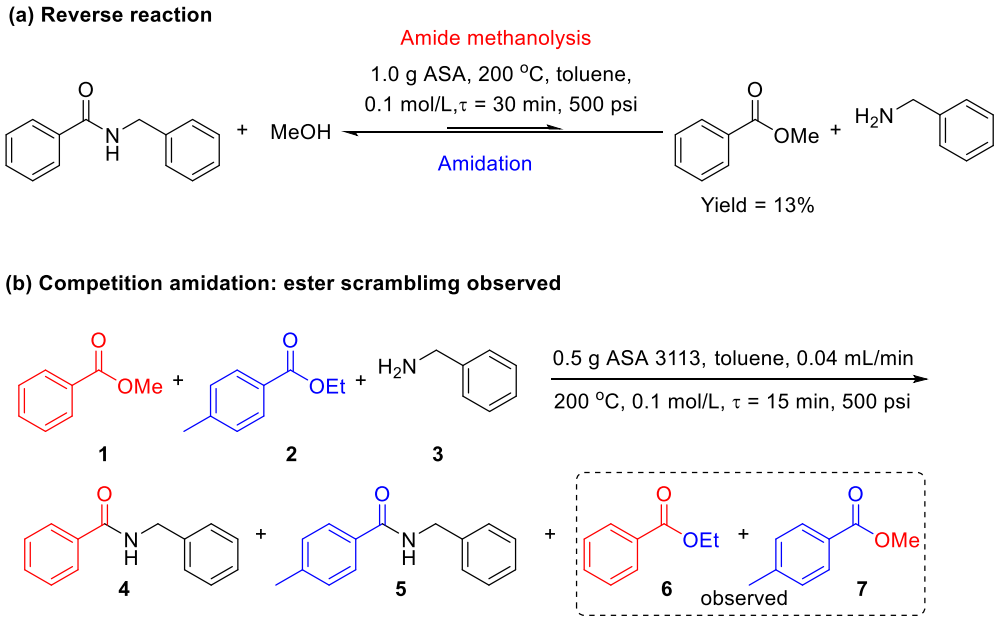

Furthermore, simultaneous amidation of a mixture of methyl benzoate and ethyl 4-methylbenzoate revealed scrambling of the esters. In addition to the expected amide products **4** and **5**, the esters ethyl benzoate **6** and methyl 4-methylbenzoate **7** were also recovered

(Scheme 3b). The new esters are formed by the alcoholysis of the amides, thereby demonstrating the reversibility of the amidation reaction.

The expected dependence of the position of chemical equilibrium on the alcohol concentration suggests an explanation for the inverse effect of pressure on the flow amidation reaction, in which amide yields are much higher at low pressures. The conversion of methyl benzoate at 170 °C is only ca. 40% conversion at > 200 psi, but it rises abruptly to exceed 90 % at < 150 psi (Figure 3.5). We speculate that methanol is partially vaporized in the flow reactor at the lower pressures, and this vaporization shifts the equilibrium towards the amide resulting in higher conversion and yield.

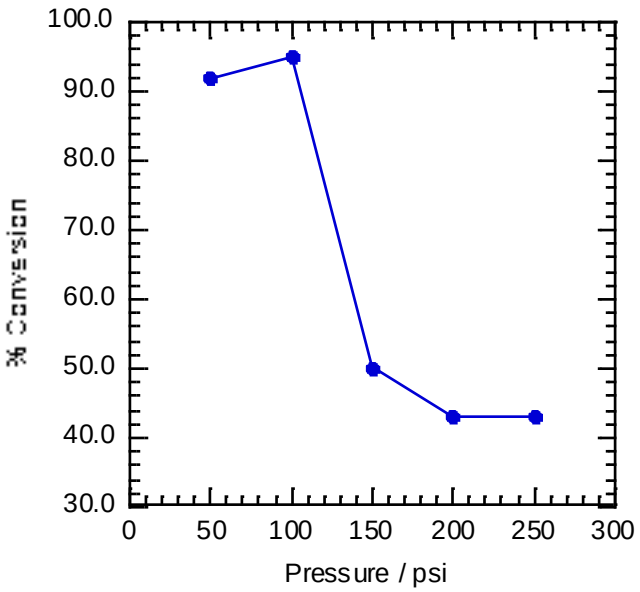

Figure 3.5 Pressure dependence of the conversion of methyl benzoate (0.2 M) to amide by reaction with benzylamine (0.24 M, 1.2 Equiv.) in toluene at 170 °C, catalyzed by 500 mg ASA catalyst in a continuous flow reactor at a flow rate of 0.04 mL/min. The conversion was detected by GC-MS, using *n*-dodecane as an internal standard.

To understand whether partial solvent vaporization also contributes to the observed pressure effect on the amidation reaction, similar experiments were conducted using *p*-xylene as solvent. Its normal boiling point of 138 °C is significantly higher than toluene (111 °C). In p-xylene, the conversion of methyl benzoate was only 42% at 300 psi (Table 3.3, entry 3) and did not increase when the pressure was reduced to 50 psi (instead, it decreased to 31%, entry 4). However, the conversion increased abruptly to 81% when the pressure was further reduced to 30 psi (entry 5). Therefore partial solvent vaporization may play a role in the efficiency of the reaction, presumably by increasing the concentrations of the reactants.

Table 3.4. Solvent dependence of the pressure effect on amidation of methyl benzoate catalyzed by ASA in a continuous flow reactor [a]

Entry	Solvent	Pressure (psi)	Conv. [b] (%)
1	toluene	300	36
2	toluene	50	84
3	p-xylene	300	42
4	p-xylene	50	31
5	p-xylene	30	81

[a] Continuous flow reactions were conducted with 0.20 M methyl benzoate and 0.24 M benzylamine at 180 °C, with a volumetric flow rate of 0.1 mL/min (corresponding to a residence time of 23 min), with 1.00 g ASA 3113 as the catalyst in a packed-bed reactor. [b] Conversion was detected by GC-MS using *n*-dodecane as an internal standard.

These results suggest that the flow reactor is a complex environment containing gas, liquid, and solid phases.

The practical application of this heterogeneous catalyst for continuous-flow ester amidation was demonstrated in the direct multi-gram synthesis of the anti-depressant drug molecule Moclobemide, starting from commercially available materials. Accordingly, the reactor was operated with long-term stability for 50 h under the reaction conditions in Scheme 3.3, providing 8.66 g of Moclobemide, corresponding to 85% isolated yield after purification.

Scheme 3.3. Synthesis of anti-depressant drug from 4-chlorobenzoic acid methyl ester and *N*-ethylaminomorpholine1-amine in toluene under continuous-flow conditions[a]

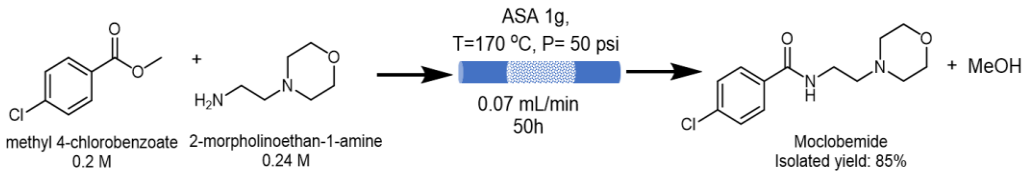

a

4-chlorobenzoic acid methyl ester 0.2 M ,*N*-ethylaminomorpholine1-amine 0.24 M in toluene

3.4 Conclusion

In this chapter, we have demonstrated high yields for the continuous flow ester amidation reaction using a simple, commercially available amorphous silica-alumina as a heterogeneous catalyst. Amorphous silica-alumina is a more effective catalyst at more than three times that currently reported in the literature, with a corresponding five times lower residence time, and is demonstrated to work for a broad substrate scope. We also observed a novel pressure effect which improves yield considerably.

Acknowledgments.

Pfizer Global R&D is gratefully acknowledged for the financial support of this work.

Contributions

This is a collaborative project completed with the help of Dr. Jing Wu, Costanza Leonardi, and Dr. Allison Wesley. I contributed to the experiments to study kinetics by performing entries 1-5 of Table 3.3. I came up with synthesizing Moclobemide to demonstrate the practical application of the ester amidation protocol and contributed to setting up the gram scale synthesis of Moclobemide. I also participated in writing the introduction part of the paper.

References

1. Pattabiraman, V. R.; Bode, J. W., Rethinking amide bond synthesis. *Nature* **2011,** *480* (7378), 471-479.
2. Montalbetti, C. A. G. N.; Falque, V., Amide bond formation and peptide coupling. *Tetrahedron* **2005,** *61* (46), 10827-10852.
3. Carey, J. S.; Laffan, D.; Thomson, C.; Williams, M. T., Analysis of the reactions used for the preparation of drug candidate molecules. *Org. Biomol. Chem.* **2006,** *4* (12), 2337-2347.
4. Deming, T. J., Synthetic polypeptides for biomedical applications. *Prog. Polym. Sci.* **2007,** *32* (8-9), 858-875.
5. Wang, X., Challenges and outlook for catalytic direct amidation reactions. *Nature Catalysis* **2019,** *2* (2), 98-102.
6. Lundberg, H.; Tinnis, F.; Selander, N.; Adolfsson, H., Catalytic amide formation from non-activated carboxylic acids and amines. *Chem. Soc. Rev.* **2014,** *43* (8), 2714-42.
7. Brow, D. G.; Bostrom, J., Analysis of Past and Present Synthetic Methodologies on Medicinal Chemistry: Where Have All the New Reactions Gone? *J. Med. Chem.* **2016,** *59* (10), 4443-4458.
8. Sabatini, M. T.; Boulton, L. T.; Sneddon, H. F.; Sheppard, T. D., A green chemistry perspective on catalytic amide bond formation. *Nature Catalysis* **2019,** *2* (1), 10-17.
9. Valeur, E.; Bradley, M., Amide bond formation: beyond the myth of coupling reagents. *Chem. Soc. Rev.* **2009,** *38* (2), 606-631.
10. El-Faham, A.; Albericio, F., Peptide Coupling Reagents, More than a Letter Soup. *Chem. Rev.* **2011,** *111* (11), 6557-6602.

11. Dunetz, J. R.; Magano, J.; Weisenburger, G. A., Large-Scale Applications of Amide Coupling Reagents for the Synthesis of Pharmaceuticals. *Org. Process Res. Dev.* **2016,** *20* (2), 140-177.

12. Owen, D. R.; Allerton, C. M. N.; Anderson, A. S.; Aschenbrenner, L.; Avery, M.; Berritt, S.; Boras, B.; Cardin, R. D.; Carlo, A.; Coffman, K. J.; Dantonio, A.; Di, L.; Eng, H.; Ferre, R.; Gajiwala, K. S.; Gibson, S. A.; Greasley, S. E.; Hurst, B. L.; Kadar, E. P.; Kalgutkar, A. S.; Lee, J. C.; Lee, J.; Liu, W.; Mason, S. W.; Noell, S.; Novak, J. J.; Obach, R. S.; Ogilvie, K.; Patel, N. C.; Pettersson, M.; Rai, D. K.; Reese, M. R.; Sammons, M. F.; Sathish, J. G.; Singh, R. S. P.; Steppan, C. M.; Stewart, A. E.; Tuttle, J. B.; Updyke, L.; Verhoest, P. R.; Wei, L.; Yang, Q.; Zhu, Y. An Oral SARS-CoV-2 Mpro Inhibitor Clinical Candidate for the Treatment of COVID-19. *Science* **2021**, *374* (6575), 1586–1593.

13. Noda, H.; Furutachi, M.; Asada, Y.; Shibasaki, M.; Kumagai, N., Unique physicochemical and catalytic properties dictated by the B3NO2 ring system. *Nature Chemistry* **2017,** *9* (6), 571-577.

14. Sabatini, M. T.; Boulton, L. T.; Sheppard, T. D., Borate esters: Simple catalysts for the sustainable synthesis of complex amides. *Science Advances* **2017,** *3* (9).

15. de Azambuja, F.; Parac-Vogt, T. N., Water-Tolerant and Atom Economical Amide Bond Formation by Metal-Substituted Polyoxometalate Catalysts. *ACS Catal.* **2019,** *9* (11), 10245-10252.

16. Allen, C. L.; Williams, J. M. J., Metal-catalysed approaches to amide bond formation. *Chem. Soc. Rev.* **2011,** *40* (7), 3405-3415.

17. de Figueiredo, R. M.; Suppo, J. S.; Campagne, J. M., Nonclassical Routes for Amide Bond Formation. *Chem. Rev.* **2016,** *116* (19), 12029-12122.

18. Basha, A.; Lipton, M.; Weinreb, S. M., Mild, General Method for Conversion of Esters to Amides. *Tetrahedron Lett.* **1977,** (48), 4171-4174.

19. Lipton, M. F.; Basha, A.; Weinreb, S. M., Conversion of Esters to Amides with Dimethylaluminum Amides - N,N-Dimethylcyclohexanecarboxamide. *Org. Synth.* **1988,** *50-9*, 492-495.

20. Wang, W. B.; Roskamp, E. J., Tin(Ii) Amides - New Reagents for the Conversion of Esters to Amides. *J. Org. Chem.* **1992,** *57* (23), 6101-6103.

21. Munoz, J. D.; Alcazar, J.; de la Hoz, A.; Diaz-Ortiz, A.; de Diego, S. A. A., Preparation of amides mediated by isopropylmagnesium chloride under continuous flow conditions. *Green Chem.* **2012,** *14* (5), 1335-1341.

22. Ohshima, T.; Hayashi, Y.; Agura, K.; Fujii, Y.; Yoshiyama, A.; Mashima, K., Sodium methoxide: a simple but highly efficient catalyst for the direct amidation of esters. *Chem. Commun. (Cambridge, U. K.)* **2012,** *48* (44), 5434-5436.

23. Caldwell, N.; Jamieson, C.; Simpson, I.; Watson, A. J. B., Catalytic amidation of unactivated ester derivatives mediated by trifluoroethanol. *Chem. Commun. (Cambridge, U. K.)* **2015,** *51* (46), 9495-9498.

24. Ishihara, K.; Kuroki, Y.; Hanaki, N.; Ohara, S.; Yamamoto, H., Antimony-templated macrolactamization of tetraamino esters. Facile synthesis of macrocyclic spermine alkaloids, (+/-)-buchnerine, (+/-)-verbacine, (+/-)-verbaskine, and (+/-)-verbascenine. *J. Am. Chem. Soc.* **1996,** *118* (6), 1569-1570.

25. Han, C.; Lee, J. P.; Lobkovsky, E.; Porco, J. A., Catalytic ester-amide exchange using group (IV) metal alkoxide-activator complexes. *J. Am. Chem. Soc.* **2005,** *127* (28), 10039-10044.

26. Tsuji, H.; Yamamoto, H., Hydroxy-Directed Amidation of Carboxylic Acid Esters Using a Tantalum Alkoxide Catalyst. *J. Am. Chem. Soc.* **2016,** *138* (43), 14218-14221.

27. Morimoto, H.; Fujiwara, R.; Shimizu, Y.; Morisaki, K.; Ohshima, T., Lanthanum(III) triflate catalyzed direct amidation of esters. *Org. Lett.* **2014,** *16* (7), 2018-21.

28. Hie, L.; Fine Nathel, N. F.; Hong, X.; Yang, Y. F.; Houk, K. N.; Garg, N. K., Nickel-Catalyzed Activation of Acyl C-O Bonds of Methyl Esters. *Angew. Chem. Int. Ed.* **2016,** *55* (8), 2810-4.

29. Ben Halima, T.; Masson-Makdissi, J.; Newman, S. G., Nickel-Catalyzed Amide Bond Formation from Methyl Esters. *Angew. Chem. Int. Ed.* **2018,** *57* (39), 12925-12929.

30. Ben Halima, T.; Vandavasi, J. K.; Shkoor, M.; Newman, S. G., A Cross-Coupling Approach to Amide Bond Formation from Esters. *ACS Catal.* **2017,** *7* (3), 2176-2180.

31. Cheung, C. W.; Ploeger, M. L.; Hu, X., Direct amidation of esters with nitroarenes. *Nat. Commun.* **2017,** *8*, 14878.

32. Ji, C. L.; Xie, P. P.; Hong, X., Computational Study of Mechanism and Thermodynamics of Ni/IPr-Catalyzed Amidation of Esters. *Molecules* **2018,** *23* (10).

33. Zheng, Y.-L.; Newman, S. G., Methyl Esters as Cross-Coupling Electrophiles: Direct Synthesis of Amide Bonds. *ACS Catal.* **2019,** *9* (5), 4426-4433.

34. Wali, A.; Unnikrishnan, S.; Pillai, S. M.; Kaushik, V. K.; Satish, S., Montmorillonite clay catalysis: Conversion of methyl benzoate and NH3 into benzonitrile and amides. *J. Catal.* **1998,** *173* (1), 84-94.

35. Sun, H.; Page, M. I.; Atherton, J. H.; Hall, A., Kinetics of the conversion of methyl benzoate to benzamide by the alumina catalysed reaction with liquid ammonia at 120 °C. *Catal. Sci. Technol.* **2014,** *4* (11), 3870-3878.

36. Ali, M. A.; Moromi, S. K.; Touchy, A. S.; Shimizu, K.-i., Direct Synthesis of Cyclic Imides from Carboxylic Anhydrides and Amines by Nb_2O_5 as a Water-Tolerant Lewis Acid Catalyst. *ChemCatChem* **2016,** *8* (5), 891-894.

37. Ali, M. A.; Siddiki, S. M.; Kon, K.; Hasegawa, J.; Shimizu, K., Versatile and sustainable synthesis of cyclic imides from dicarboxylic acids and amines by Nb2O5 as a base-tolerant heterogeneous Lewis acid catalyst. *Chemistry* **2014,** *20* (44), 14256-60.

38. Ali, M. A.; Siddiki, S. M. A. H.; Kon, K.; Shimizu, K.-i., A Heterogeneous Niobium(V) Oxide Catalyst for the Direct Amidation of Esters. *ChemCatChem* **2015,** *7* (17), 2705-2710.

39. Ali, M. A.; Siddiki, S. M. A. H.; Onodera, W.; Kon, K.; Shimizu, K.-i., Amidation of Carboxylic Acids with Amines by Nb2O5as a Reusable Lewis Acid Catalyst. *ChemCatChem* **2015,** *7* (21), 3555-3561.

40. Siddiki, S. M. A. H.; Rashed, M. N.; Ali, M. A.; Toyao, T.; Hirunsit, P.; Ehara, M.; Shimizu, K. i., Lewis Acid Catalysis of Nb_2O_5 for Reactions of Carboxylic Acid Derivatives in the Presence of Basic Inhibitors. *ChemCatChem* **2018,** *11* (1), 383-396.

41. Nammalwar, B.; Muddala, N. P.; Watts, F. M.; Bunce, R. A., Efficient conversion of acids and esters to amides and transamidation of primary amides using OSU-6. *Tetrahedron* **2015,** *71* (48), 9101-9111.

42. Sultan, S.; Kumar, M.; Devari, S.; Mukherjee, D.; Ali Shah, B., Copper-Manganese Spinel Oxide Catalyzed Synthesis of Amides and Azobenzenes via Aminyl Radical Cations. *ChemCatChem* **2016,** *8* (4), 703-707.

43. Britton, J.; Majumdar, S.; Weiss, G. A., Continuous flow biocatalysis. *Chem. Soc. Rev.* **2018,** *47* (15), 5891-5918.

44. Britton, J.; Raston, C. L., Multi-step continuous-flow synthesis. *Chem. Soc. Rev.* **2017,** *46* (5), 1250-1271.

45. Colella, M.; Carlucci, C.; Luisi, R., Supported Catalysts for Continuous Flow Synthesis. *Top Curr Chem (Cham)* **2018,** *376* (6), 46.

46. Gérardy, R.; Emmanuel, N.; Toupy, T.; Kassin, V.-E.; Tshibalonza, N. N.; Schmitz, M.; Monbaliu, J.-C. M., Continuous Flow Organic Chemistry: Successes and Pitfalls at the Interface with Current Societal Challenges. *Eur. J. Org. Chem.* **2018,** *2018* (20-21), 2301-2351.

47. Gilmore, K.; Seeberger, P. H., Continuous flow photochemistry. *Chem. Rec.* **2014,** *14* (3), 410-8.

48. Isbrandt, E. S.; Sullivan, R. J.; Newman, S. G., High Throughput Strategies for the Discovery and Optimization of Catalytic Reactions. *Angew. Chem. Int. Ed.* **2019,** *58* (22), 7180-7191.

49. Langille, E.; Bottaro, C. S.; Drouin, A., A novel use of catalytic zinc-hydroxyapatite columns for the selective deprotection of N-tert-butyloxycarbonyl (BOC) protecting group using flow chemistry. *Journal of Flow Chemistry* **2020**.

50. Pan, X.; Liu, Z., The preparation of novel chiral auxiliaries SAMIQ/RAMIQ and their application in the asymmetric Michael addition. *Tetrahedron* **2014,** *70* (31), 4602-4610.

51. Pastre, J. C.; Browne, D. L.; Ley, S. V., Flow chemistry syntheses of natural products. *Chem. Soc. Rev.* **2013,** *42* (23), 8849-69.

52. Plutschack, M. B.; Pieber, B.; Gilmore, K.; Seeberger, P. H., The Hitchhiker's Guide to Flow Chemistry parallel. *Chem. Rev.* **2017,** *117* (18), 11796-11893.

53. Rogers, L.; Jensen, K. F., Continuous manufacturing – the Green Chemistry promise? *Green Chem.* **2019,** *21* (13), 3481-3498.

54. Santoro, S.; Ferlin, F.; Ackermann, L.; Vaccaro, L., C-H functionalization reactions under flow conditions. *Chem. Soc. Rev.* **2019,** *48* (10), 2767-2782.

55. Scott, S. L., A Matter of Life(time) and Death. *ACS Catal.* **2018,** *8* (9), 8597-8599.

56. Trobe, M.; Burke, M. D., The Molecular Industrial Revolution: Automated Synthesis of Small Molecules. *Angew. Chem. Int. Ed.* **2018,** *57* (16), 4192-4214.

57. Britton, J.; Jamison, T. F., The assembly and use of continuous flow systems for chemical synthesis. *Nat. Protoc.* **2017,** *12* (11), 2423-2446.

58. Tanimu, A.; Jaenicke, S.; Alhooshani, K., Heterogeneous catalysis in continuous flow microreactors: A review of methods and applications. *Chem. Eng. J.* **2017,** *327*, 792-821.

59. Gutmann, B.; Cantillo, D.; Kappe, C. O., Continuous-flow technology-a tool for the safe manufacturing of active pharmaceutical ingredients. *Angew. Chem. Int. Ed.* **2015,** *54* (23), 6688-728.

60. Tsubogo, T.; Oyamada, H.; Kobayashi, S., Multistep continuous-flow synthesis of (R)- and (S)-rolipram using heterogeneous catalysts. *Nature* **2015,** *520* (7547), 329-32.

61. Spare, L. K.; Laude, V.; Harman, D. G.; Aldrich-Wright, J. R.; Gordon, C. P., An optimised approach for continuous-flow solid-phase peptide synthesis utilising a rudimentary flow reactor. *Reaction Chemistry & Engineering* **2018,** *3* (6), 875-882.

62. Gordon, C. P., The renascence of continuous-flow peptide synthesis - an abridged account of solid and solution-based approaches. *Org. Biomol. Chem.* **2018,** *16* (2), 180-196.

63. Polster, C. S.; Cole, K. P.; Burcham, C. L.; Campbell, B. M.; Frederick, A. L.; Hansen, M. M.; Harding, M.; Heller, M. R.; Miller, M. T.; Phillips, J. L.; Pollock, P. M.; Zaborenko, N., Pilot-Scale Continuous Production of LY2886721: Amide Formation and Reactive Crystallization. *Org. Process Res. Dev.* **2014,** *18* (11), 1295-1309.

64. White, T. D.; Berglund, K. D.; Groh, J. M.; Johnson, M. D.; Miller, R. D.; Yates, M. H., Development of a Continuous Schotten-Baumann Route to an Acyl Sulfonamide. *Org. Process Res. Dev.* **2012,** *16* (5), 939-957.

65. Vrijdag, J. L.; Delgado, F.; Alonso, N.; De Borggraeve, W. M.; Perez-Macias, N.; Alcazar, J., Practical preparation of challenging amides from non-nucleophilic amines and esters under flow conditions. *Chem. Commun. (Camb.)* **2014,** *50* (95), 15094-7.

66. Fuse, S.; Mifune, Y.; Nakamura, H.; Tanaka, H., Total synthesis of feglymycin based on a linear/convergent hybrid approach using micro-flow amide bond formation. *Nat. Commun.* **2016,** *7*, 13491.

67. Rashed, M.N.; Masuda, K.; Ichitsuka, T.; Koumura, N.; Sato, K.; Kobayashi, S. Zirconium Oxide-Catalyzed Direct Amidation of Unactivated Esters under Continuous-Flow Conditions. *Adv. Synth. Catal.* **2021***, 363* (10), 2529-2535.

68. Sanchez Escribano, V.; Garbarino, G.; Finocchio, E.; Busca, G. γ-Alumina and Amorphous Silica–Alumina: Structural Features, Acid Sites and the Role of Adsorbed Water. *Top Catal* **2017***, 60* (19), 1554–1564.

69. Moses, A. W.; Raab, C.; Nelson, R. C.; Leifeste, H. D.; Ramsahye, N. A.; Chattopadhyay, S.; Eckert, J.; Chmelka, B. F.; Scott, S. L. Spectroscopically Distinct Sites Present in Methyltrioxorhenium Grafted onto Silica−Alumina, and Their Abilities to Initiate Olefin Metathesis. *J. Am. Chem. Soc.* **2007**, *129* (28), 8912–8920.

70. Hie, L.; Fine Nathel, N. F.; Shah, T. K.; Baker, E. L.; Hong, X.; Yang, Y. F.; Liu, P.; Houk, K. N.; Garg, N. K., Conversion of amides to esters by the nickel-catalysed activation of amide C-N bonds. *Nature* **2015,** *524* (7563), 79-83.

71. Li, J.-F.; Wang, Y.-F.; Wu, Y.-Y.; Liu, W.-J.; Wang, J.-W., Nickel-Catalyzed Esterification of Amides Under Mild Conditions. *Catal. Lett.* **2019,** *150* (3), 874-880.

72. Mashima, K.; Nishii, Y.; Nagae, H., Catalytic Cleavage of Amide C-N Bond: Scandium, Manganese, and Zinc Catalysts for Esterification of Amides. *Chem. Rec.* **2019**.

73. Shirshin, K. K.; Esipovich, A. L.; Kazantsev, O. A.; Gushchin, A. V., Amidation of fatty acid methyl ester using metal oxides and hydroxides as catalysts. *Chem. Pap.* **2019,** *73* (6), 1571-1574.

74. Siddiki, S. M. A. H.; Touchy, A. S.; Tamura, M.; Shimizu, K.-i., Versatile and sustainable alcoholysis of amides by a reusable CeO2 catalyst. *RSC Adv.* **2014,** *4* (67), 35803-35807.

Appendix 3

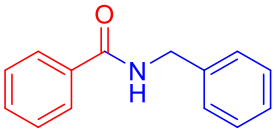

^{1}H NMR (600 MHz, Chloroform-*d*) δ 7.83 – 7.76 (m, 2H), 7.47 (m, 1H), 7.38 (m, 2H), 7.31 (m, 4H), 7.27 (m, 1H), 6.83 (s, 1H), 4.59 (m, 2H). ^{13}C NMR (151 MHz, cdcl$_3$) δ 167.46, 138.31, 134.39, 131.46, 128.69, 128.50, 127.81, 127.47, 127.05, 44.00.

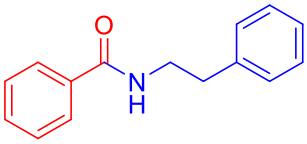

^{1}H NMR (600 MHz, Chloroform-*d*) δ 7.72 – 7.65 (m, 2H), 7.48 – 7.43 (m, 1H), 7.38 (t, *J* = 7.6 Hz, 2H), 7.31 (t, *J* = 7.5 Hz, 2H), 7.25 – 7.20 (m, 3H), 6.31 (s, 1H), 3.70 (td, *J* = 7.0, 5.8 Hz, 2H), 2.92 (t, *J* = 7.0 Hz, 2H). ^{13}C NMR (151 MHz, cdcl$_3$) δ 167.50, 138.92, 134.66, 131.36, 128.80, 128.69, 128.52, 126.83, 126.57, 41.16, 35.71.

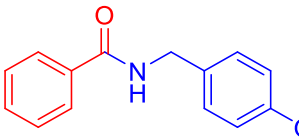

^{1}H NMR (600 MHz, Chloroform-d) δ 7.79 – 7.75 (m, 2H), 7.47 (d, J = 7.5 Hz, 1H), 7.40 (t, J = 7.7 Hz, 2H), 7.26 (d, J = 8.4 Hz, 2H), 6.89 – 6.84 (m, 2H), 6.54 (s, 1H), 4.55 (d, J = 5.6 Hz, 2H), 3.79 (s, 3H). 13C NMR (151 MHz, cdcl3) δ 167.40, 159.19, 134.56, 131.56, 130.41, 129.37, 128.64, 127.06, 114.24, 55.41, 43.71.

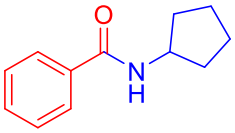

^{1}H NMR (600 MHz, Chloroform-*d*) δ 7.79 – 7.70 (m, 2H), 7.48 – 7.43 (m, 1H), 7.39 (t, *J* = 7.6 Hz, 2H), 6.48 – 6.16 (m, 1H), 4.43 – 4.34 (m, 1H), 2.06 (ddd, *J* = 12.6, 7.4, 4.9 Hz, 2H), 1.71 (dddd, J = 11.0, 8.3, 6.5, 3.2 Hz, 2H), 1.64 (dtd, J = 12.2, 7.5, 3.8 Hz, 2H), 1.56 – 1.42 (m, 2H). 13C NMR (151 MHz, cdcl3) δ 167.26, 135.02, 131.23, 128.49, 126.95, 51.76, 33.21, 23.89.

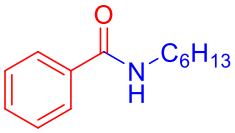

^{1}H NMR (600 MHz, Chloroform-*d*) δ 7.79 – 7.74 (m, 2H), 7.49 – 7.44 (m, 1H), 7.39 (ddd, *J* = 9.1, 6.9, 1.8 Hz, 2H), 6.44 (s, 1H), 3.42 (qd, *J* = 7.6, 6.7, 2.0 Hz, 2H), 1.64 – 1.55 (m, 2H), 1.42 – 1.22 (m, 6H), 0.92 – 0.84 (m, 3H). ^{13}C NMR (151 MHz, $cdcl_3$) δ 167.63, 134.98, 131.30, 128.55, 126.96, 40.22, 31.60, 29.72, 26.77, 22.65, 14.10.

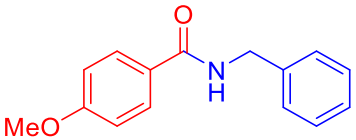

^{1}H NMR (600 MHz, Chloroform-*d*) δ 7.79 – 7.71 (m, 2H), 7.29 (q, *J* = 3.2, 2.2 Hz, 4H), 7.25 (ddd, *J* = 6.6, 4.1, 2.2 Hz, 1H), 6.85 (ddd, *J* = 9.0, 4.4, 2.2 Hz, 3H), 4.55 (dd, *J* = 5.7, 2.7 Hz, 2H), 3.79 (d, *J* = 3.2 Hz, 3H). ^{13}C NMR (151 MHz, $cdcl_3$) δ 167.07, 162.19, 138.62, 128.91, 128.68, 127.81, 127.40, 126.70, 113.72, 55.41, 43.98.

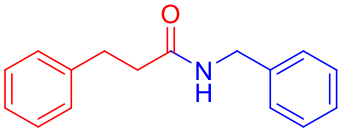

^{1}H NMR (600 MHz, Chloroform-*d*) δ 7.32 – 7.23 (m, 5H), 7.23 – 7.17 (m, 3H), 7.16 – 7.11 (m, 2H), 4.38 (d, *J* = 5.7 Hz, 2H), 2.99 (t, *J* = 7.6 Hz, 2H), 2.51 (t, *J* = 7.6 Hz, 2H). ^{13}C NMR (151 MHz, cdcl$_3$) δ 172.00, 140.88, 138.28, 128.73, 128.64, 128.49, 127.80, 127.51, 126.33, 43.64, 38.54, 31.82.

^{1}H NMR (600 MHz, Chloroform-*d*) δ 7.66 (d, *J* = 15.6 Hz, 1H), 7.46 (dt, *J* = 5.5, 3.3 Hz, 2H), 7.36 – 7.28 (m, 6H), 7.28 – 7.24 (m, 1H), 6.44 (dd, *J* = 15.6, 3.2 Hz, 1H), 6.31 – 6.16 (m, 1H), 4.54 (d, *J* = 5.7 Hz, 2H). ^{13}C NMR (151 MHz, cdcl$_3$) δ 165.95, 141.43, 138.33, 134.91, 129.79, 128.91, 128.83, 128.00, 127.99, 127.91, 127.65, 120.64, 43.95.

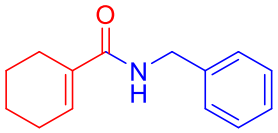

^{1}H NMR (600 MHz, Chloroform-*d*) δ 7.34 – 7.30 (m, 2H), 7.30 – 7.24 (m, 3H), 6.65 (m, 1H), 6.10 – 5.98 (m, 1H), 4.48 (d, *J* = 5.7 Hz, 2H), 2.24 (m, 2H), 2.15 (m, 2H), 1.70 – 1.64 (m, 2H), 1.62 – 1.56 (m, 2H).^{13}C NMR (151 MHz, cdcl$_3$) δ 168.44, 138.59, 133.73, 133.04, 128.66, 127.80, 127.40, 43.60, 25.36, 24.31, 22.13, 21.52.

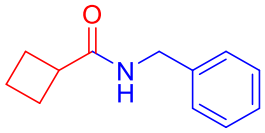

^{1}H NMR (600 MHz, Chloroform-*d*) δ 7.34 – 7.27 (m, 2H), 7.27 – 7.21 (m, 3H), 5.95 (s, 1H), 4.39 (d, *J* = 5.8 Hz, 2H), 3.01 (td, *J* = 8.5, 1.0 Hz, 1H), 2.33 – 2.24 (m, 2H), 2.16 – 2.08 (m, 2H), 1.99 – 1.89 (m, 1H), 1.86 (d, *J* = 1.2 Hz, 1H).^{13}C NMR (151 MHz, cdcl$_3$) δ 174.90, 138.64, 128.69, 127.78, 127.43, 43.46, 39.93, 25.41, 18.24.

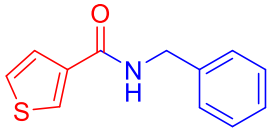

^{1}H NMR (600 MHz, Chloroform-*d*) δ 7.53 (s, 1H), 7.48 – 7.38 (m, 1H), 7.28 (m, 4H), 7.02 (s, 1H), 6.68 (s, 1H), 4.56 (s, 2H). ^{13}C NMR (151 MHz, cdcl$_3$) δ 161.94, 138.89, 138.14, 130.04, 128.71, 128.21, 127.86, 127.64, 127.54, 77.30, 77.09, 76.88, 43.92.

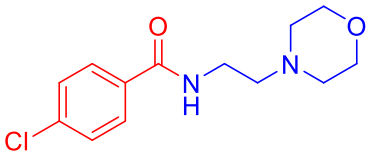

^{1}H NMR (400 MHz, CDCl$_3$) *δ* 7.71 (d, *J* = 8.6 Hz, 2H), 7.41 (d, *J* = 8.6 Hz, 2H), 6.74 (br. s., 1H), 3.72 (t, *J* = 4.6 Hz, 4H), 3.54 (dt, *J* = 5.8, 10.8 Hz, 2H), 2.59 (t, *J* = 5.8 Hz, 2H), 2.50 (t, *J* = 4.6 Hz, 4H). ^{13}C NMR (100 MHz, CDCl$_3$) δ 166.3, 137.7, 133.0, 128.8, 128.4, 67.0, 56.8, 53.3, 36.1.

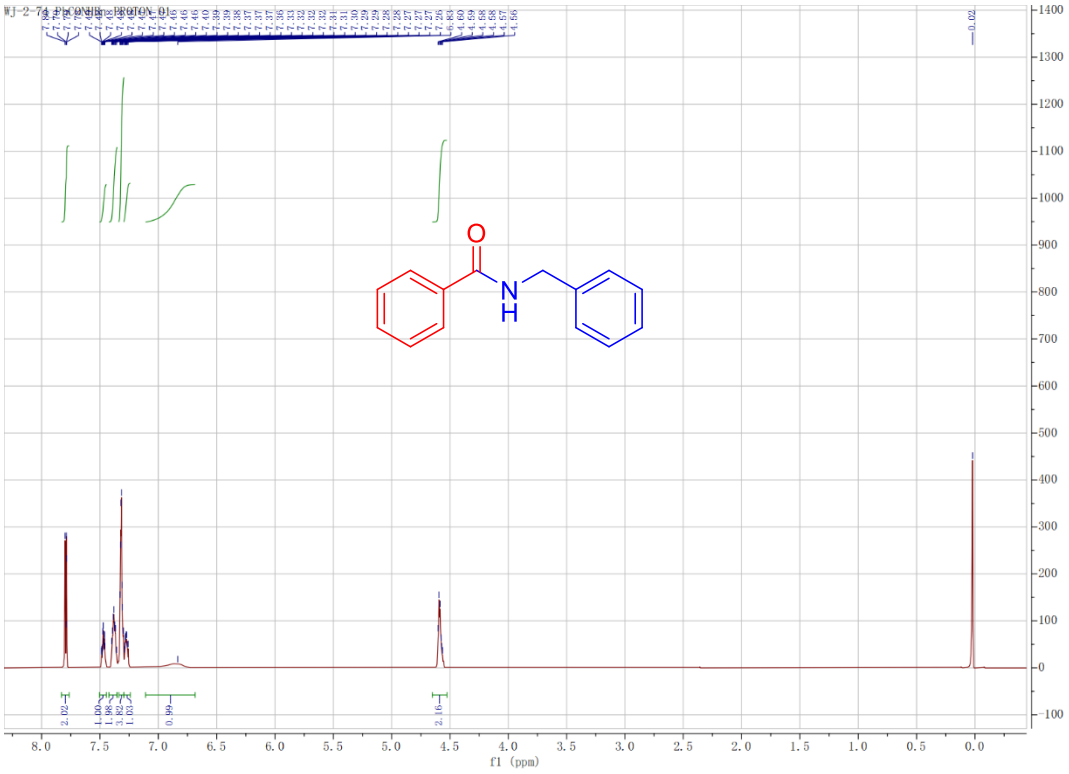
f1 (ppm)

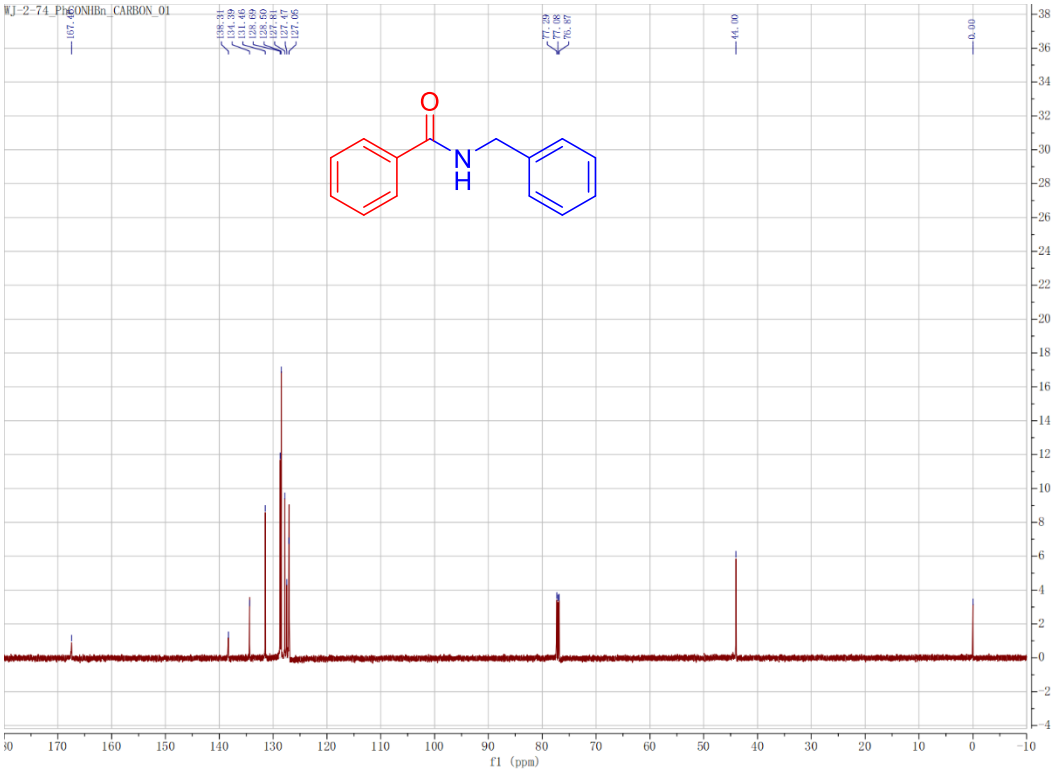
f1 (ppm)

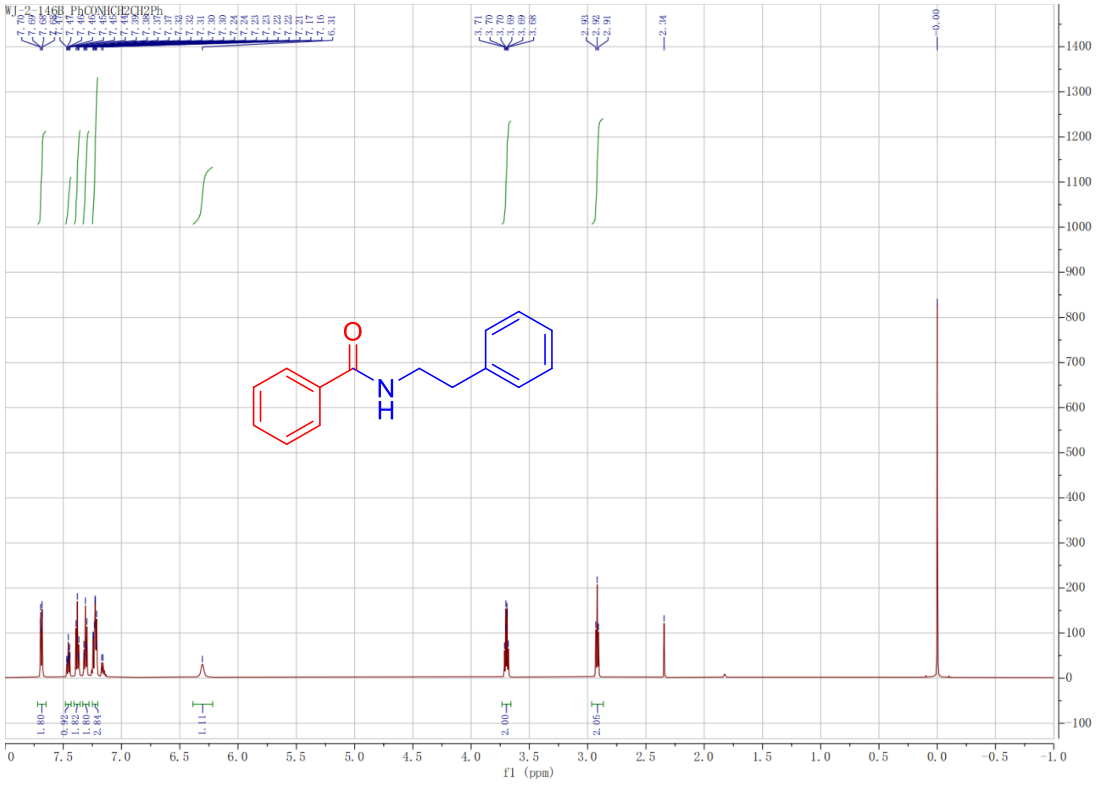
WJ-2-146B PhCONHCH2CH2Ph
f1 (ppm)

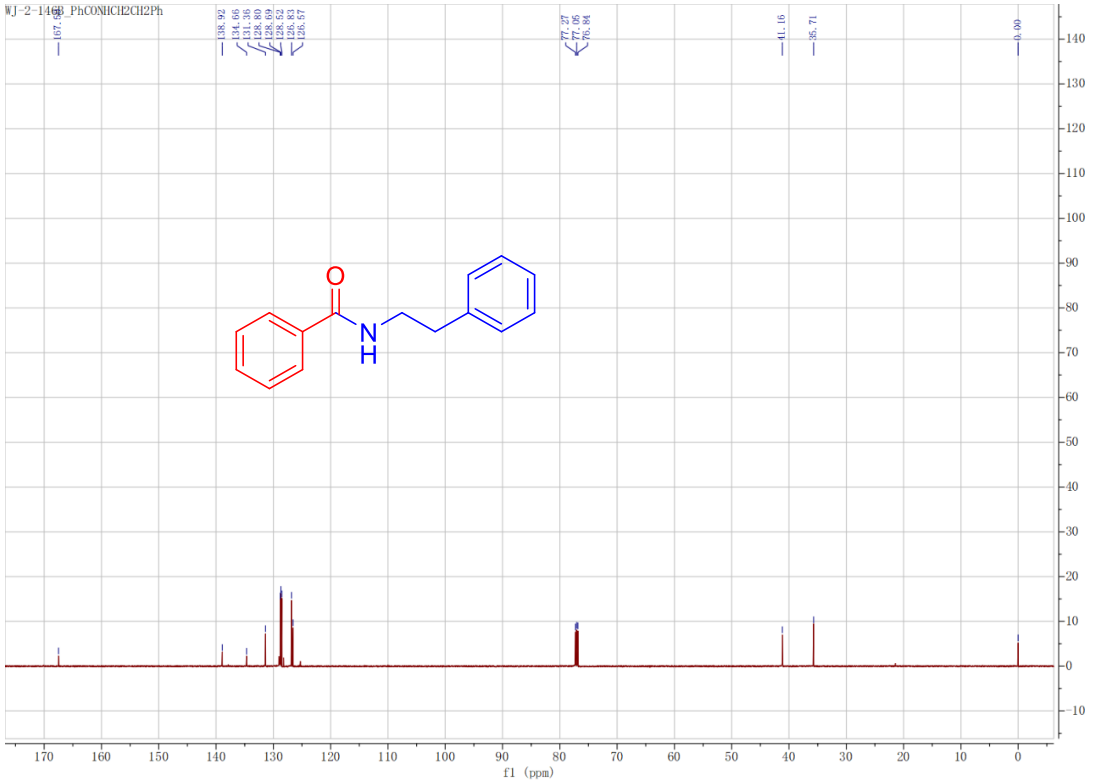
WJ-2-146B PhCONHCH2CH2Ph
f1 (ppm)

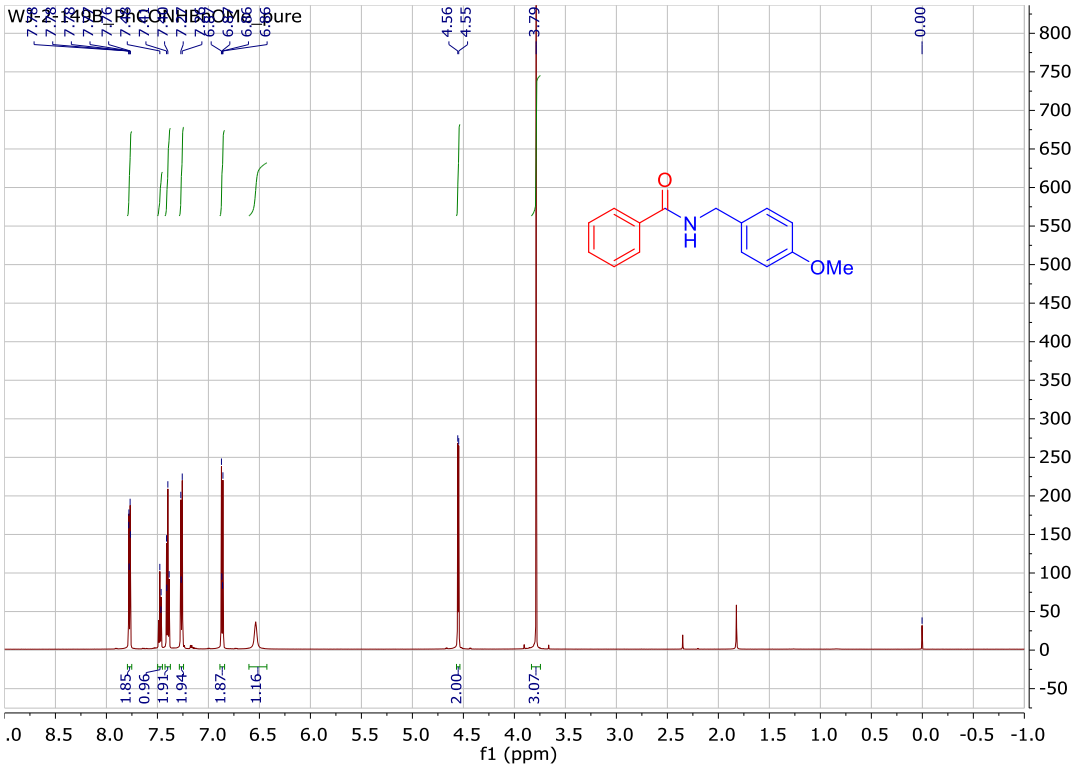
WJ-2-149B_PhCONHBnOMe_pure
4.56
4.55
3.79
0.00
1.85
0.96
1.91
1.94
1.87
1.16
2.00
3.07
O
N
H
OMe
f1 (ppm)

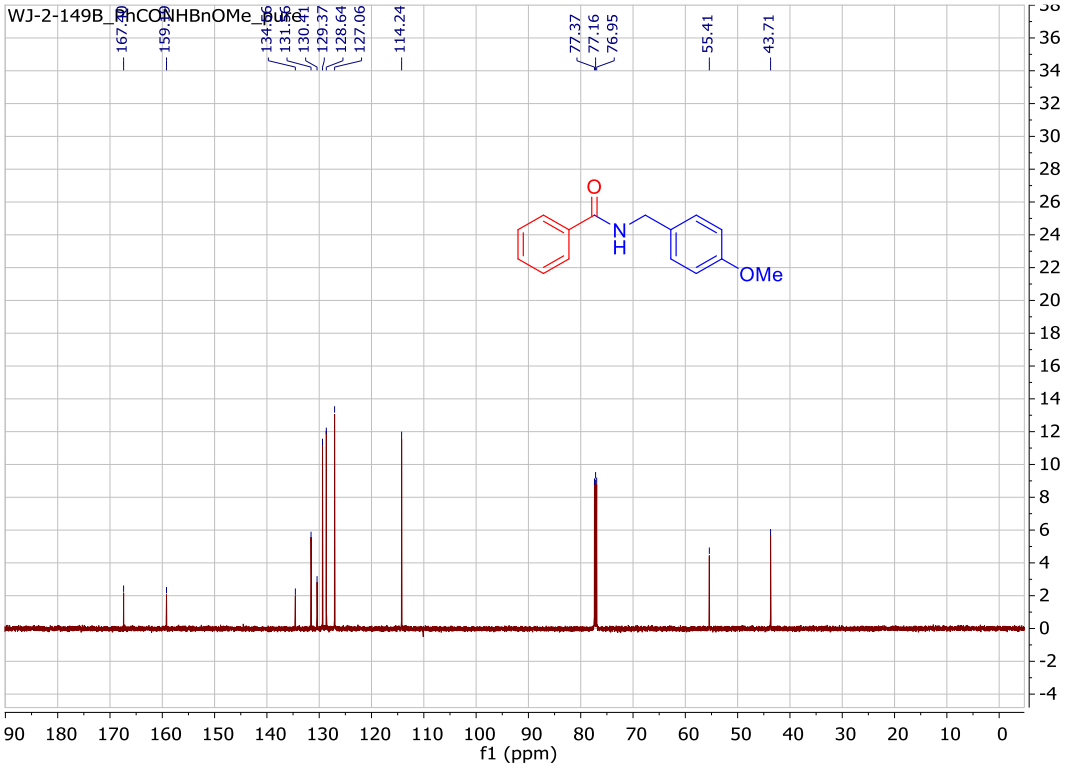
WJ-2-149B_PhCONHBnOMe_pure
167.30
159.11
134.16
131.16
130.41
129.37
128.64
127.06
114.24
77.37
77.16
76.95
55.41
43.71
O
N
H
OMe
f1 (ppm)

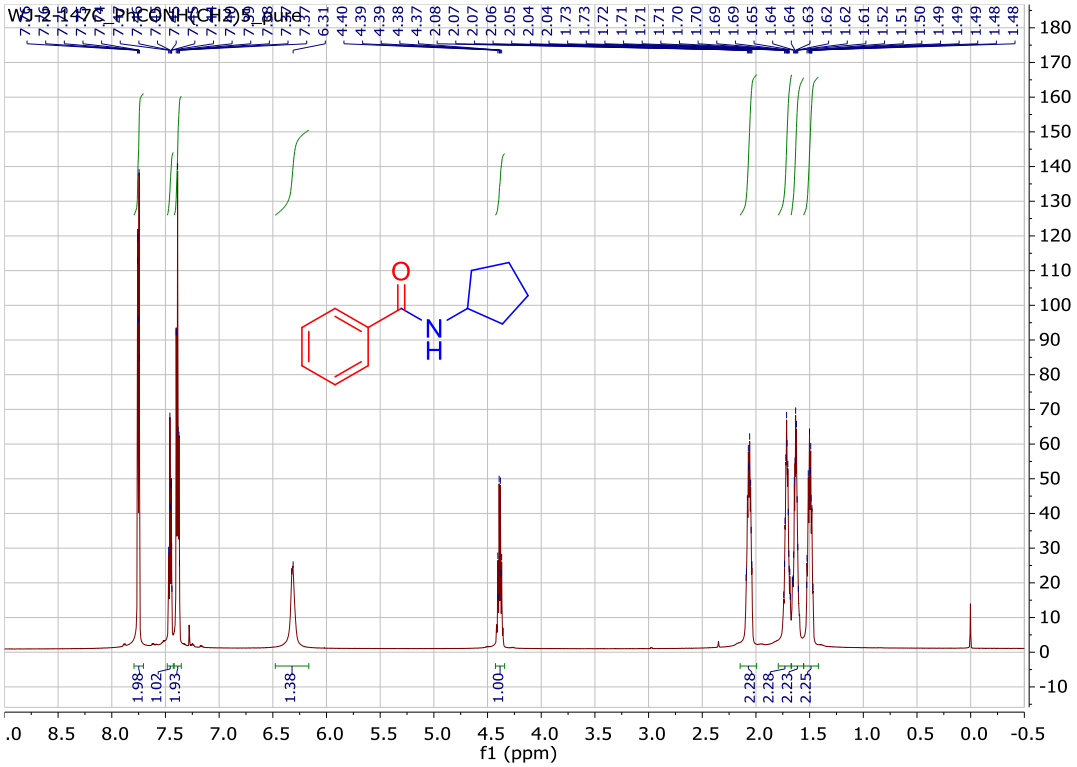
WJ-2-147C_PhCONH(CH2)5_pure
f1 (ppm)

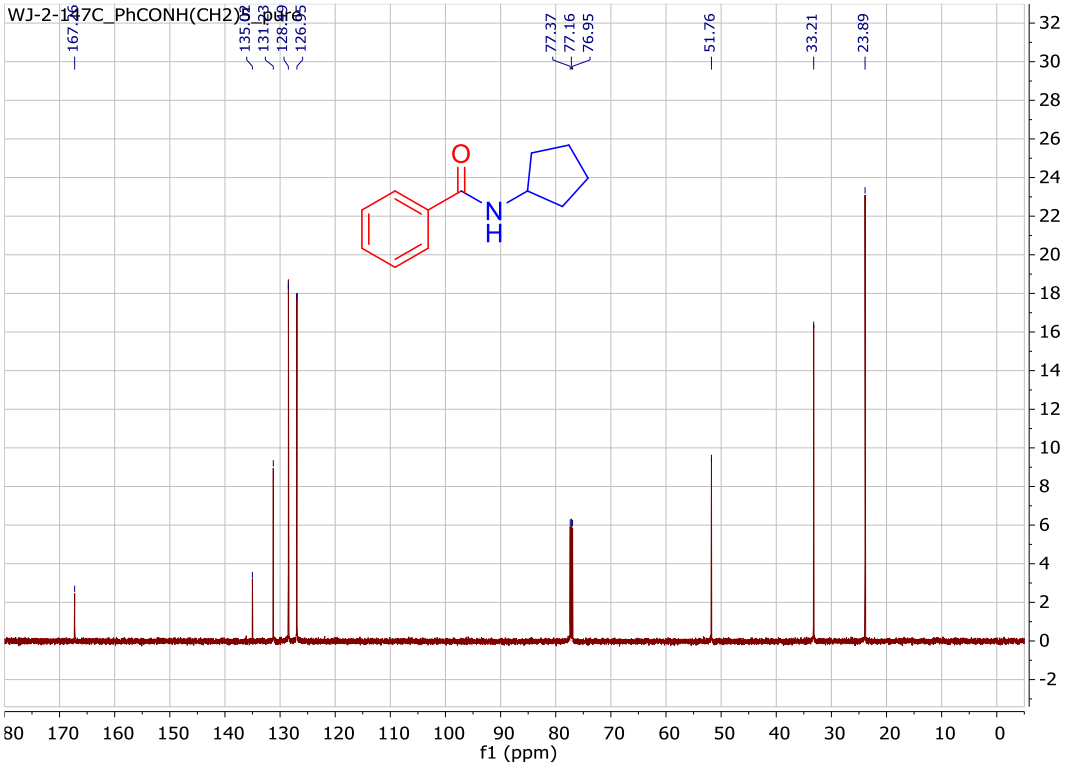
WJ-2-147C_PhCONH(CH2)5_pure
f1 (ppm)

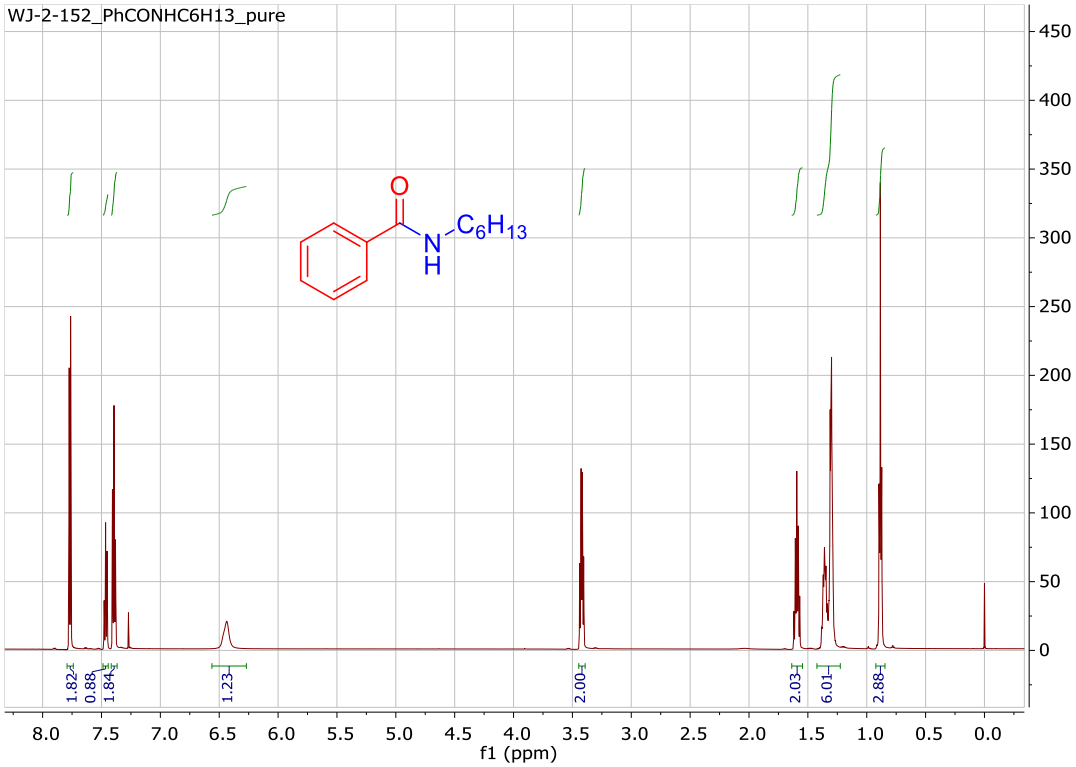
WJ-2-152_PhCONHC6H13_pure
O
N
H
C6H13
1.82
0.88
1.84
1.23
2.00
2.03
6.01
2.88
f1 (ppm)

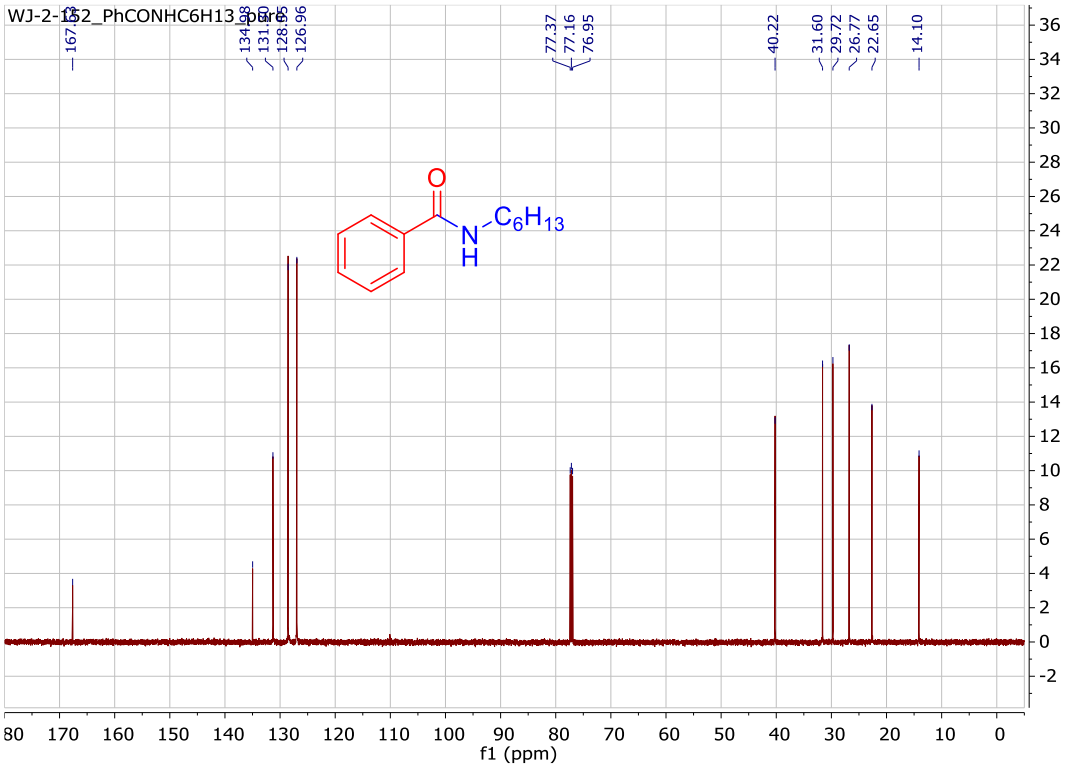
WJ-2-152_PhCONHC6H13_pure
167.23
134.88
131.60
128.65
126.96
77.37
77.16
76.95
40.22
31.60
29.72
26.77
22.65
14.10
O
N
H
C6H13
f1 (ppm)

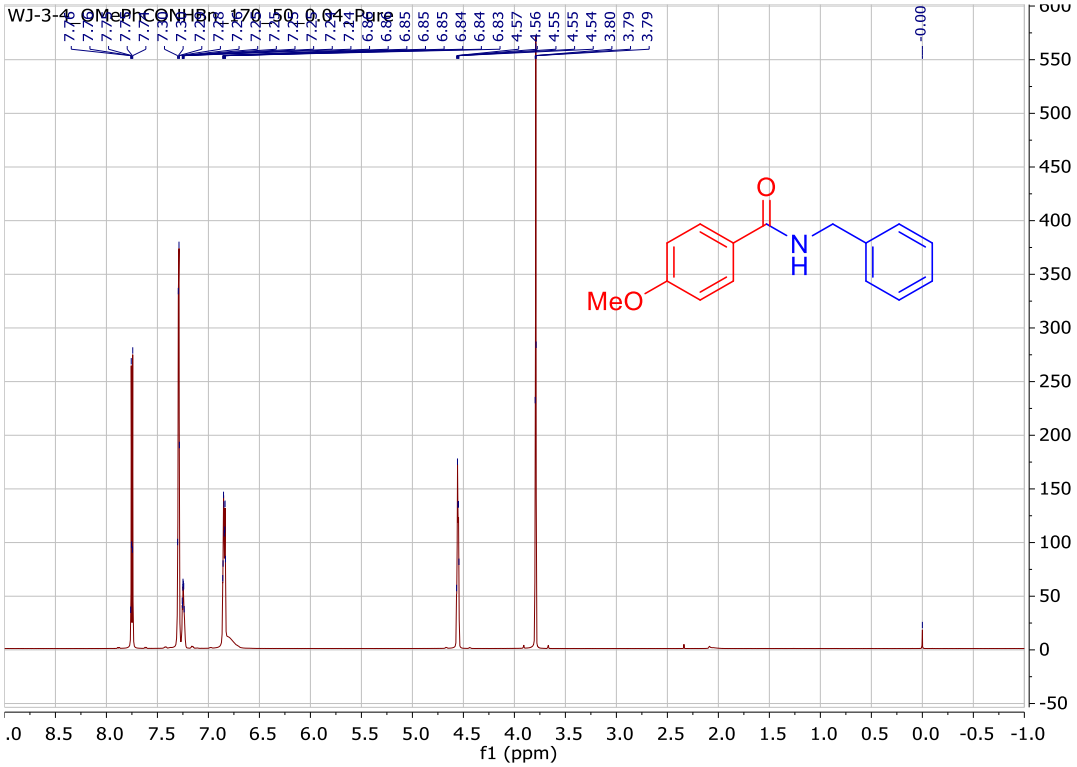
WJ-3-4 OMePhCONHBn 170 50 0.04 Pure
O
N
H
MeO
f1 (ppm)

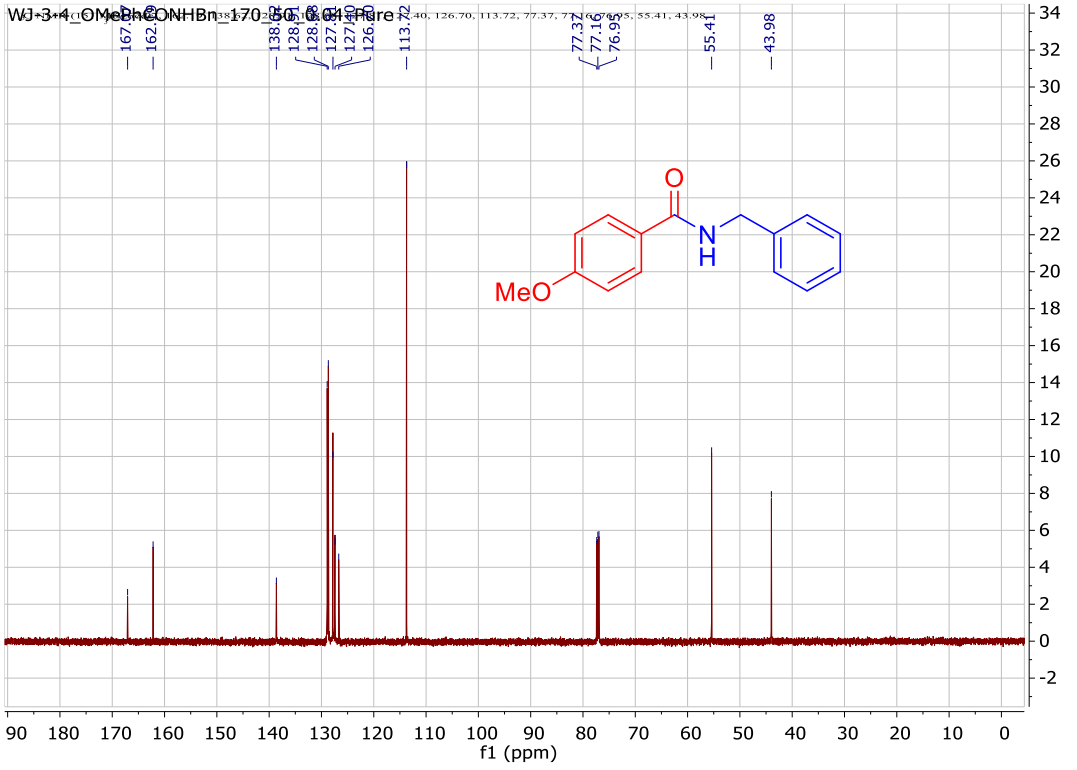
WJ-3-4_OMePhCONHBn_170_50_C13_Pure
O
N
H
MeO
f1 (ppm)

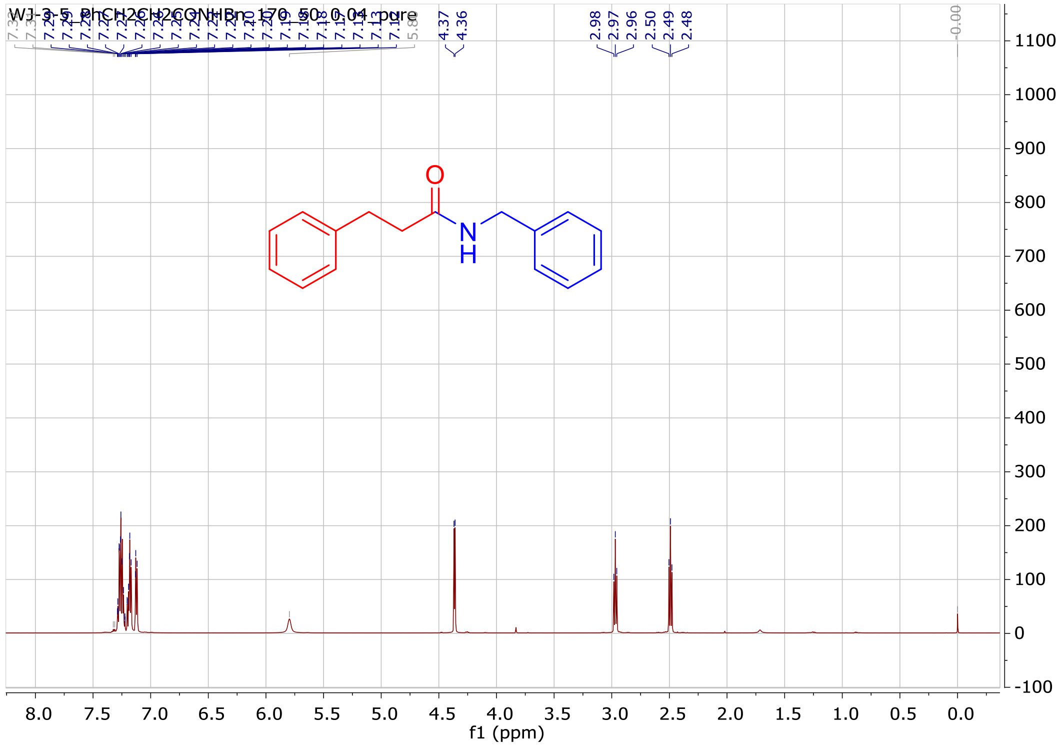
WJ-3-5_PhCH2CH2CONHBn_170_50_0.04_pure
4.37
4.36
2.98
2.97
2.96
2.50
2.49
2.48
0.00
O
N
H
f1 (ppm)

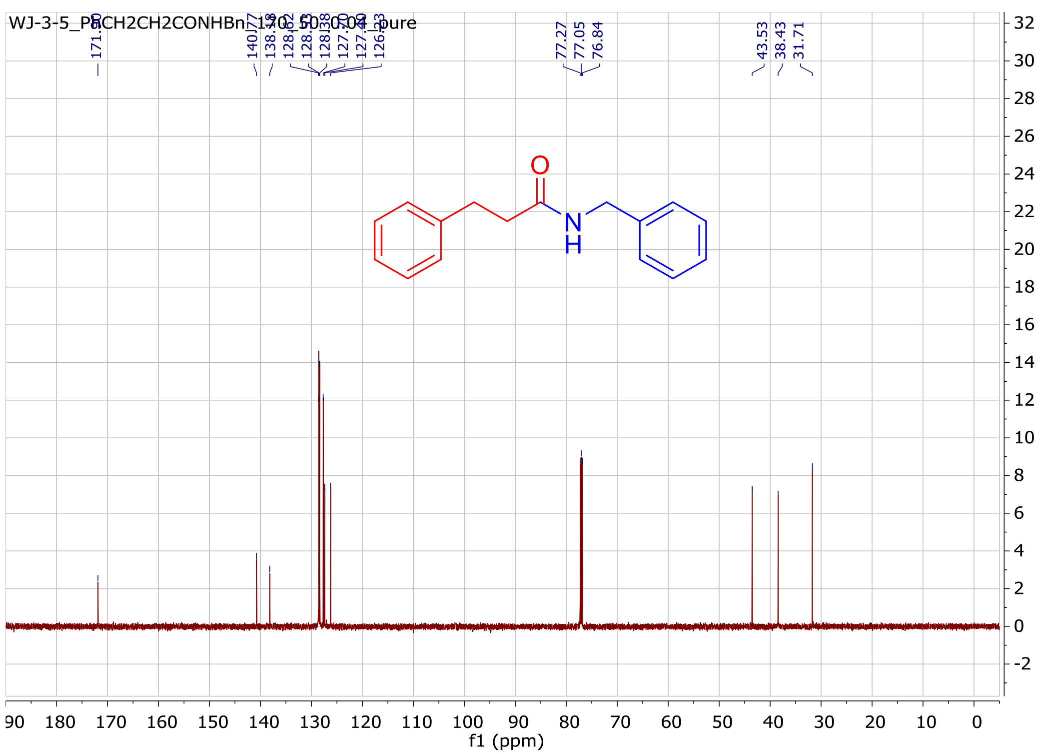
WJ-3-5_PhCH2CH2CONHBn_170_50_0.04_pure
77.27
77.05
76.84
43.53
38.43
31.71
O
N
H
f1 (ppm)

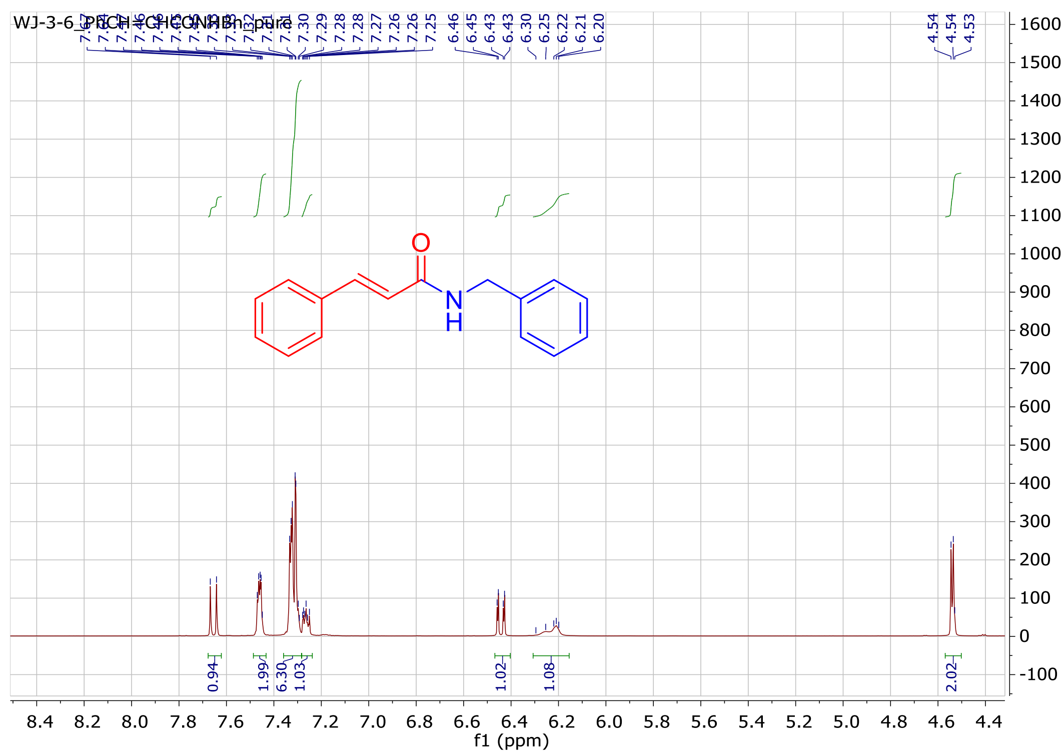
WJ-3-6_PhCH=CHCONHBn_pure
f1 (ppm)

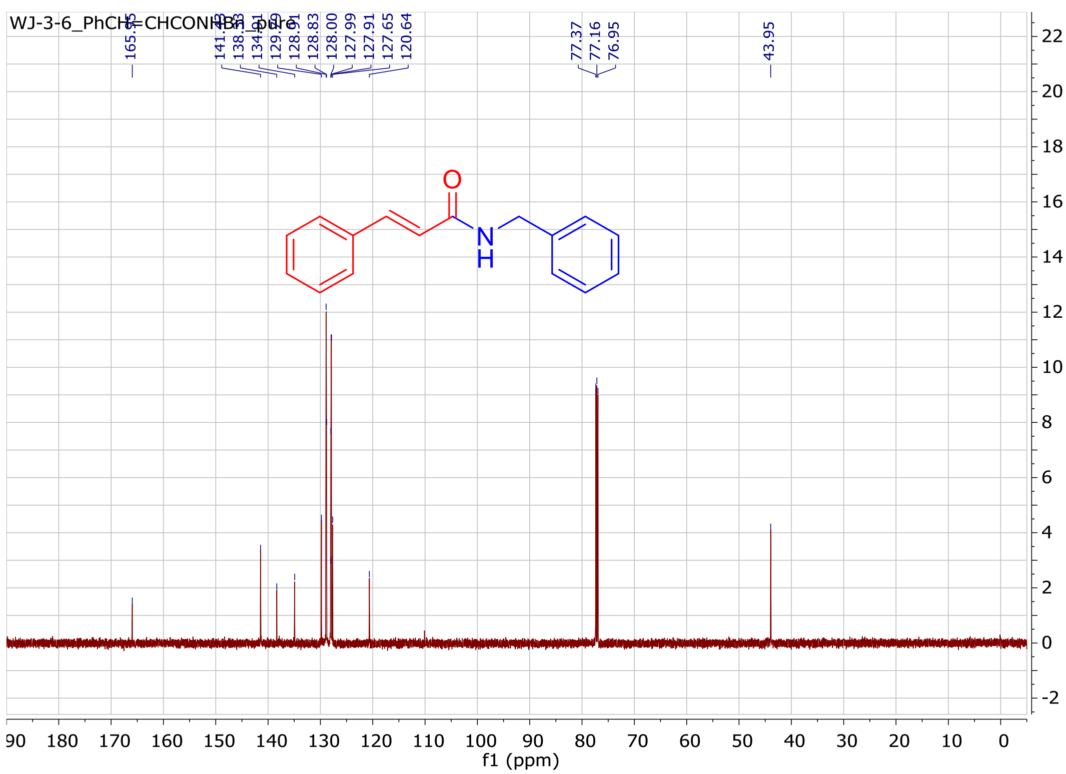
WJ-3-6_PhCH=CHCONHBn_pure
165.85
141.43
138.33
134.91
129.90
128.91
128.83
128.00
127.99
127.91
127.65
120.64
77.37
77.16
76.95
43.95
f1 (ppm)

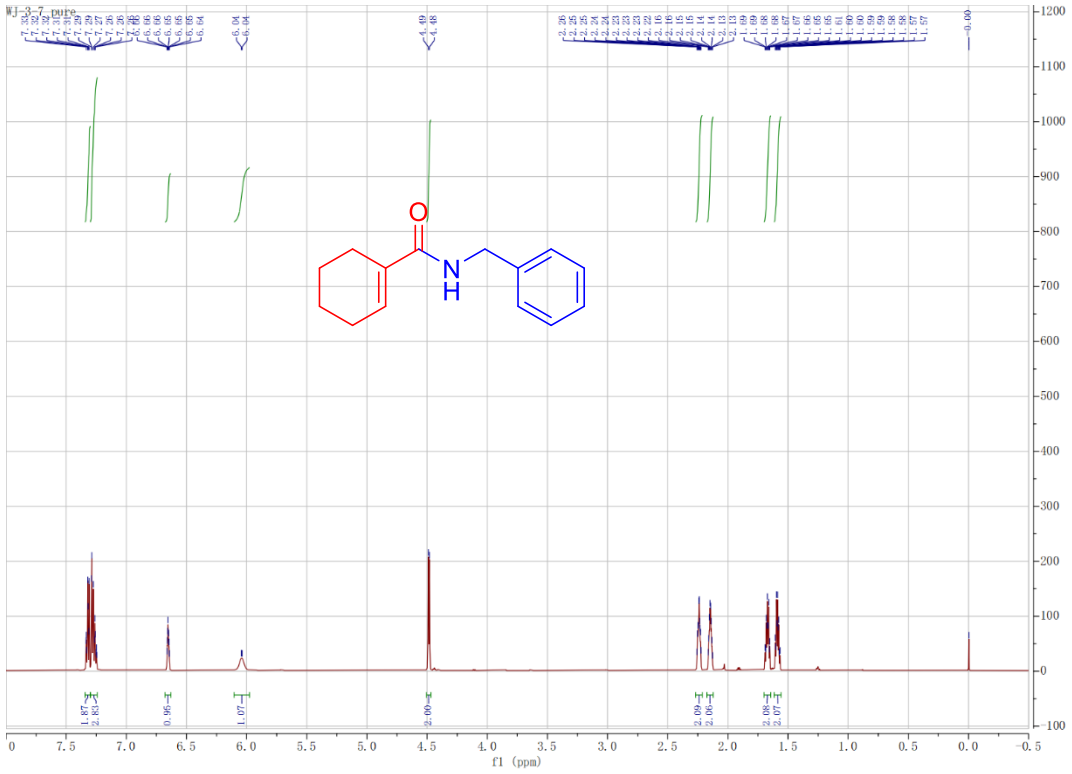
f1 (ppm)

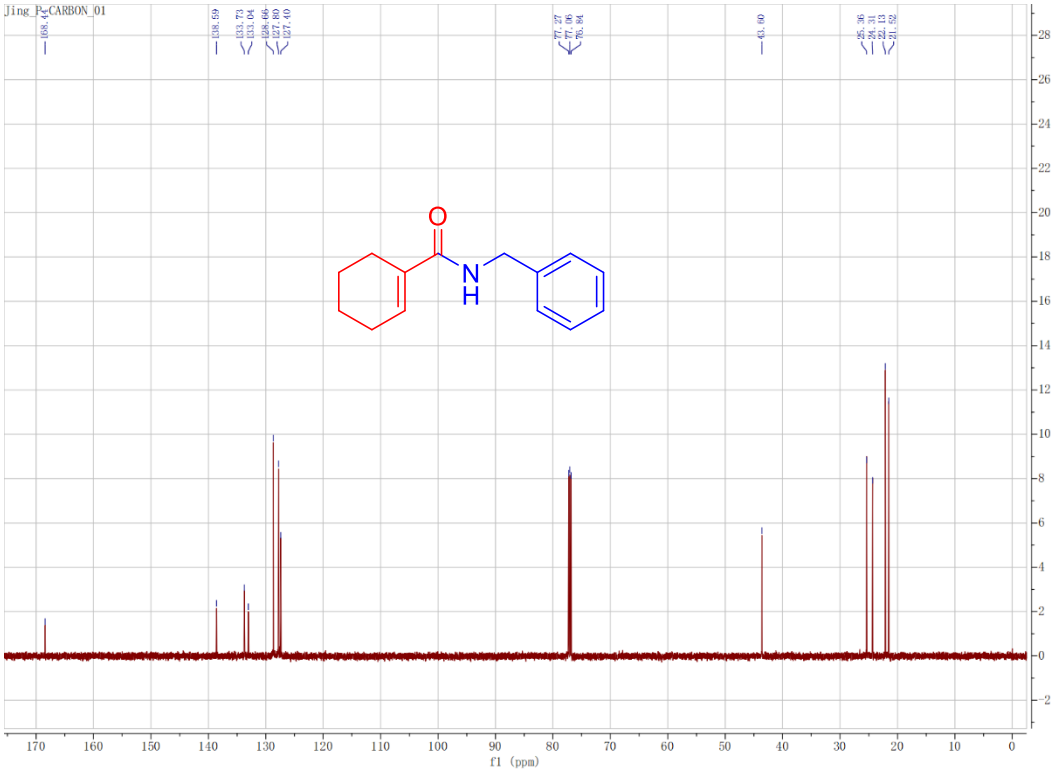
Jing_P_CARBON_01
f1 (ppm)

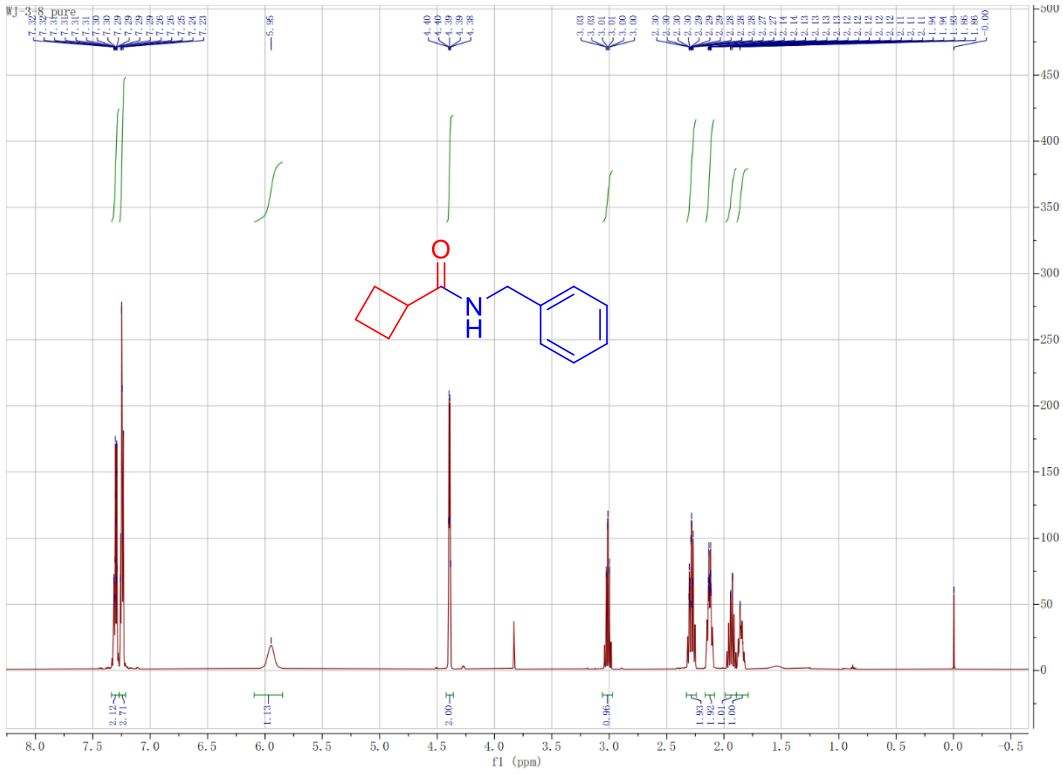
WJ-3-8 pure
f1 (ppm)

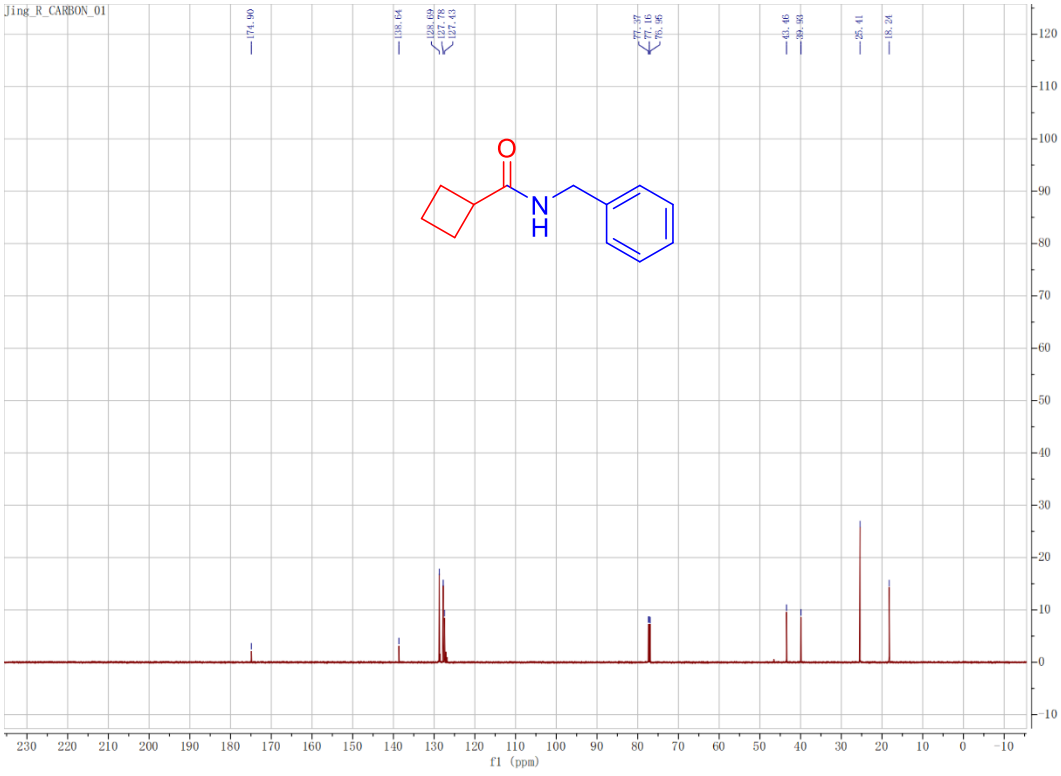
Jing_R_CARBON_01
f1 (ppm)

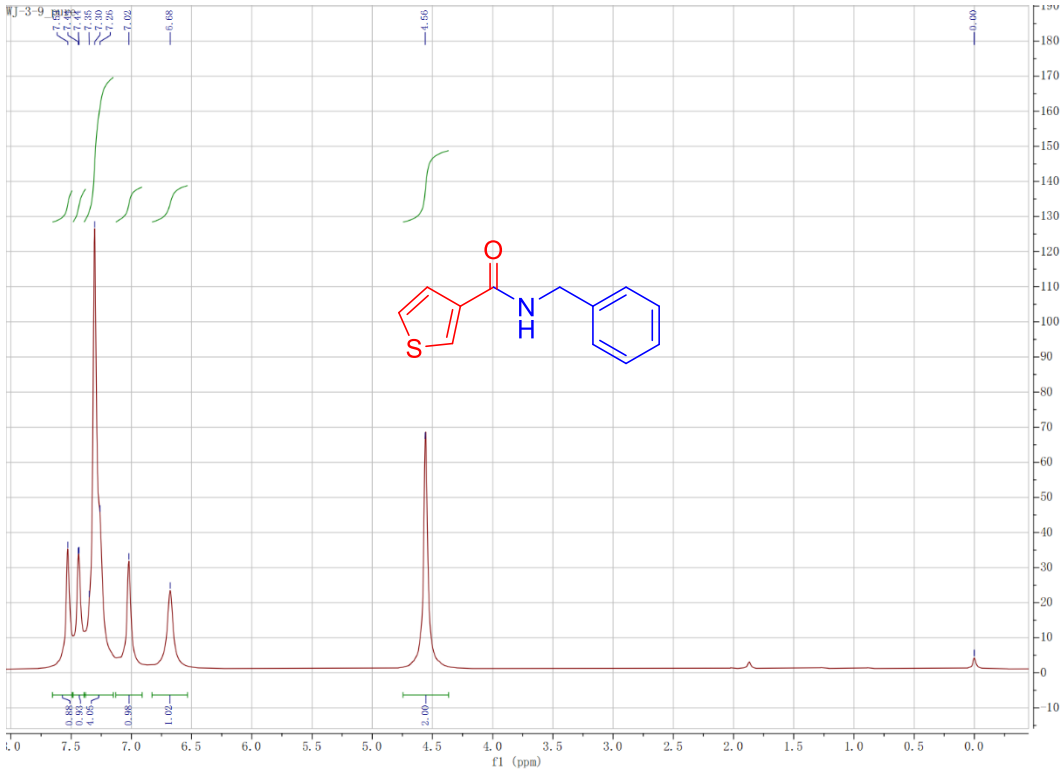
7.68
7.67
7.35
7.30
7.26
7.02
6.68
4.56
0.00
0.88
0.93
4.00
0.98
1.02
2.00
f1 (ppm)

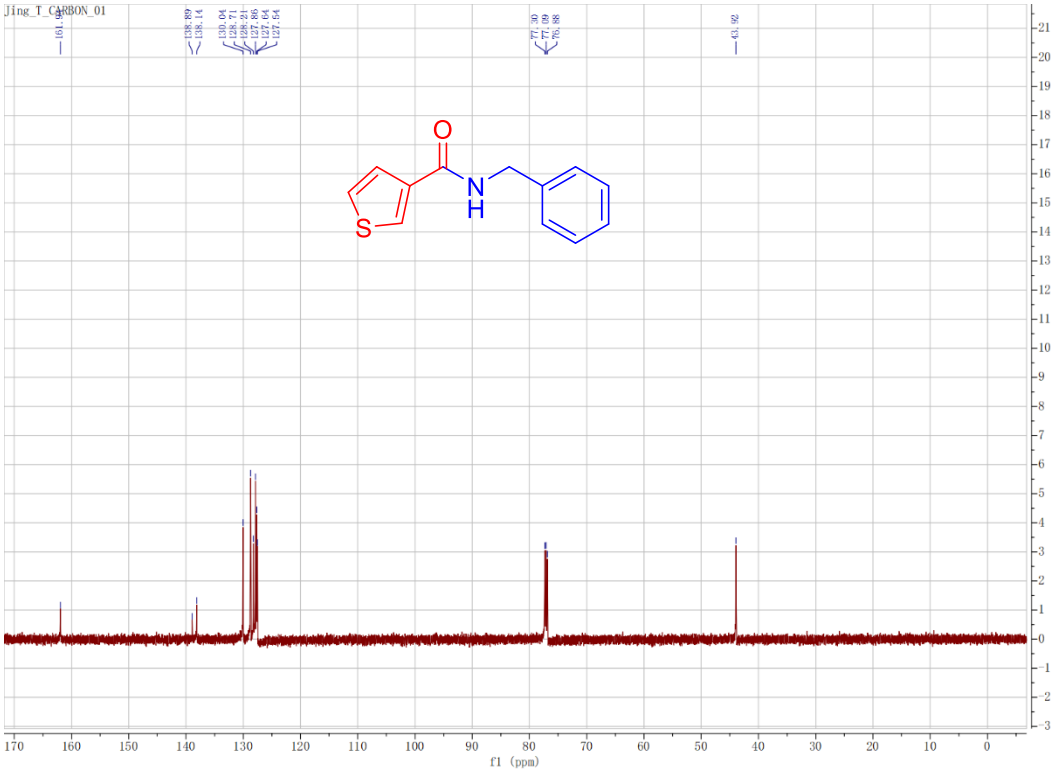
Jing_T_CARBON_01
161.07
138.89
138.14
130.04
128.71
128.24
127.86
127.54
127.54
77.39
77.09
76.88
43.92
f1 (ppm)

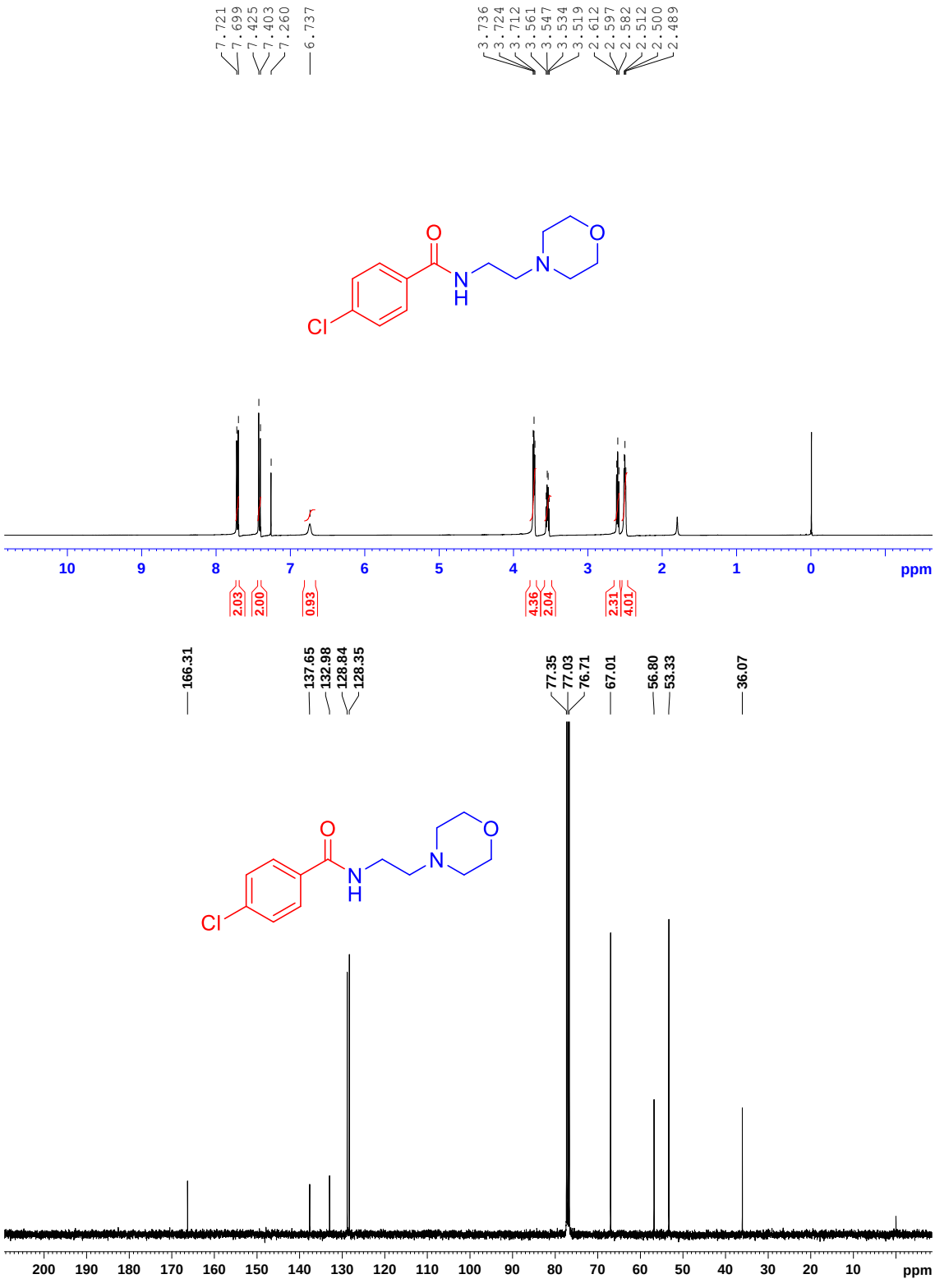
7.721
7.699
7.425
7.403
7.260
6.737
3.736
3.724
3.712
3.561
3.547
3.534
3.519
2.612
2.597
2.582
2.512
2.500
2.489
O
O
N
N
H
Cl
10
9
8
7
6
5
4
3
2
1
0
ppm
2.03
2.00
0.93
4.36
2.04
2.31
4.01
166.31
137.65
132.98
128.84
128.35
77.35
77.03
76.71
67.01
56.80
53.33
36.07
200
190
180
170
160
150
140
130
120
110
100
90
80
70
60
50
40
30
20
10
ppm

CONCLUSION

In Summary, we developed two new synthetic protocols catalyzed by readily available amorphous silica-alumina in continuous flow.

The method for making azacycles is atom economical and greener since water is the only byproduct. This method works well with a variety of cyclic ethers and with aromatic/aliphatic amines. Pyrrolidines, piperidines, and pyrroles were obtained in excellent yields (> 90 %) in several cases, and the practical application of this method was demonstrated in the preparation of a key intermediate towards the synthesis of an H3 antagonist. A gram-scale synthesis of *N*-phenylpyrrolidine was sustained over 68 h, providing > 14 g (nearly 100 mmol) pure product in over 99% yield, with isolation by simple solvent evaporation.

The protocol for preparing amides from esters used comparatively low loading of catalyst. Amorphous silica-alumina is more than three times more effective catalyst than currently reported in the literature, with a corresponding five times lower residence time with a broad substrate scope. The practical application of this protocol was demonstrated by the gram scale synthesis of Moclobemide, an anti-depressant. We were able to synthesize 8.66 g of Moclobemide over 50 hours without significant loss in the activity of the catalyst. However, there are some limitations since both protocols used high temperatures (170^{o}C-200^{o}C). For some challenging substrates in azacycle synthesis, we used very high pressure (up to 600 psi) and a very low flow rate (0.04 ml/min).